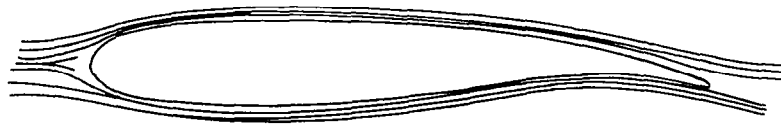


NASA
CP
2218
c.1

NASA Conference Publication 2218

Laminar Flow Control

*1981 Research and
Technology Studies*



LOAN COPY
AFWL TECHNICAL LIBRARY
KIRTLAND AFB, N. M.

*Presentations made at the Oral Status Review
of the NASA Aircraft Energy Efficiency (ACEE)
Laminar Flow Control (LFC) Program held at
Dryden Flight Research Center
Edwards, California
September 17-18, 1981*

NASA



NASA Conference Publication 2218

Laminar Flow Control

*1981 Research and
Technology Studies*

Dal V. Maddalon, *Editor*
Langley Research Center
Hampton, Virginia

Presentations made at the Oral Status Review
of the NASA Aircraft Energy Efficiency (ACEE)
Laminar Flow Control (LFC) Program held at
Dryden Flight Research Center
Edwards, California
September 17-18, 1981

NASA

National Aeronautics
and Space Administration

**Scientific and Technical
Information Branch**

FOREWORD

Laminar flow control (LFC) technology has undergone tremendous progress in recent years as focused research efforts in structures, materials, aerodynamics, and systems have begun to pay off. This work, conducted under the NASA Aircraft Energy Efficiency (ACEE) Laminar Flow Control Program, was begun in 1976. The objective is to demonstrate practical, reliable, LFC technology for application to commercial transport aircraft. Earlier work has shown that an LFC system greatly reduces aircraft fuel use and operating costs.

Ongoing research studies described in these papers complement the major strides being made by industry airframe manufacturers, under NASA sponsorship, in the development of LFC structures and materials and in the demonstration of flight systems. Research and technology developments discussed herein include: fundamental studies of improved analytical techniques in boundary-layer stability prediction (together with confirming experimental measurements); a greatly expanded experimental data base characterized by detailed transonic wind-tunnel measurements on supercritical airfoils specially designed for LFC; theoretical and experimental design studies of high-lift systems applicable to LFC airfoils; reduced cost and complexity of LFC structures from technology such as superplastically formed-diffusion bonded titanium materials; and the impact of routine airline operations on the reliability and maintenance of laminar flow control systems under actual weather conditions. Six research papers are presented by representatives of NASA Langley Research Center, Rockwell International, Douglas Aircraft Company, and Virginia Polytechnic Institute and State University. The material given here is essentially the same as that used in oral presentations at the review. Order of papers is in the actual order of speaker appearance.

This review was a part of the ACEE Project Oral Status Review and KC-135 Winglet Program Review held September 14-18, 1981, at Dryden Flight Research Center in Edwards, California. The conference included comprehensive reviews of major flight-test and structures contracts by the two major ACEE LFC contractors, Douglas Aircraft Company and Lockheed-Georgia Company. In addition, two sessions included selected papers describing LFC research and technology. The NASA sponsored work in this latter area is collected in this NASA Conference Publication.

Use of trade names or names of manufacturers in this report does not constitute an official endorsement of such products or manufacturers, either expressed or implied, by the National Aeronautics and Space Administration.

Grateful appreciation is expressed to the authors whose efforts characterized the technical excellence of this session.

Dal V. Maddalon
Session Chairman
Langley Research Center

CONTENTS

Foreword..... iii

1. NASA Langley Laminar Flow Control Airfoil Experiment 1
W. D. Harvey and J. D. Pride, Jr.
NASA Langley Research Center

2. Status of NASA Advanced LFC Airfoil High-Lift Study 43
Zachary T. Applin
NASA Langley Research Center

3. Stability of Boundary Layers With Porous Suction Strips: Experiment and
Theory 63
G. A. Reynolds, W. S. Saric, H. L. Reed, and A. H. Nayfeh
Virginia Polytechnic Institute and State University

4. Probability of Laminar Flow Loss Because of Ice Crystal Encounters 75
Richard E. Davis
NASA Langley Research Center

5. SPF/DB Titanium Concepts for Structural Efficiency 95
V. E. Wilson
Rockwell International

6. SPF/DB Titanium LFC Porous Panel Concept 111
Neil R. Williams
Douglas Aircraft Company

NASA LANGLEY LAMINAR FLOW CONTROL AIRFOIL EXPERIMENT

W. D. Harvey and J. D. Pride
NASA Langley Research Center
Hampton, VA

ABSTRACT

In an effort to significantly reduce drag and increase aircraft energy efficiency, the NASA Langley Research Center has designed and is constructing an advanced swept supercritical LFC airfoil which is scheduled for wind tunnel testing to confirm performance and to establish a technology base for future long range commercial transports. The swept LFC airfoil was designed for a given thickness ratio and lift coefficient, with emphasis placed on high critical Mach number with shock-free flow. It is compatible with satisfactory low speed and buffeting characteristics and minimizing the suction laminarization. Further emphasis was placed on achieving shock-free flow over a wide range of off-design conditions including trailing edge flap control. This presentation further briefly describes the requirements and design of the suction system and modifications to the Langley 8-Foot Transonic Pressure Tunnel including contouring of all nonporous test section walls for free air simulation and flow quality improvements. Tunnel installation is scheduled for completion and initial testing is to begin in early 1982. Specific objectives for the LFC experiment are given in figure 1.

SPECIFIC OBJECTIVES

- DEVELOP AN ADVANCED SWEPT SUPERCRITICAL AIRFOIL WITH PERFORMANCE COMPARABLE TO ADVANCED TURBULENT AIRFOILS AND WITH FEATURES WHICH WILL SIMPLIFY LAMINARIZATION
- VERIFY PERFORMANCE OF THE SELECTED AIRFOIL THROUGH WIND-TUNNEL TESTING AT SIMULATED DESIGN AND OFF-DESIGN CONDITIONS AT REQUIRED CROSSFLOW REYNOLDS NUMBERS
- EVALUATE BOTH SLOTTED AND POROUS CONCEPTS IN THE UPPER SURFACE WING BOX REGION
- EXTEND DATA BASE AND VALIDATE EFFICIENCY OF UPDATED STABILITY CODES WITH EMPHASIS ON THE COMBINED EFFECTS OF CROSSFLOW AND LOCAL SUPERSONIC FLOW

Figure 1

SYMBOLS

a	amplitude
B	growth factor; $\beta\theta R_\theta$
b	span of model
C_d	total drag, $C_{d, \text{suct}} + C_{d, \text{wake}}$
C_L	section lift coefficient
C_p	pressure coefficient; $\frac{p - p_\infty}{q_\infty}$
C_Q	coefficient of suction, $-\left(\frac{(\rho u)_w}{\rho_\infty U_\infty}\right)$
c	chord length
D	diameter
e	= 2.71
f	frequency
G	Goertler parameter; $R_\theta(\theta/r)^{1/2}$
H	height
h	plenum (or nozzle) height or surface wave height
l	length
M	Mach number
N	amplitude ratio; $\ln a/a_0$
p	pressure
Q	mass flow rate
q_∞	dyanmic pressure, $1/2 \rho_\infty U_\infty^2$
R_∞	free stream unit Reynolds number
Re_c	Reynold numbers based on chord (local or freestream)
Re_s	slot Reynolds number

Re_w	crossflow Reynolds number
Re_x	local Reynolds number based on coordinate x
R_θ	momentum thickness Reynolds number
r	radius of surface curvature
s	slot width
t	thickness
U_s	slot velocity
U_∞	freestream velocity
u	velocity in flow direction
V_0	local velocity component normal to suction surface
v	velocity perpendicular to flow direction
x	coordinate in chord direction
z	sucked height of local boundary layer
α	angle of attack or mass flow discharge coefficient
β	Taylor-Goertler vortex growth parameter
β_{flap}	trailing edge flap angle
δ	total boundary-layer thickness
θ	momentum thickness
λ	wavelength
Λ	leading edge sweep angle
μ	viscosity
ρ	density

Subscripts

∞	freestream
\perp	normal to leading edge
DD	drag divergence

n nozzle
sd suction duct
w wall value
o reference
e edge value

Superscript

' prime denotes rms value

TEST SETUP FOR LFC EXPERIMENT IN LaRC 8-FT TPT

A schematic of the overall LFC experiment hardware in the Langley 8-ft TPT is shown in figure 2, along with modifications. The LaRC 8-ft TPT has been dedicated to the development and testing of low drag airfoils at transonic speeds with and without suction control. The major component consists of a large-chord swept supercritical LFC airfoil of aspect ratio nearly one and spans the full tunnel height. Airfoil suction air is removed by a 10 000 CFM compressor through the airflow system evacuation lines, control boxes, and sonic nozzles. To produce transonic wind-tunnel flow which simulates free-air flow about an infinite yawed airfoil, all nonporous bonding walls have been contoured. Length of the contoured liner is about 6 times the tunnel height including nozzle contraction, test section and diffuser. An adjustable two-wall choke (sonic throat) is located downstream of the LFC model to block upstream noise propagation. Tunnel modifications include installation of a honeycomb followed by five screens for suppression of turbulence.

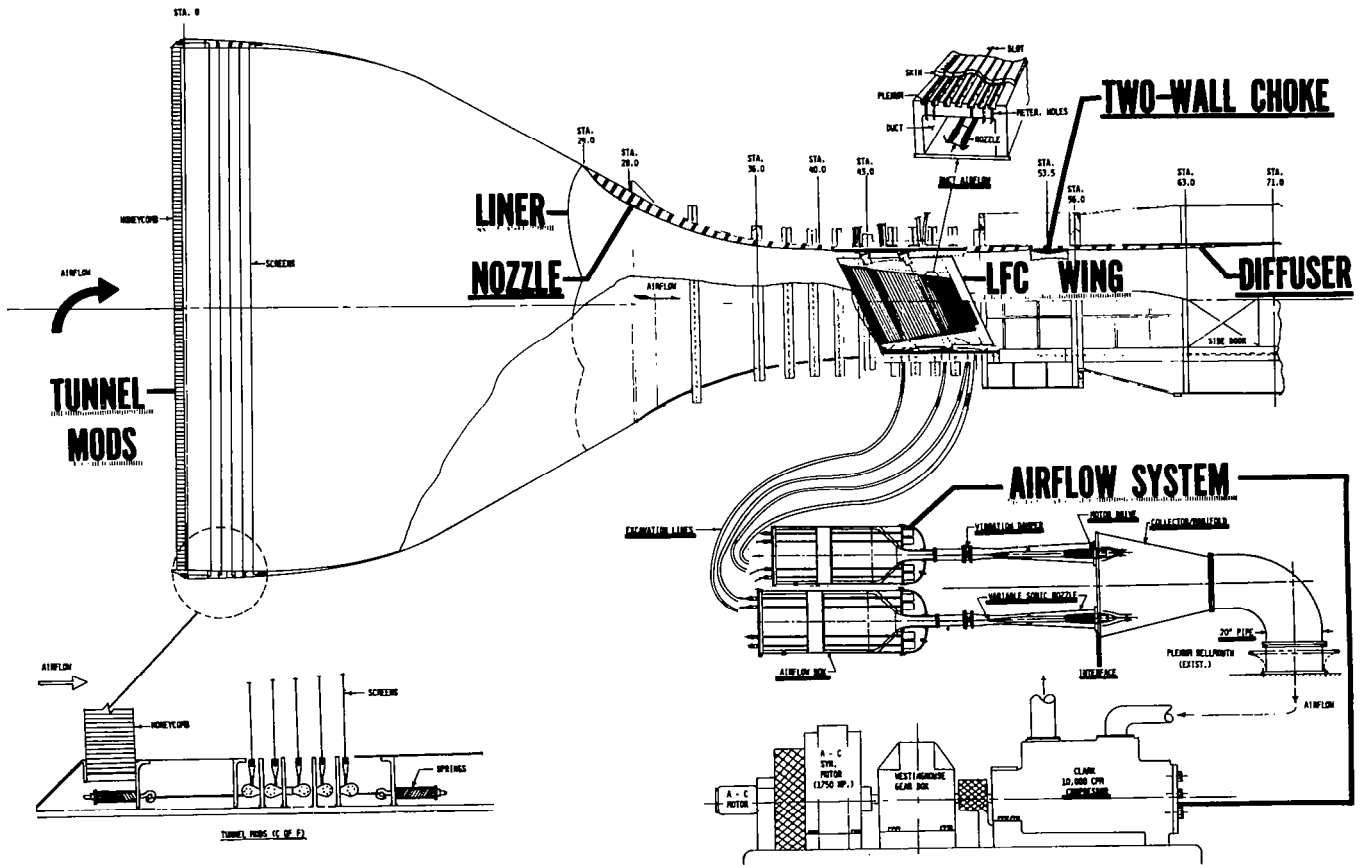


Figure 2

LFC AIRFOIL EXPERIMENT SCHEDULE

Figure 3 is a current ACEE/PERT schedule indicating major milestones for the design, fabrication, and installation of various components of the LFC experiment, and test start date of January 1982. Also included for tracking purposes are the associated tunnel modifications. Filled symbols to the left of the current vertical dashed line at September 1981 represent completed task milestones. It should be noted that the original LFC test date of July 1981 was delayed about 6 months due to high-priority Shuttle tests (CLOT) conducted recently in the 8-ft TPT. However, the LFC experiment fabrication and installation is on schedule with the tunnel modifications (honeycomb and screens, liner) in progress.

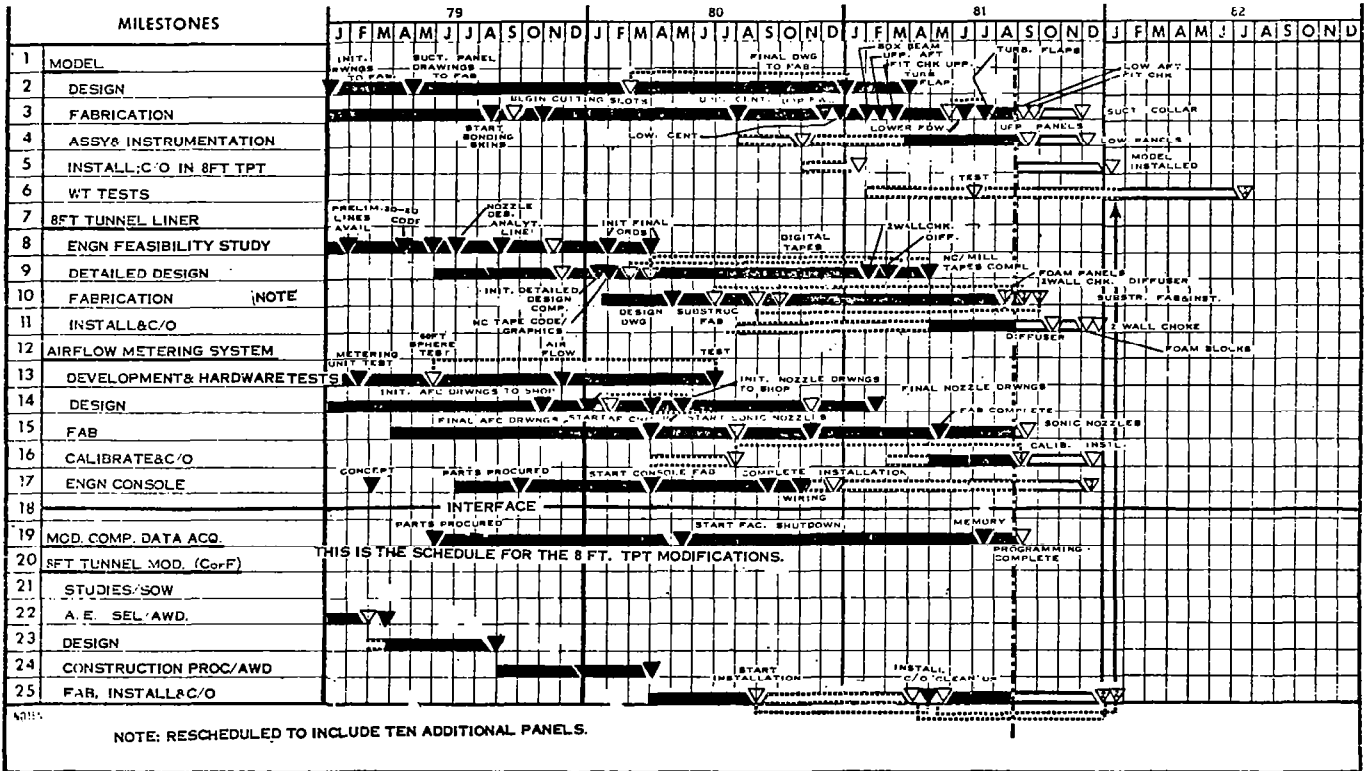


Figure 3

EFFECT OF TUNNEL TURBULENCE LEVEL ON
MAINTAINING FULL-CHORD LAMINAR FLOW

Previous LFC experiments (ref. 1) have shown that the characteristics of low-drag airfoils can be successfully measured only in low-turbulence tunnels. Figure 4 illustrates the effect of tunnel disturbance levels on maintaining full-chord laminar flow on airfoils and bodies of revolution with suction applied through closely spaced slots in several wind tunnels, compared to X-21 flight results. Results indicate that tunnels, whose level of turbulence is very low ($u'/V_\infty \leq 0.05\%$), are required to achieve extensive LFC on airfoils at high Re_c 's approaching flight conditions. Also shown is the design point established for the LFC experiment corresponding to $u'/V_\infty = 0.05\%$ and $Re_c = 20 \times 10^6$ at $M_\infty = 0.82$. Realization of this goal is expected based on flow quality tests (ref. 2) and installation of a wall choke and turbulence screens for the LFC experiment.

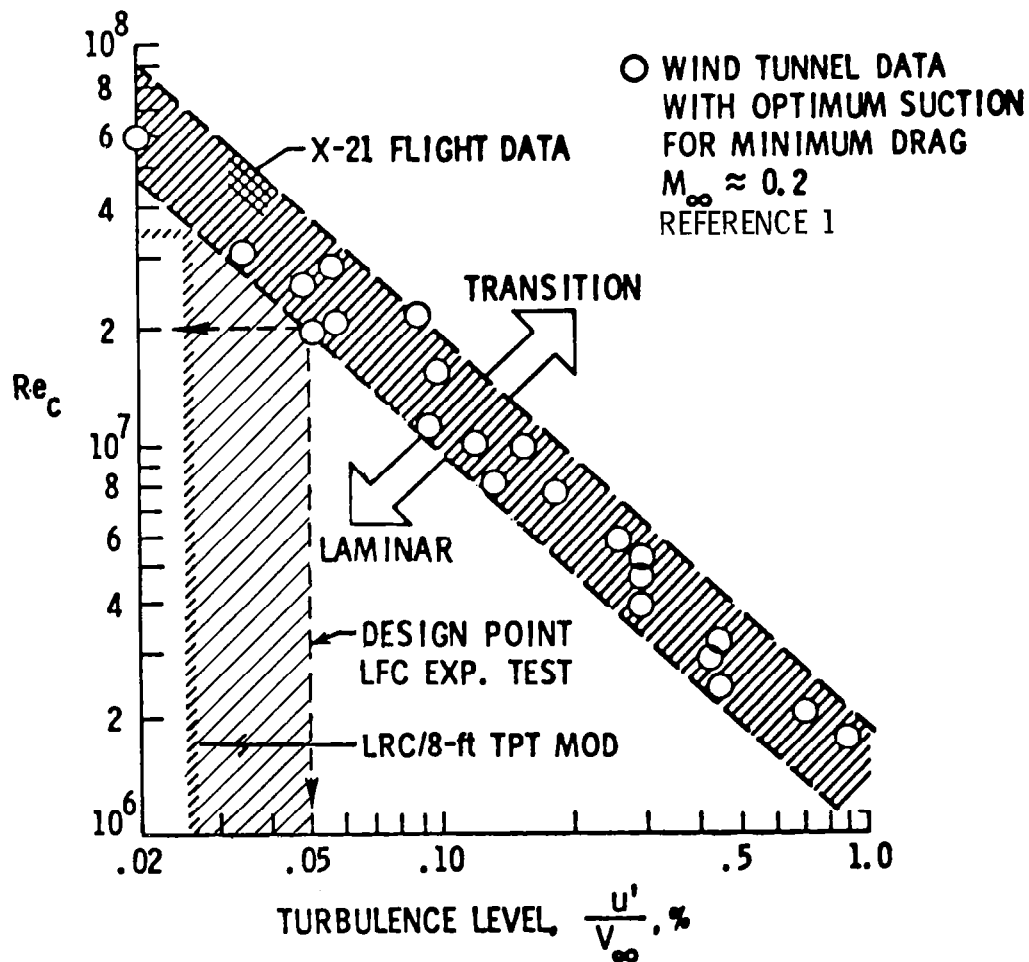


Figure 4

CROSSFLOW REYNOLDS NUMBER (Re_w) SIMULATION

Aside from the basic considerations of model scale, fabrication, and boundary-layer stability and control, optimization with regard to choices of leading edge sweep, chord Reynolds number, and crossflow Reynolds number is of major importance. Achievement of moderately high chord Reynolds numbers on a practical-size wind-tunnel LFC model inherently requires high unit Reynolds number testing that is several times larger than that encountered on a vehicle at cruise. Considering the maximum feasible airfoil chord for testing in the LaRC 8-ft TPT, the flight Mach number and constant crossflow Reynolds number simulation was selected based on future full-scale LFC aircraft cruise conditions. Figure 5 shows the design point chord Reynolds number ($Re_c \sim C \cos \Lambda$) and sweep angle for $Re_w = \text{constant}$. While exact flight simulation could not be achieved, the test range of $10 \times 10^6 \leq Re_c \leq 40 \times 10^6$ at $\Lambda = 23^\circ$ approaches flight simulation at cruise for future commercial transports.

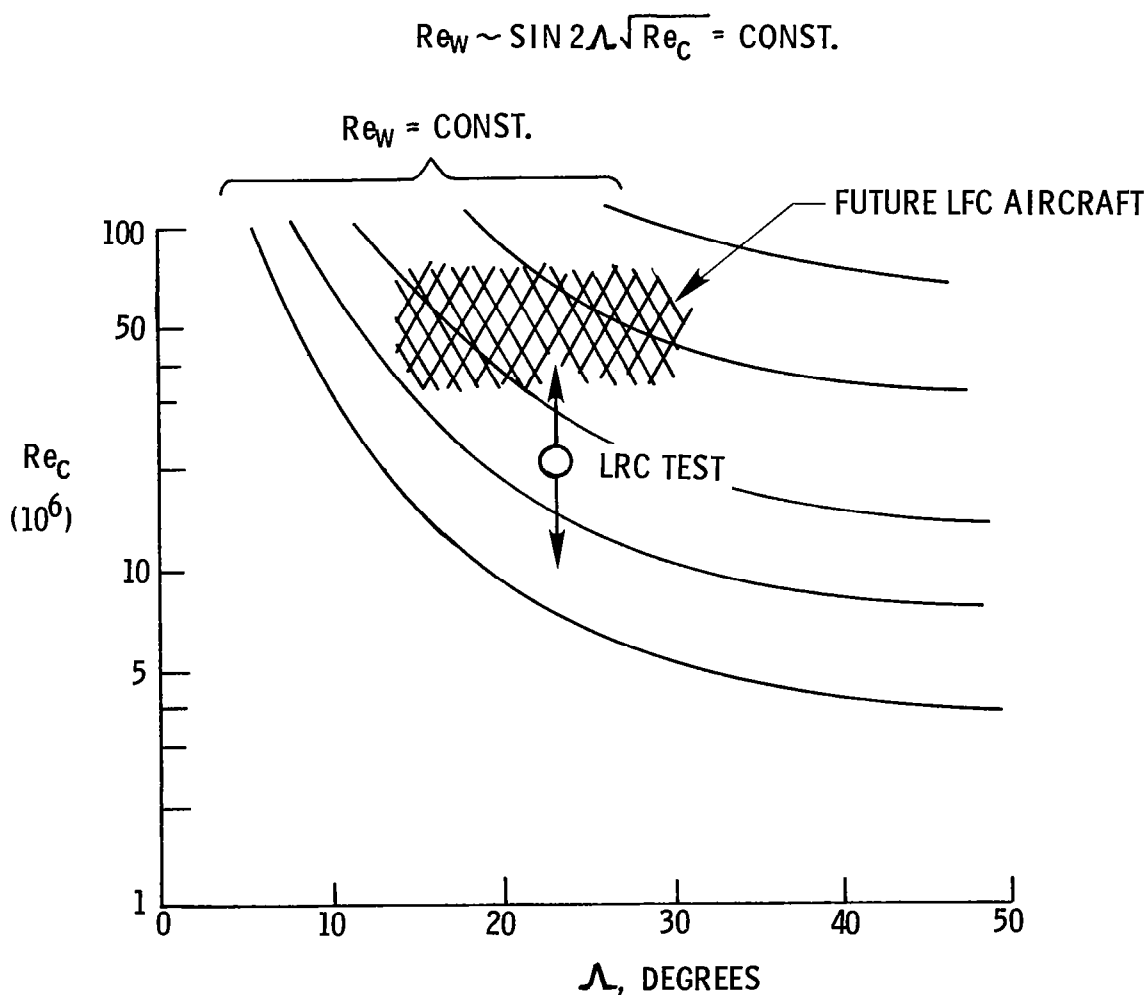


Figure 5

LFC AIRFOIL AERODYNAMIC DESIGN CYCLE

A block diagram of the design cycle for the LFC airfoil is shown in figure 6 along with typical outputs from the various design codes. The codes used represent updated aerodynamics design tools and advanced boundary-layer stability theories for optimization and prediction of suction requirements. Airfoil pressure distribution is determined from a transonic inviscid code ("Korn-Garabedian") (ref. 3). The boundary-layer code (ref. 4) used has been modified to include the effects of mass transfer at the wall and computation of the surface displacement thickness. The boundary-layer code (ref. 4) is combined with the transonic inviscid code (ref. 3) to analyze transonic flow over a finite swept airfoil with LFC. Interaction of the results from the boundary-layer analysis with the stability code (ref. 5) provides the required suction rates. The stability analysis is based on various types of growth disturbances (crossflow, T-S (Tollmien-Schlichting), T-G (Taylor-Goertler)) in the different regions of the airfoil. It should be noted that final design suction results for the LFC airfoil have been verified utilizing several alternate stability codes (refs. 6-8) and independent calculations (refs. 7 and 8), including incompressible and compressible effects.

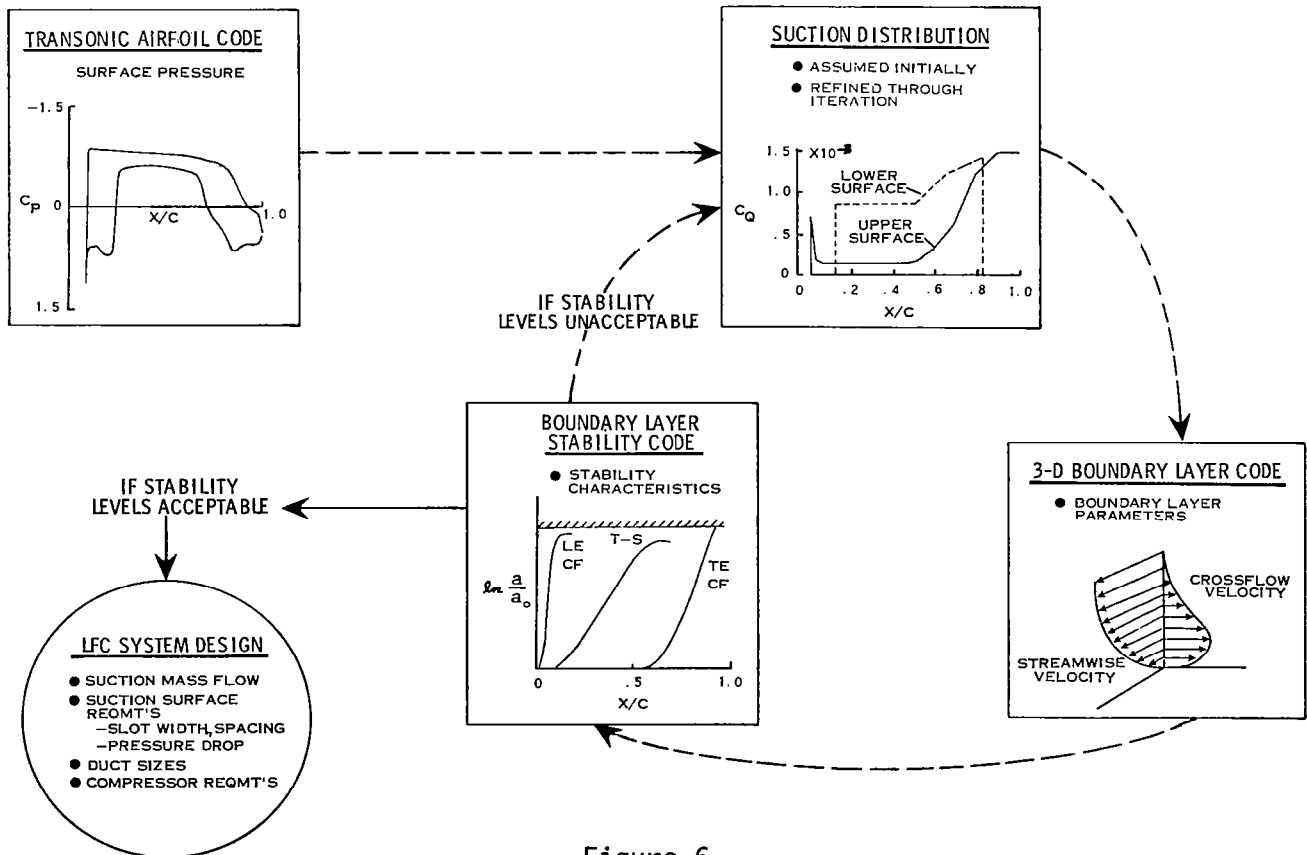


Figure 6

SUPERCRITICAL LFC AIRFOIL DESIGN AND OFF-DESIGN PRESSURE DISTRIBUTION

The chordwise pressure distributions and sonic lines on the upper and lower surfaces of the LFC airfoil are shown in figure 7 for the shock-free design point and a representative off-design case and are determined for the Korn-Garabedian code (ref. 3) analysis using a 320-point mesh. The airfoil geometry and pressure distribution represent an effort to minimize boundary-layer growth disturbances and subsequent suction control requirements, using concepts developed by Pfenninger (ref. 9). To minimize lift (at a given t/c and M_∞), the airfoil thickness is reduced in the structurally less critical front and rear areas by undercutting the lower surface. The central region provides bending strength and torsional stiffness and insignificant lift contribution. This concept avoids excessively large pitching moments. Boundary-layer crossflow was substantially reduced by decreasing sweep and leading-edge thickness and by the choice of pressure and suction distribution. The upper surface pressure distribution has a steep acceleration in the nose region followed by a gradual deceleration and flat profile to $x/c \approx 0.4$. Downstream, the flow decelerates rapidly, followed by a steep subsonic pressure rise with suction towards the trailing edge analogous to a Stratford-type recovery. The supersonic zone on the upper surface extends over about 80% chord. Flow accelerates rapidly around the leading edge lower surface and towards the concave region at high static pressure and decelerates before further acceleration downstream to sonic velocity in the midchord region. Suction control is required for the minimization of centrifugal Taylor-Goertler-type boundary-layer instabilities and interactions in the concave regions. A small-chord ($0.1 c$) trailing-edge flap provides lift recovery at off-design. Application of a suitable leading-edge lift device (Krueger type) appears feasible in the small nose and lower concave (low-velocity) region to ensure satisfactory low-speed characteristics.

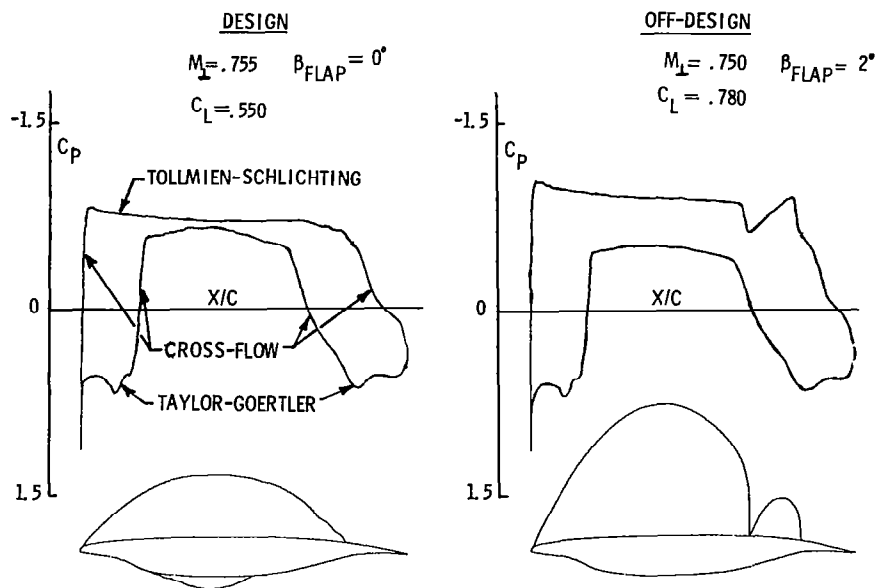


Figure 7

LFC AIRFOIL SHOCK-FREE LIMIT

The flow around supercritical airfoils is basically sensitive to changes in the external flow conditions. Design and off-design analyses indicate that shock-free full-chord LFC airfoils at transonic potential flow appear feasible at the design point and within a narrow operating range. Figure 8 shows the LFC airfoil shock-free C_L limit with normal chord Mach number for various model flap and incremental angle-of-attack ($\Delta\alpha$) adjustments. In order to test under shock-free conditions at lower-than-design Mach number, the shock-free C_L limit must be adjusted by selecting an appropriate combination of M , α , and β . Lowering the flap increases the local supersonic Mach numbers and raises the sonic bubble on the upper surface. Thus, the interacting supersonic and receiving rearward subsonic flows cause surface static pressure discontinuities and shock waves to occur as flap deflection progressively changes. At sufficiently high Mach number and flap deflection, strong shocks develop at the downstream end of the supersonic zone. Further limitations are imposed by the supersonic bubble/tunnel wall interaction as Mach number decreases. Thus operation beyond the indicated design and off-design boundaries requires increases in suction control and streamline contouring to be evaluated during testing.

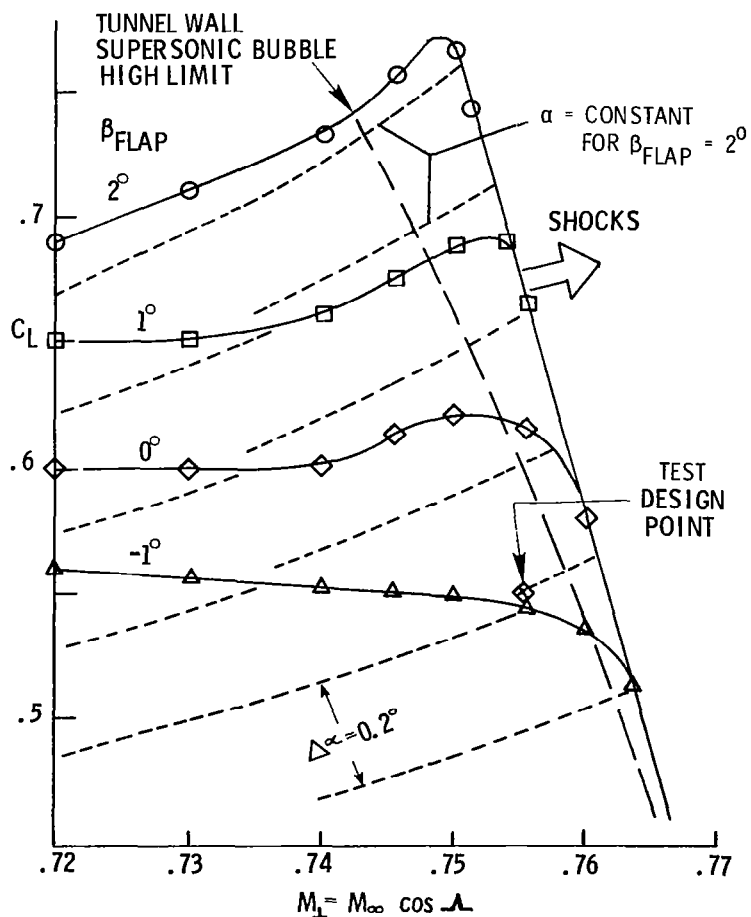


Figure 8

AIRFOIL DRAG DIVERGENCE WITH THICKNESS

Emphasis was placed on achievement of high design-critical Mach number at drag divergence with shock-free flow for a given thickness ratio t/c and lift coefficients. The developed swept supercritical LFC airfoil is to have performance comparable to advanced turbulent airfoils with features which simplify laminarization. Figure 9 shows the variation of Mach number at drag divergence with t/c for conventional and advanced turbulent supercritical airfoils with the LFC airfoil design point. Operation at higher Mach numbers requires flap deflection to avoid shocks and subsequent drag increase, comparable to turbulent airfoils.

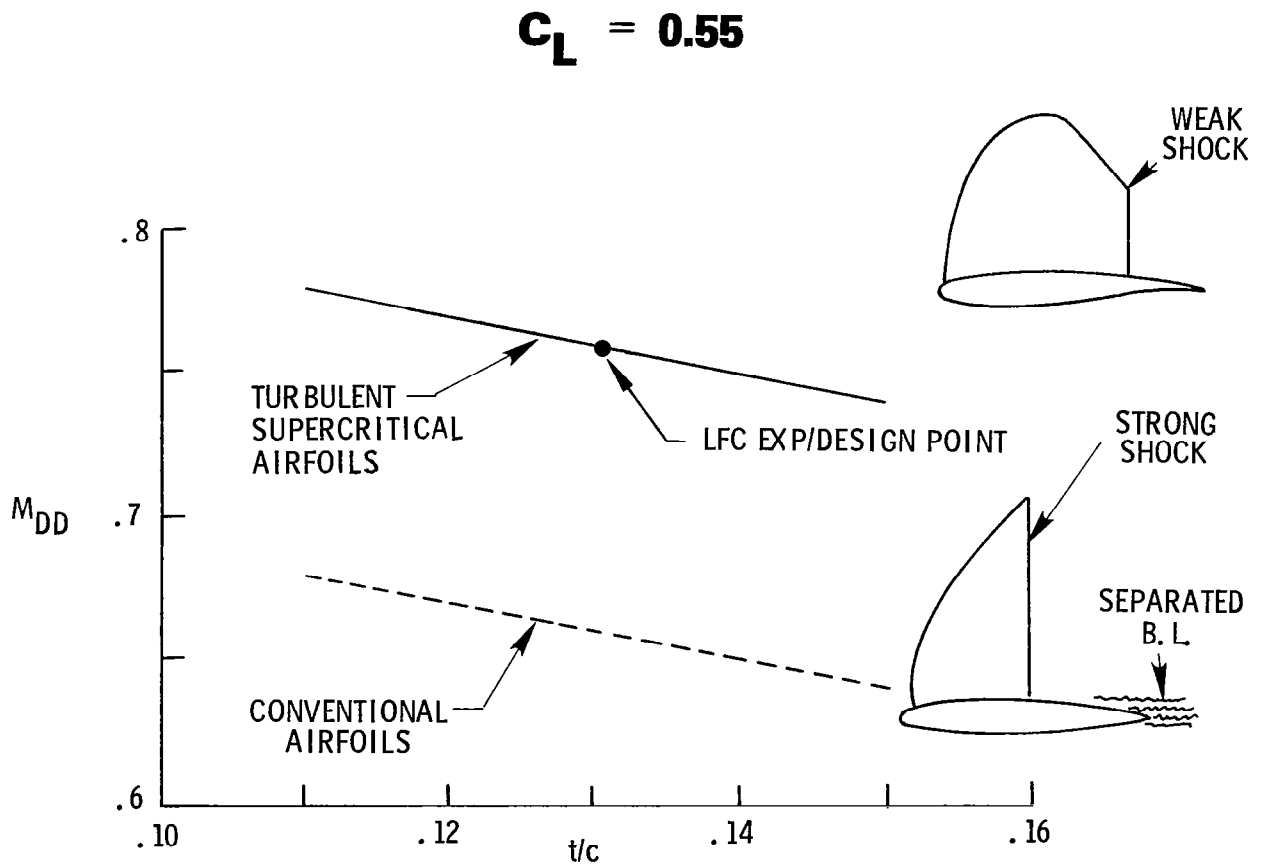
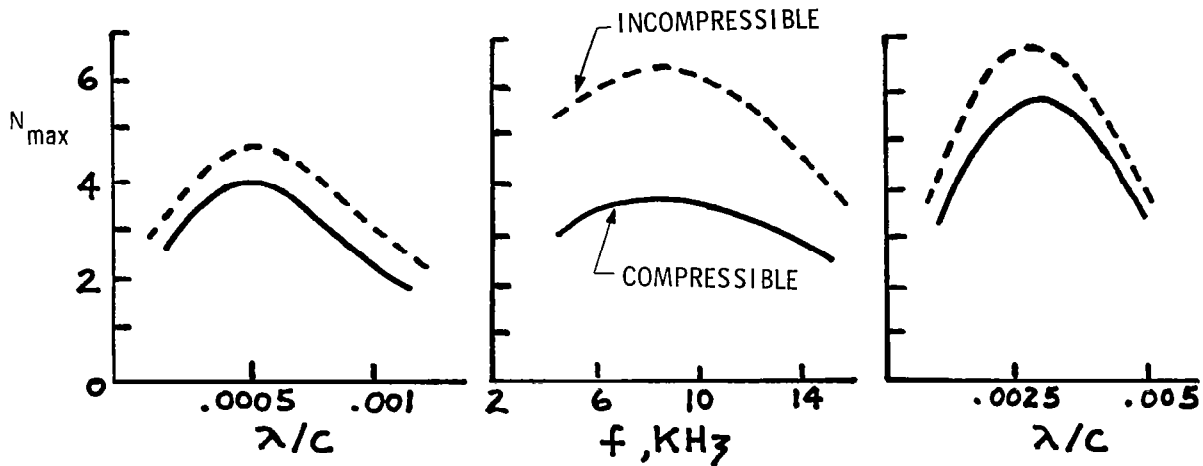


Figure 9

MAXIMUM DISTURBANCE AMPLITUDE RATIO ($N = \ln a/a_0$)
 SWEEPED LFC AIRFOIL UPPER SURFACE DESIGN

The design of swept LFC airfoils at high Re_c 's is primarily influenced by boundary-layer crossflow considerations. A linearized incompressible boundary-layer crossflow stability code (refs. 6 and 8) was initially used to calculate the crossflow and T-S boundary layer disturbances with later calculations and verifications conducted using updated linear incompressible and compressible codes (refs. 5 and 7). Figure 10 shows the maximum disturbance amplitude ratios calculated in the nose, midchord, and aft upper surface regions. The results shown are from the envelope method which represents the N_{max} variation with frequency (f) or normalized wavelength (λ/c) in each region of the airfoil. In general, the crossflow growth disturbances dominate and the most amplified were found for $f = 0$. Upper-surface T-S waves are optimized by stabilizing the boundary layer, particularly upstream, through the use of higher suction rates followed by progressively weaker downstream suction rates. Therefore, increased level and corresponding trends in the required suction coefficient with x/c occur with increasing R . Compressibility effects (ref. 5) are seen to significantly reduce N_{max} in the different airfoil regions with subsequent reduced suction requirements, indicating that the incompressible calculations were conservative.



- | <u>NOSE REGION</u> | <u>MID-CHORD REGION</u> | <u>AFT REGION</u> |
|--|--|---|
| <ul style="list-style-type: none"> - CROSSFLOW INSTABILITY - STATIONARY DISTURB. ($f=0$) - $0 \leq \sqrt{Re_x} \leq 1600$ - 15% DECREASE IN N_{max} | <ul style="list-style-type: none"> - T-S INSTABILITY - $0 \leq \sqrt{Re_x} \leq 3300$ - 40% DECREASE IN N_{max} | <ul style="list-style-type: none"> - CROSSFLOW INSTABILITY - STATIONARY DISTURB. ($f=0$) - $\sqrt{Re_x} \geq 3900$ - 15% DECREASE IN N_{max} |

Figure 10

MAXIMUM DISTURBANCE AMPLITUDE RATIO ($N = \ln a/a_0$)
 SWEEPED LFC AIRFOIL LOWER SURFACE DESIGN

In comparison with the upper-surface stability analysis, figure 11 shows the maximum disturbance amplitude ratio with frequency or normalized wavelength for the nose, midchord, and aft lower surface regions. The linearized incompressible stability results again indicate that boundary-layer crossflow in the forward and aft concave surface regions is more difficult to control, especially in the rear. However, laminarization of the LFC airfoil lower surface strongly depends on the feasibility and suction control of the more dominating centrifugal Taylor-Goertler-type instability in the concave surface regions which may cause transition.

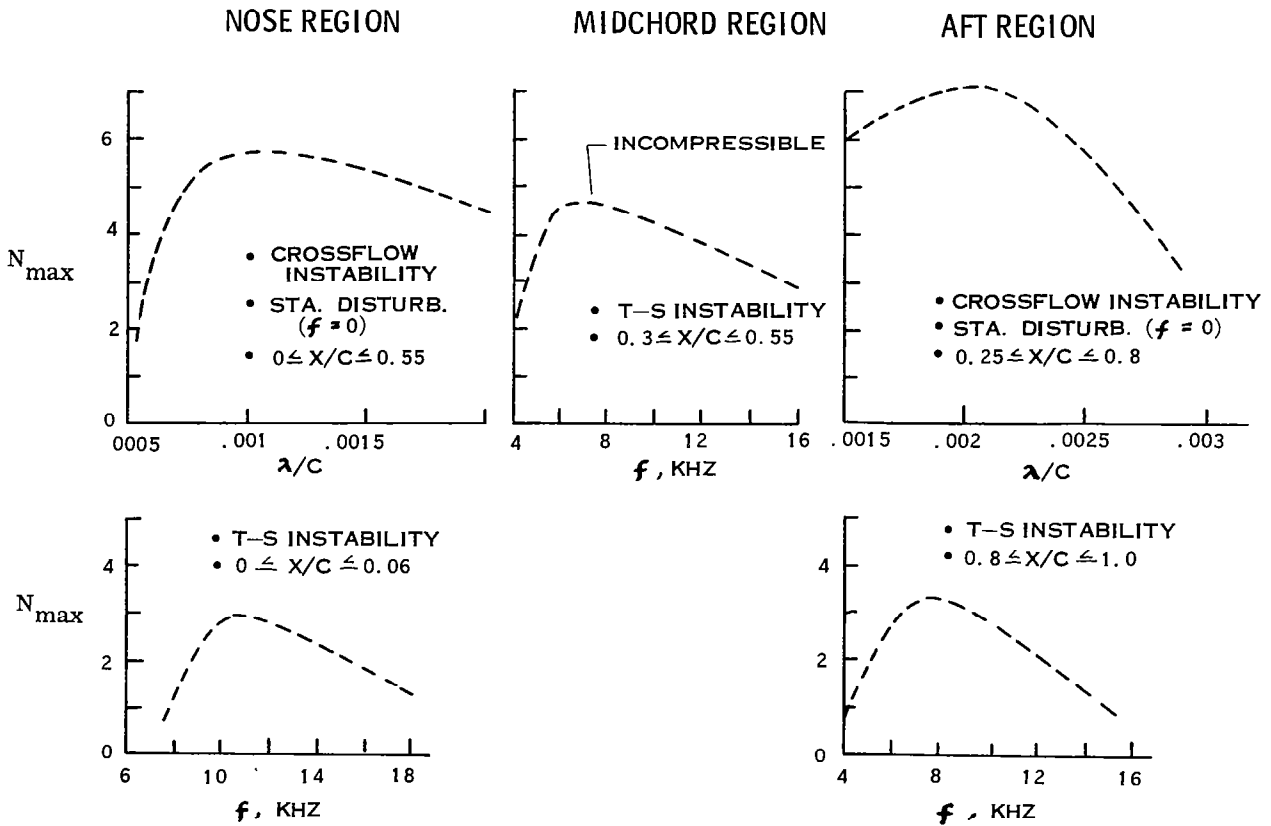


Figure 11

LINEARIZED MAXIMUM GROWTH FACTOR B OF TAYLOR-GOERTLER
VORTICES VERSUS GOERTLER PARAMETER G FOR INCOMPRESSIBLE
FLOW WITH/WITHOUT SUCTION

Results from linearized analysis (refs. 10 and 11) of the T-G instability with and without asymptotic area suction were used to determine amplification factors for the LFC airfoil lower concave surface regions. Figure 12 shows the variation of the linearized maximum growth factor B with Goertler number G for disturbances with and without suction. Suction pulls the T-G vortices closer towards the wall where stronger viscous forces tend to damp their growth. Values of B are evaluated between the theoretical boundaries shown and calculated values of G based on airfoil radius of surface curvature r and R_θ from boundary-layer analysis. These values are then used to obtain the T-G vortex growth rate in the concave regions.

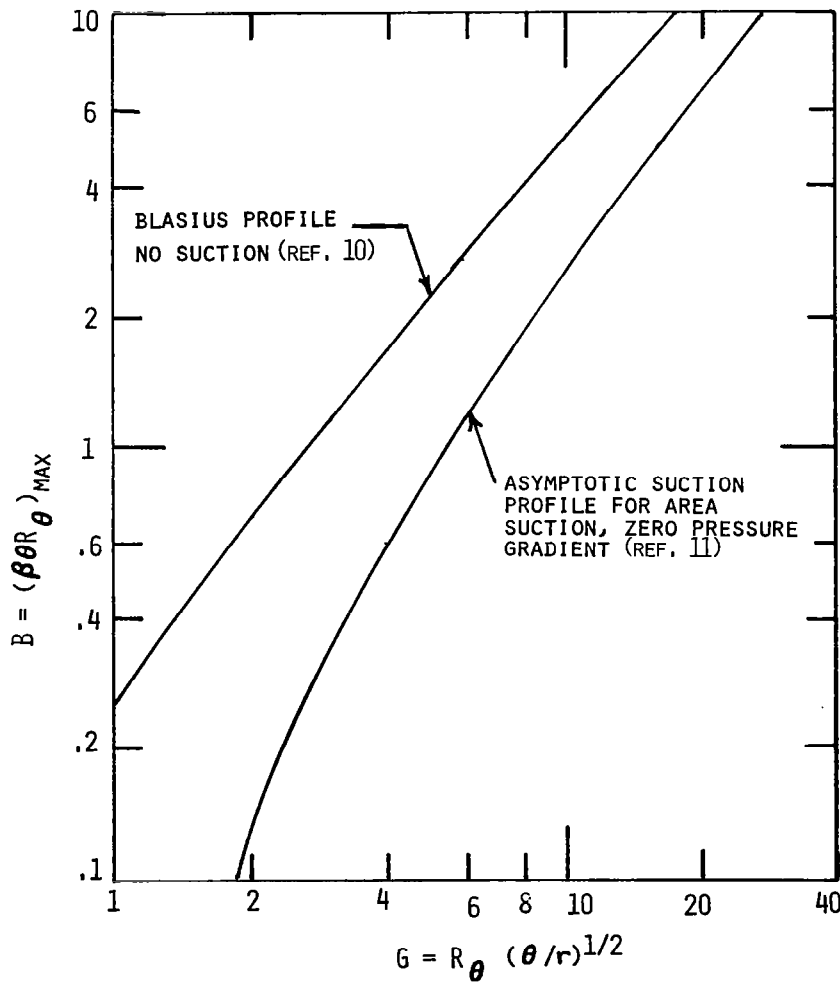


Figure 12

MAXIMUM DISTURBANCE AMPLITUDE RATIO N_{max} FOR TAYLOR-GOERTLER
VORTICES AND FLOW TURN INCREMENT, LFC AIRFOIL LOWER-SURFACE DESIGN

In principle, turning of the flow in the concave curvature region through several "corner" locations was analyzed instead of the usual gradual turn over a larger chordwise distance. Figure 13 shows representative values of N_{max} with incremental turn of the flow, $\Delta x/c$, for the Blasius and asymptotic suction amplification factors previously discussed and evaluated for the LFC airfoil. The insert illustrates typical variations of the normalized curvature c/r with x/c for several possible increments of turn. Even though the Goertler number G and local growth rate B of the T-G vortices with a rapid turn and small r are large, the integrated growth rate N_{max} decreases with decreasing radius of surface curvature due to shorter turns within the concave regions. Since the flow usually decelerates approaching the concave "corner" regions, local suction is required for stability of the mean boundary layer. Values of $N_{max} \approx 2.5$ to 4 in the front and near-concave regions have been applied based on the described approach.

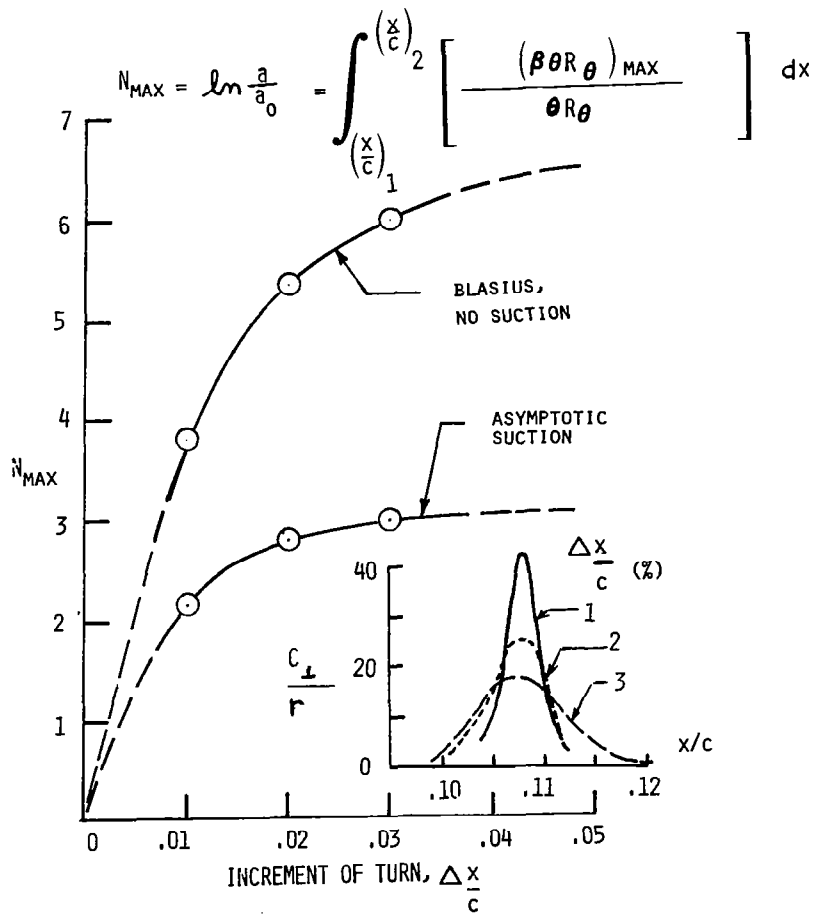


Figure 13

LFC AIRFOIL CHORDWISE SUCTION REQUIREMENTS FOR CHORD REYNOLDS NUMBER RANGE

Evaluation of the optimum suction rates required to avoid premature transition on the swept LFC airfoil was based on the conservative linearized incompressible stability calculations previously discussed for amplified boundary-layer disturbances. Figure 14 shows the chordwise suction quantity coefficient (C_Q) over the LFC airfoil upper and lower surface test region for several chord Reynolds numbers. Results shown are based on local growth rates of e^5 to e^7 for crossflow and T-S boundary layer disturbances and $e^{2.5}$ to e^4 for T-G disturbances. Suction is eliminated in the nose region for moderately high Reynolds numbers in contrast to that required for blunt noses. Suction extends to 97% chord on the upper and 84% on the lower surface; respectively. Increased suction is required in the upper aft pressure rise region and decelerated flow regions of the lower surface concave regions.

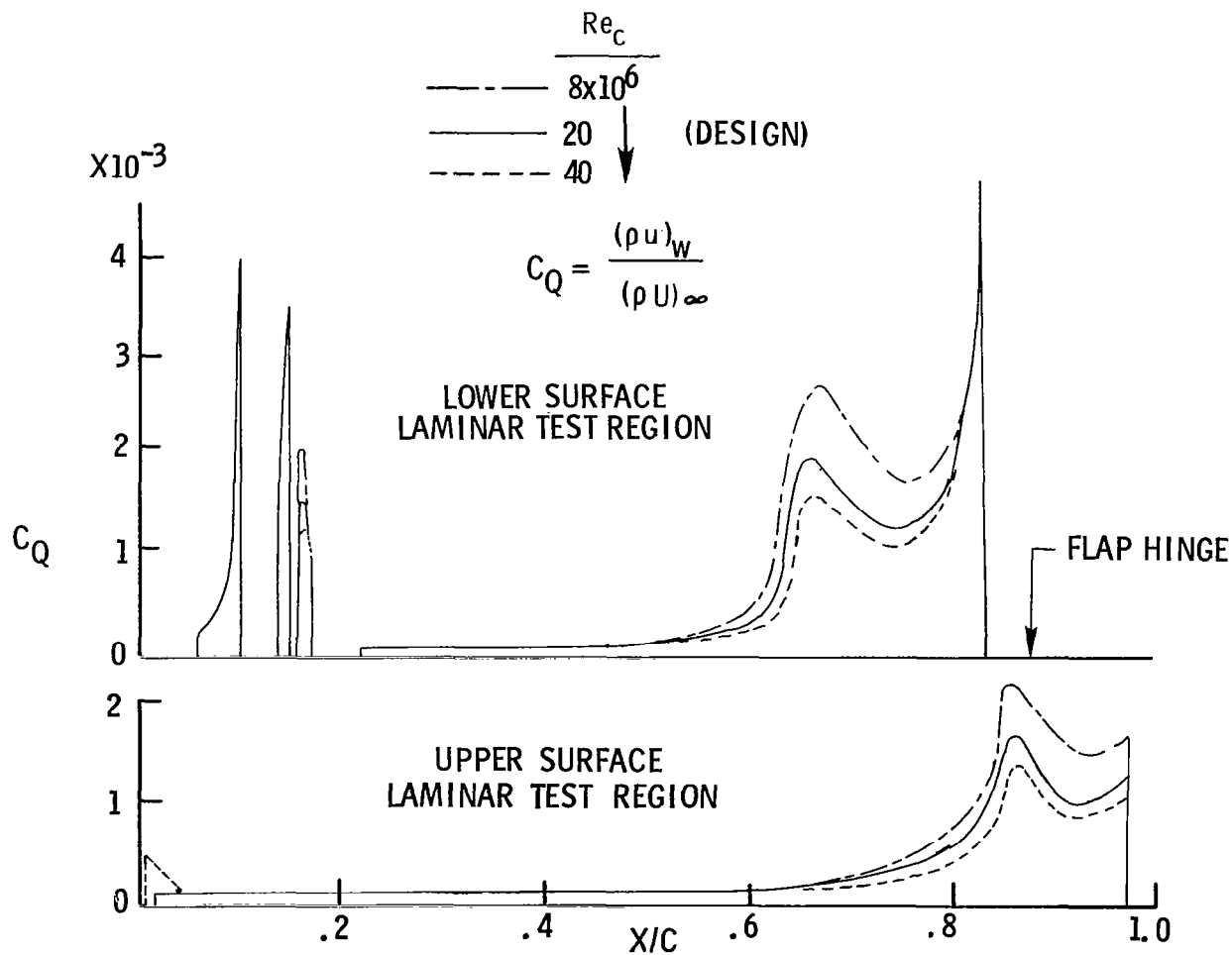


Figure 14

SPAN/CHORDWISE VARIATION OF LFC AIRFOIL UPPER AND LOWER SURFACE
LAMINAR AND TURBULENT ZONE DESIGN SUCTION DISTRIBUTION - PLAN VIEW

The oncoming tunnel wall boundary layer develops a turbulent wedge over the airfoil surface near the wall juncture, requiring suction control to insure achievement of a full-chord laminar test region. Thus, the LFC airfoil is designed with separate suction control of the upper and lower surface laminar test regions from the spanwise turbulent wedge zones. Figure 15 shows the upper and lower surface plan view of the design spanwise suction distribution at several chordwise stations. Considering the LFC airfoil volume limitations, maximum design values of the turbulent zone suction rates are indicated in terms of multiples of the corresponding laminar test zone rates and x/c locations. A 2-D boundary layer analysis (ref. 12) was conducted to evaluate the turbulent-zone suction rates required to avoid flow separation. In general, the required laminar-zone suction rates extend the full span and chordwise to $x/c = 0.6$ on the upper end and to $x/c = 0.2$ on the lower surface before increased suction is required above the laminar values with further chordwise-spanwise distance to avoid flow separation and loss of lift without further flap deflection control. On both surfaces, the laminar rates extend into the turbulent zone before increasing rapidly to the required level for control. In either the upper or lower surface turbulent zones, the plenum metering holes were selected by gradually spacing the holes closer together approaching the end of the ducts next to the walls.

SPAN/CHORDWISE VARIATION OF LFC AIRFOIL UPPER SURFACE LAMINAR AND TURBULENT ZONE DESIGN SUCTION DISTRIBUTION (PLAN VIEW)

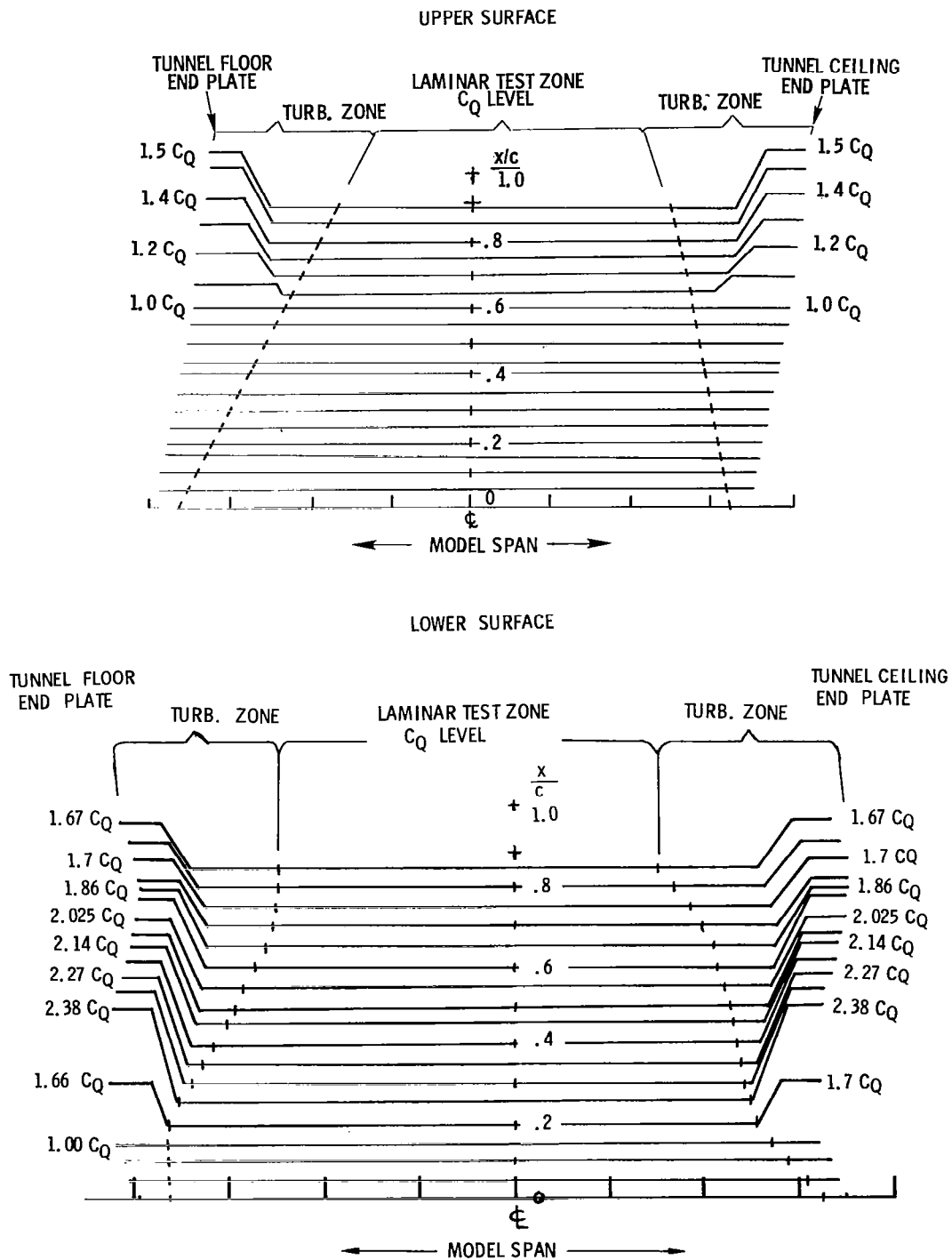
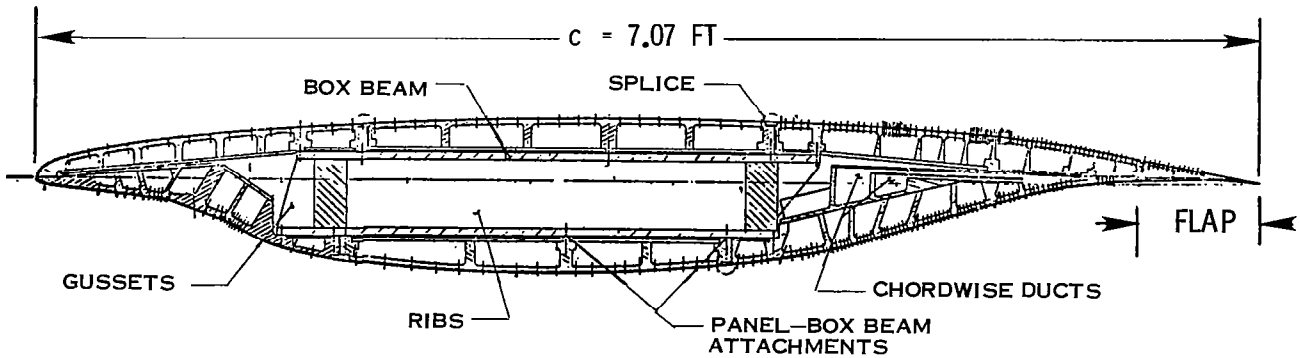


Figure 15

LFC EXPERIMENT DESIGN CONSIDERATIONS

Figure 16 is a cross-section view of the 7-ft chord model at mid-span including the design point conditions. Structural features of the model include three separate upper and lower surface suction panels that attach at the front and rear box beam assembly. A trailing edge flap (spanwise segmented) extends over the last 10% chord. Suction air is removed through closely spaced fine slots and ducts extending spanwise. A discussion of the fabrication design features will be presented subsequently.



MODEL DESIGN POINT

$$M_{\infty} = 0.82, M_{0_{\perp}} = 0.755$$

$$Re_c = 20 \times 10^6$$

$$c = 7.07', \Lambda = 23^{\circ}$$

$$(t/c)_{\perp} = 13.0\%$$

$$(C_{L_{\perp}}) = 0.55$$

$$FLAPCHORD = 10.9\%$$

Figure 16

PHOTOGRAPH OF LFC AIRFOIL UPPER
SURFACE SUCTION PANEL ASSEMBLY

Figure 17 shows a typical fit-check assembly of the three completed upper surface suction panels for the LFC airfoil. The panels have been skin-bonded, slots sawed, and internal ducting, plenums, and metering holes machined. The external surface has been polished and Tufram-coated for smoothness and hardness finish.

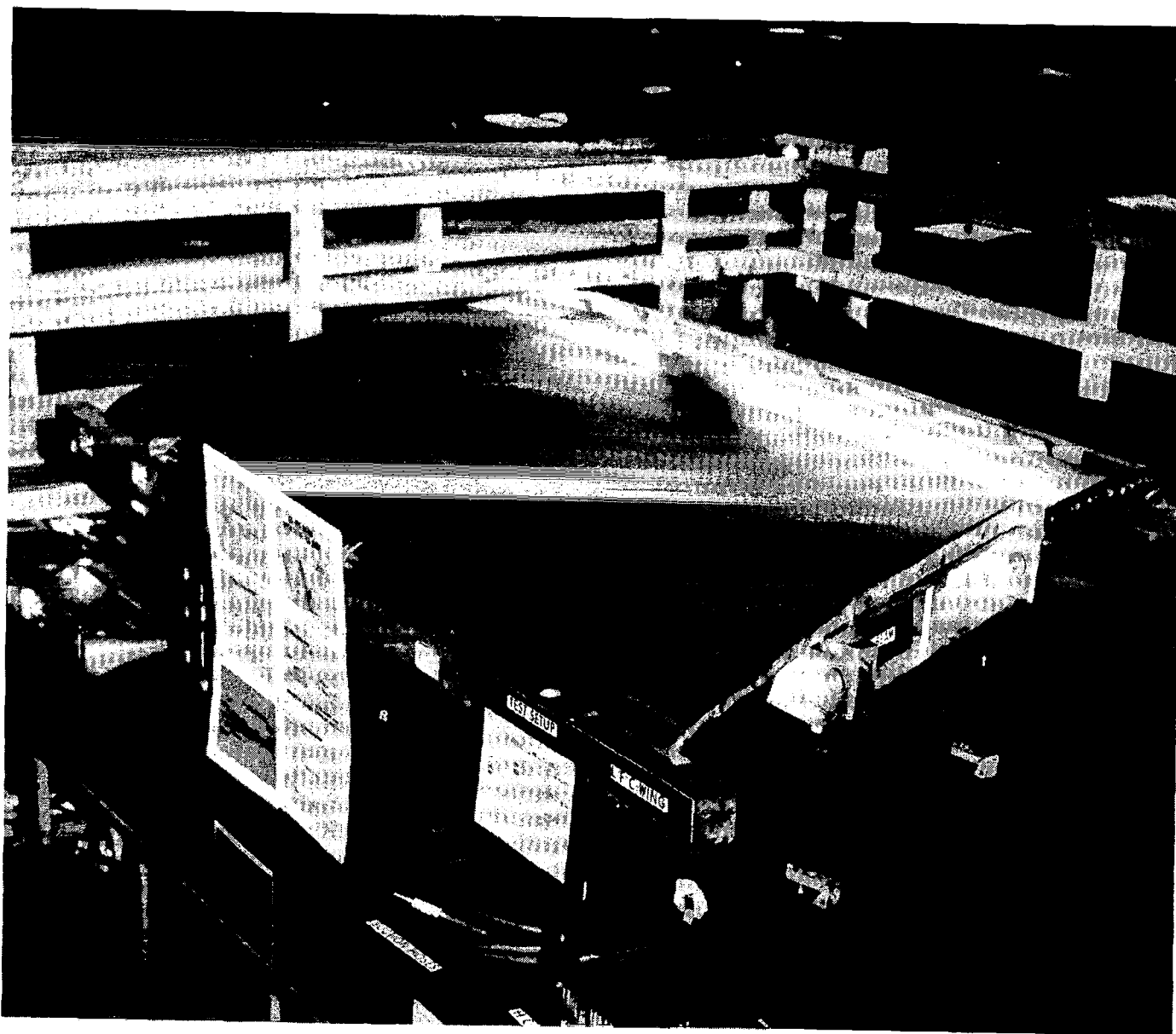


Figure 17

DOUGLAS STRUCTURAL CONCEPT

Alternate upper surface porous suction panels are being designed and fabricated for testing on the current LFC airfoil model. Figure 18 illustrates the ACEE-contracted Douglas concept which contains a suction surface constructed of electron beam drilled titanium. Hole spacing and geometry are indicated representing the asymptotic approach to area suction for comparison with the discrete slot suction approach. The EB-drilled holes form diffuser shaped flow passages that are expected to provide required pressure drop and ease of maintenance.

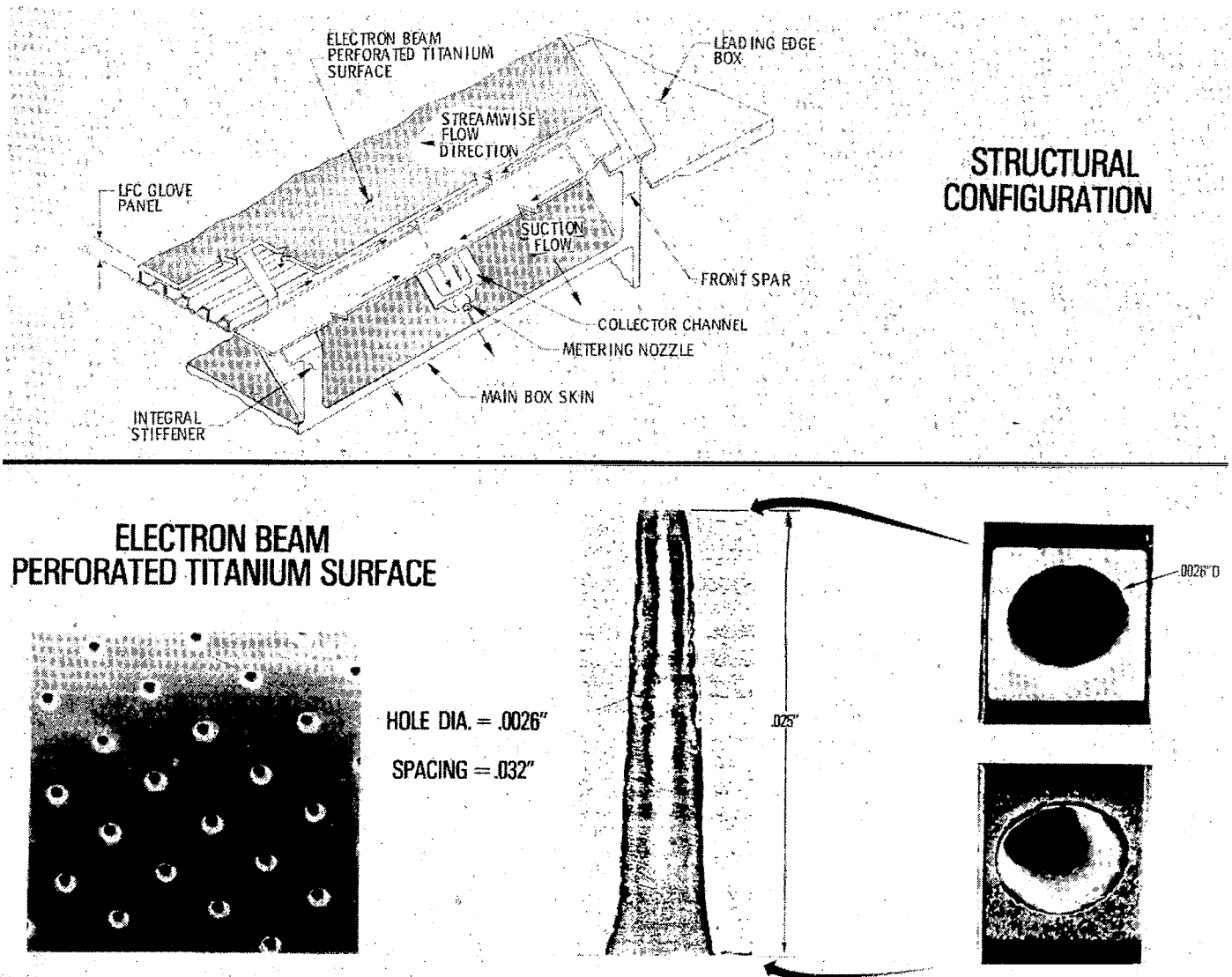


Figure 18

ESTIMATED VARIATION OF EQUIVALENT SUPERCRITICAL LFC WING PROFILE DRAG WITH REYNOLDS NUMBER

Of major importance is the achievement of lowering profile drag for the swept supercritical LFC airfoil. The total equivalent drag of an LFC wing is $C_d = C_{d_s} + C_{d_w}$. The suction drag was evaluated from the suction power required to reaccelerate the suction air to undisturbed velocity. The previously discussed variation of C_Q vs x/c for a range of Re_c was used as input. The wake drag was evaluated from theoretical values calculated for the LFC airfoil and based on momentum considerations for a swept wing according to Raetz (ref. 13). The total profile drag, C_d , for the upper and lower surfaces combined of the LFC airfoil is shown in figure 19 as compared to an equivalent laminar flat plate. The profile drag decreases with increasing Re_c primarily as a result of the corresponding reduced C_Q requirement and sweep angle. The estimated $C_d = 0.001$, with full-chord LFC is considerably smaller than for an equivalent turbulent airfoil of $C_d \approx 0.007$. These estimated results compare favorably with measured values for a single surface on previous LFC wings (refs. 14 and 15).

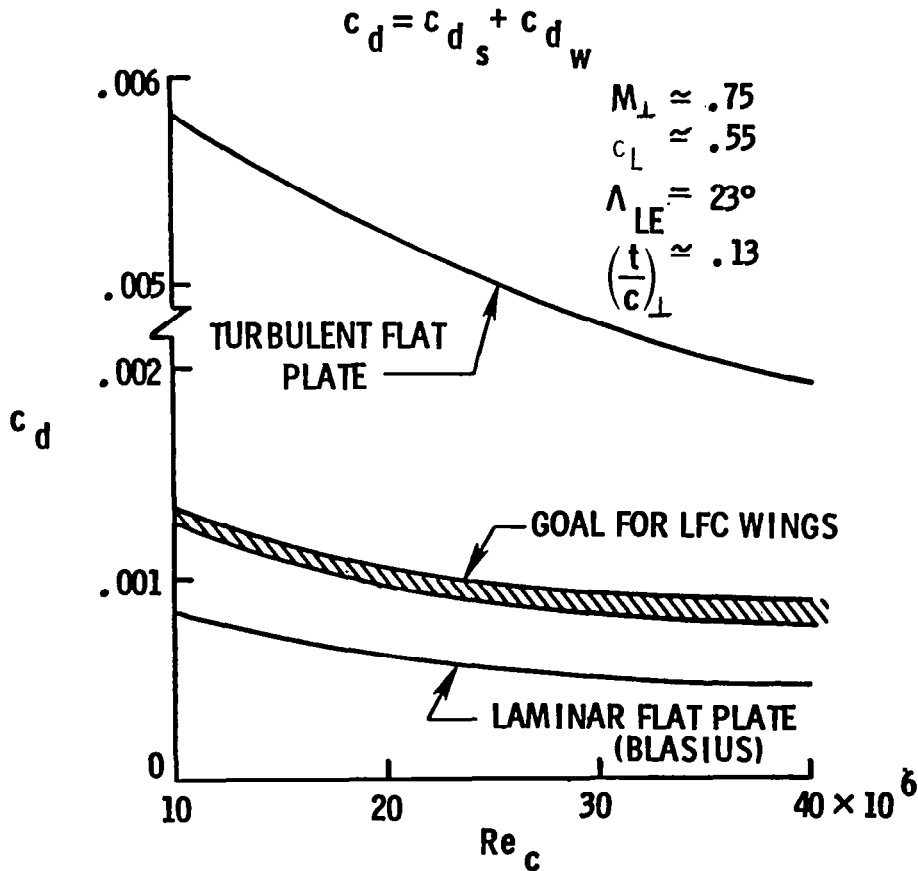


Figure 19

LFC AIRFOIL SEGMENTS OF SUCTION SYSTEM

Figure 20 shows details of the LFC airfoil surface and internal suction system for leading edge and trailing edge flap segments. Utilizing the calculated suction requirements, the LFC airfoil upper and lower surface slot widths, spacing, and internal suction airflow metering system were designed allowing for a 50% off-design suction increase capability. This system provides removal of local boundary layer air through discrete spanwise slots and metering holes located in plenums beneath each slot. Suction airflow from several chordwise slot-plenums is collected by spanwise ducts having constant cross-section with circular or 2-D suction nozzles located at the ends. The suction ducts were designed on the criterion of minimizing pressure variation along duct length (spanwise duct length, $l \sim b/\cos \Lambda$) by accounting for momentum and friction forces. Significant features are that the design maximum duct velocity, except for the extreme rearward ducts, is less than 50 ft/sec, where the normalized velocity varies as

$$\frac{U_{\text{DUCT}}}{U_{\infty}} \sim \frac{M^{3/2}}{C^{3/2} \cos^{5/2} \Lambda}$$

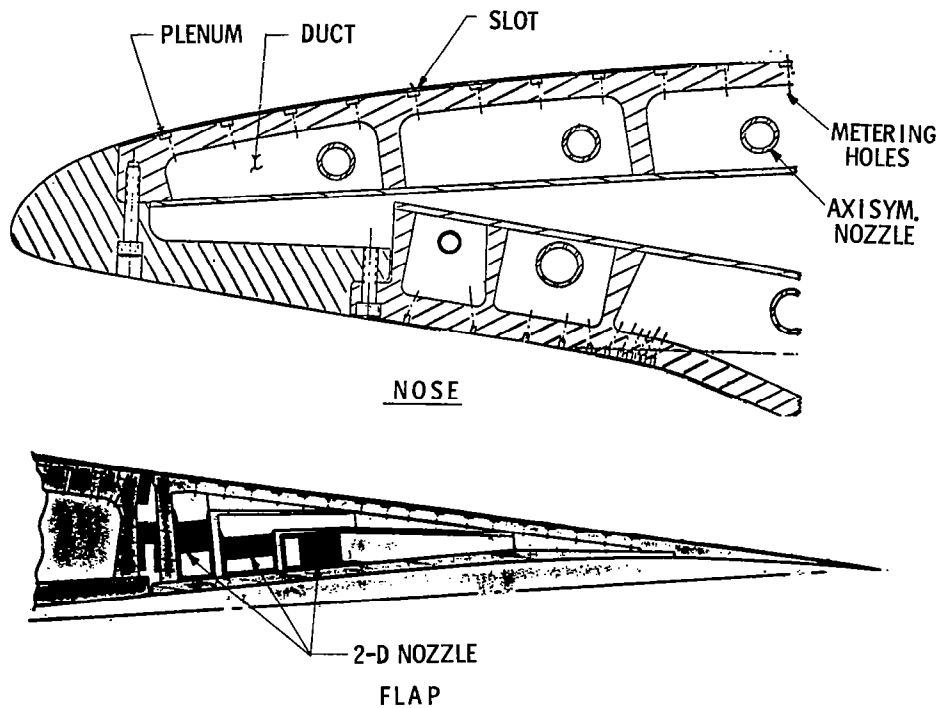


Figure 20

SLOT DESIGN EQUATIONS/CRITERIA

The equations used for slot spacing Δc_n and sucked height z were derived by equating the suction flow rate at the surface to the flow rate within the slot based on the approach of Pfenninger (ref. 15), as shown in figure 21. In general, z should be near unity, the pressure drop through the slot must be compatible with metering and duct pressure level, and the slot spacing Reynolds number should necessarily be limited to small values. For the LFC airfoil, maximum pressure drop through the plenum metering holes was limited to about 2% of the free stream dynamic pressure to avoid backflow oscillations through the slots. The equations show the effect on slot design of a constant chord wing and unit Reynolds number condition. For example, the factor $(c^{1/2}/R_\infty^{3/4})$ in the expression for z along with the relation between z and s indicate that slot widths on a typical LFC transport wing would be several times greater than the present LFC airfoil slot widths.

SLOT SPACING Δc_n AND WIDTH s

$$\rightarrow \Delta c_n = \frac{\mu_s Re_s \sqrt{c}}{\mu_\infty F_o^* \sqrt{R_\infty}} \sim \frac{Re_s}{\frac{U_s/\nu_s}{U_\infty/\nu_\infty}}$$

WHERE $F_o^* = \frac{\mu_s V_0}{\mu_\infty U_\infty} \sqrt{R_c}$

$R_\infty =$ UNIT REYNOLDS NO.

$$1.3 \lesssim s/z \lesssim 1.4$$

$$\nu = \frac{\mu}{\rho}$$

SLOT DEPTH H

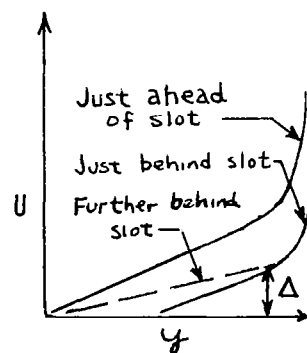
$$\frac{s}{H} \lesssim 0.4$$

SUCKED HEIGHT z

$$z \cong \left(\frac{2F_o^* \Delta c_n}{\Delta R_\infty} \right)^{\frac{1}{2}} = \left(\frac{2\mu_s Re_s}{\Delta\mu_\infty} \right)^{\frac{1}{2}} \frac{c^{\frac{1}{4}}}{R_\infty^{3/4}}$$

WHERE $\Delta =$ SLOPE OF NON-DIMENSIONAL BOUNDARY LAYER VELOCITY PROFILE

$$= (\text{CONST.}) \sqrt{\nu \frac{\Delta x}{U}}$$



$y_{\text{CRIT.}} \approx 0.2\delta$ (HEIGHT OF CRITICAL LAYER)

$z_{\text{CRIT.}} \lesssim 0.3Y_c$

Figure 21

CRITICAL SLOT REYNOLDS NUMBER AND SLOT-PLENUM
GOEMETRY FOR LFC AIRFOILS

In principle, criteria for slot design are the slot Reynolds number Re_s , the sucked height ratio z , the slot pressure drop coefficient, and Reynolds number based on slot spacing. Figure 22 shows experimental limits for the variation of the plenum height to slot width ratio, h/s , with slot Reynolds number for several limiting metering hole geometries beneath the slot. In general, Re_s should be small as practical considerations permit to avoid viscous slot wake flow oscillations. Results indicate that very shallow plenums for constant slot width are required for design at high values of Re_s , which may cause practical fabrication and maintenance problems. The LFC airfoil design criteria are indicated by the hatched region for $10 \leq h/s \leq 20$ and $Re_s \leq 150$ and are compatible with previous criteria (refs. 1, 14, 15).

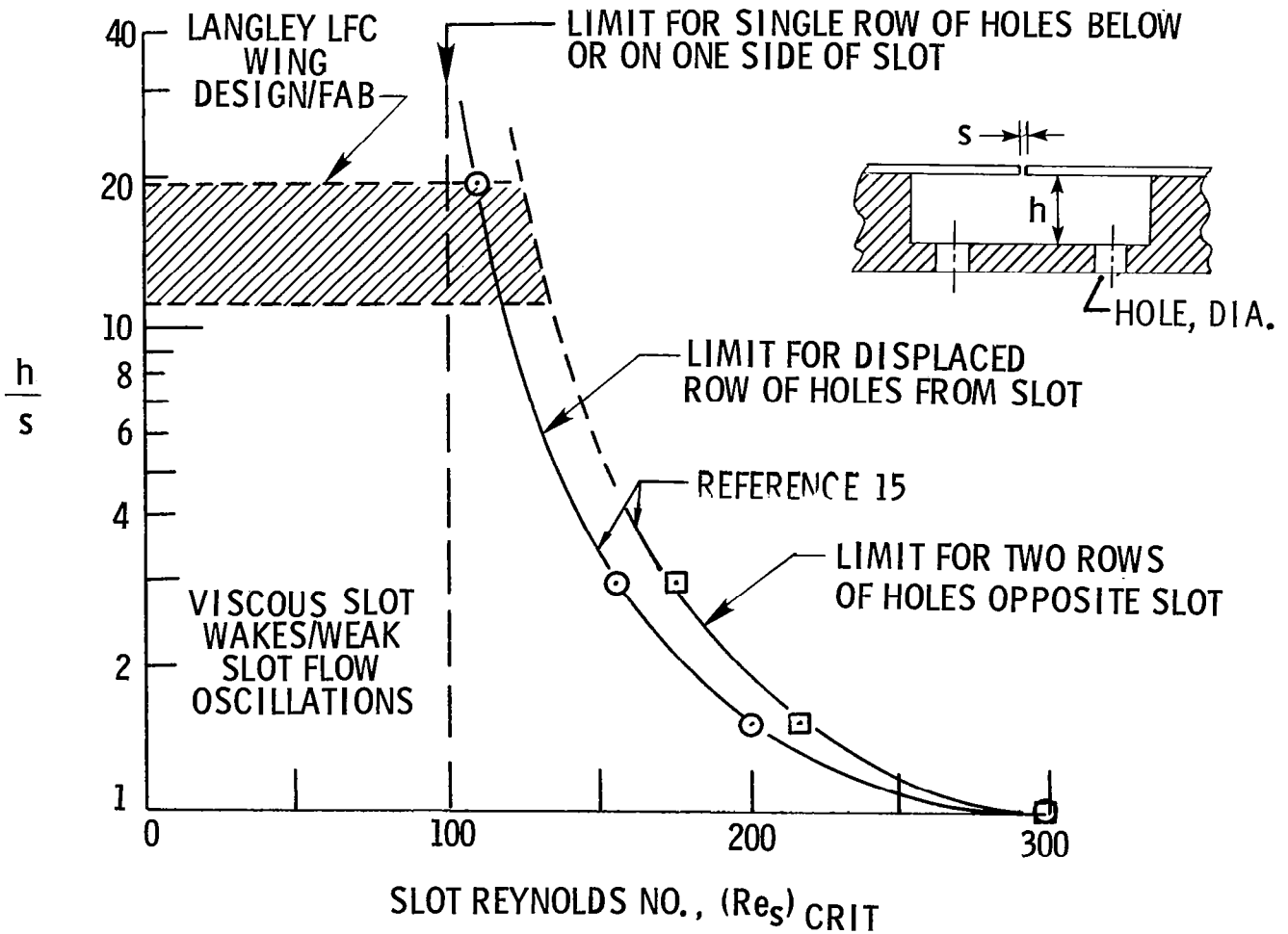


Figure 22

SKETCH OF LFC AIRFOIL SUCTION DUCT AND NOZZLES

Figure 23 illustrates the LFC airfoil internal suction ducting and nozzle layout in the chordwise and spanwise directions. The laminar test region suction ducting is separated from the turbulent zone ducting by a chordwise bulkhead for individual duct and zone control. Penetration holes in the model bulkheads for nozzles, orifice tubes, and leads are sealed to prevent leakage of flow between related turbulent and laminar spanwise ducts. An access panel seals the complete internal surface of each panel. To insure that low velocities are maintained in a given laminar test region duct, a nozzle has been placed at each duct end where required. Also shown are typical connecting suction hoses and couplings that extend from each nozzle exit through either the tunnel floor or ceiling to the suction airflow control boxes. Hose has been sized and selected such that the cross-sectional area over its length does not change within 2% at $\max \Delta p = 1.51$ to minimize both duct and hose pressure oscillations.

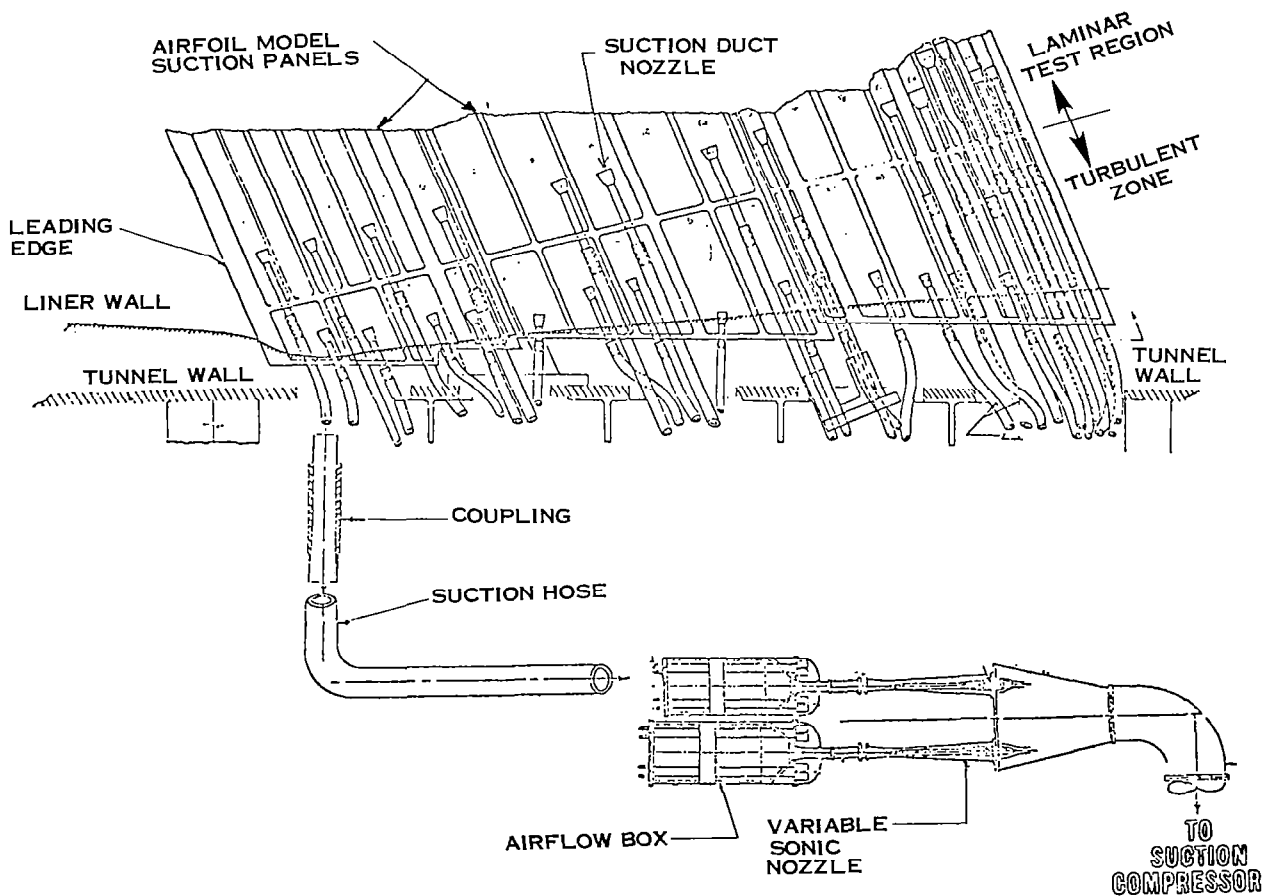


Figure 23

SKETCH OF LFC AIRFOIL SUCTION DUCT NOZZLES

Consideration of volume limitations of the LFC airfoil model and requirements for maintaining very low duct velocities necessarily resulted in the design and application of both circular and 2-D suction duct nozzles to remove and measure the suction flow rates. Figure 24 shows sketches of both nozzle types. The circular nozzles provide a smooth inlet flow followed by a straight section beginning at 2 throat diameters downstream of the lip. The 2-D nozzles were designed with half-height, $h/2$, and followed by a transition section from rectangular to circular. The nozzle half-height and width vary depending on duct dimensions in which they are installed. The nozzle sizes were designed based on limiting maximum flow velocity of 250 ft/sec to avoid choking and duct pressure oscillations. All nozzles have been calibrated for flow coefficient variation with Reynolds number based on diameter to determine flow rates during LFC testing. Each duct and nozzle throat contains a static pressure port to measure the nozzle-duct differential pressure to be used in the following expression, along with the calibrated nozzle flow coefficient to evaluate mass flow rate.

$$\dot{Q} = \frac{\alpha_n \frac{\pi D^2}{4} n \sqrt{\frac{\rho_{sd} \Delta \rho_n}{\rho_\infty q_\infty}}}{\sqrt{1 - \left(\frac{\pi D^2 n}{4 F}\right)^2}}$$

where $\Delta \rho_n = \rho_{sd} - \rho_n$ and $F =$ transverse duct area.

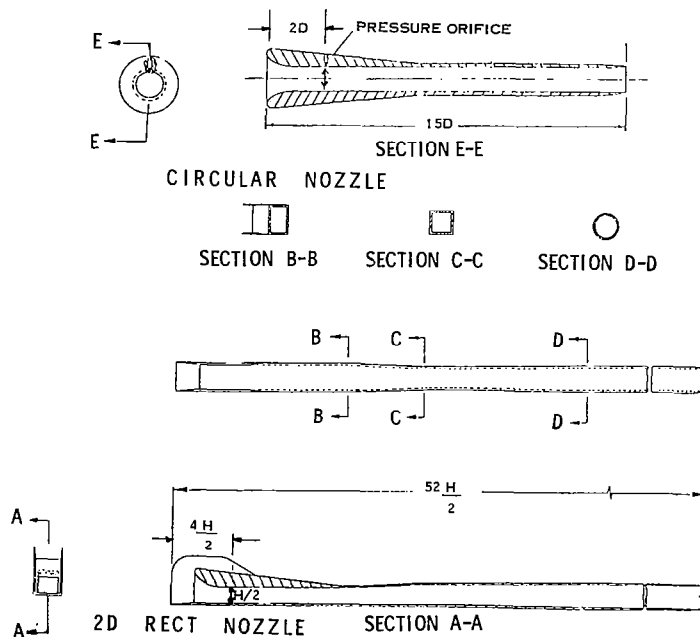


Figure 24

SKETCH OF LFC AIRFLOW CONTROL SYSTEM

The LFC airfoil suction-flow control is monitored by four suction boxes that are connected via hoses to the suction-ducting nozzles located in the model (fig. 25). The suction boxes contain arrays of motor-driven needle valves operated remotely for individual chordwise suction-ducting control on both surfaces of the airfoil. The individual suction boxes are connected downstream by variable sonic-flow nozzles which are provided for flow control to the suction compressor and feed-back noise control through the system. Operation of the suction boxes and drive motors is provided by a console located in the tunnel control room.

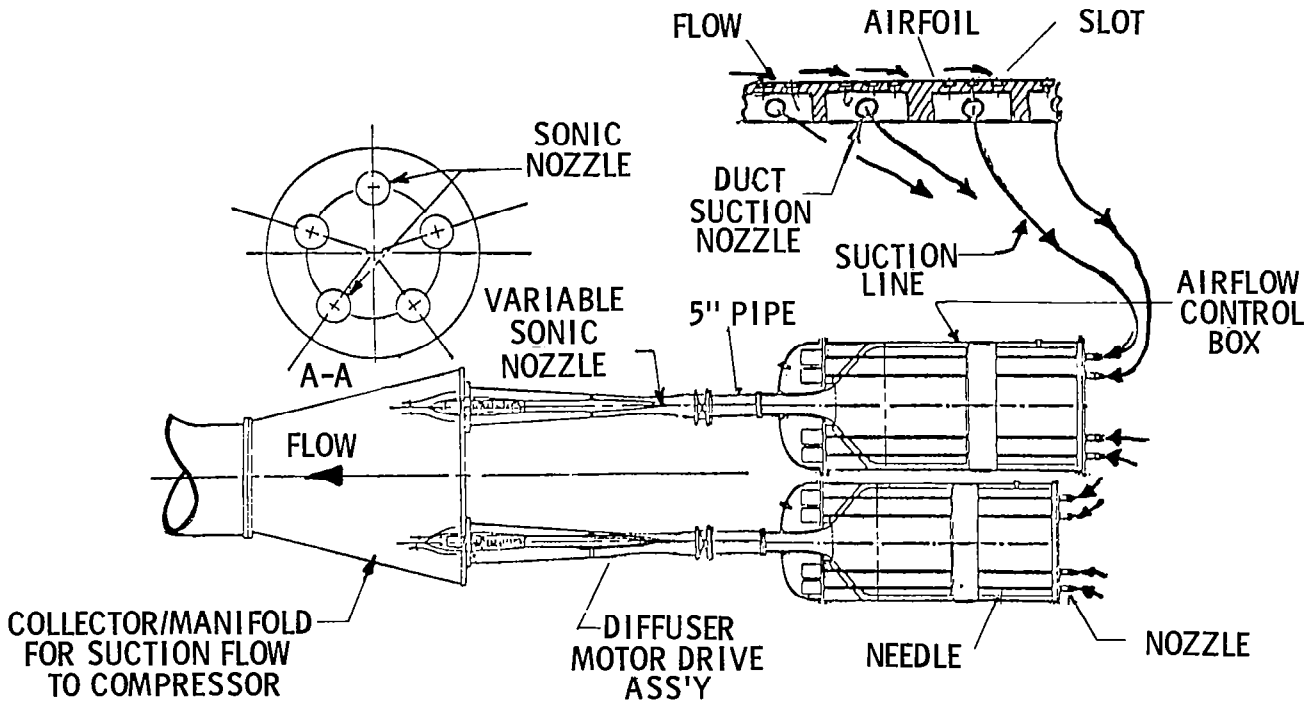


Figure 25

LFC AIRFLOW BOX ASSEMBLY

Details of the airflow control boxes for the LFC airfoil are shown in figure 26. Airflow from the individual suction duct-nozzle hoses enters the individual nozzles located at the box upstream end. Actuation of the needles in the box nozzles provides the control of suction airflow at the model. This is accomplished through 27 individual control mechanisms in each box. The boxes have been designed to maintain low velocity (~15 ft/sec) and contain a contraction section and noise damping devices (honeycomb and screen) to minimize disturbances at the needle-nozzle flow controls. The individual nozzles and associated needles have been designed for control for about 16% below design suction at low Reynolds number and 20% above design at the highest Reynolds numbers anticipated.

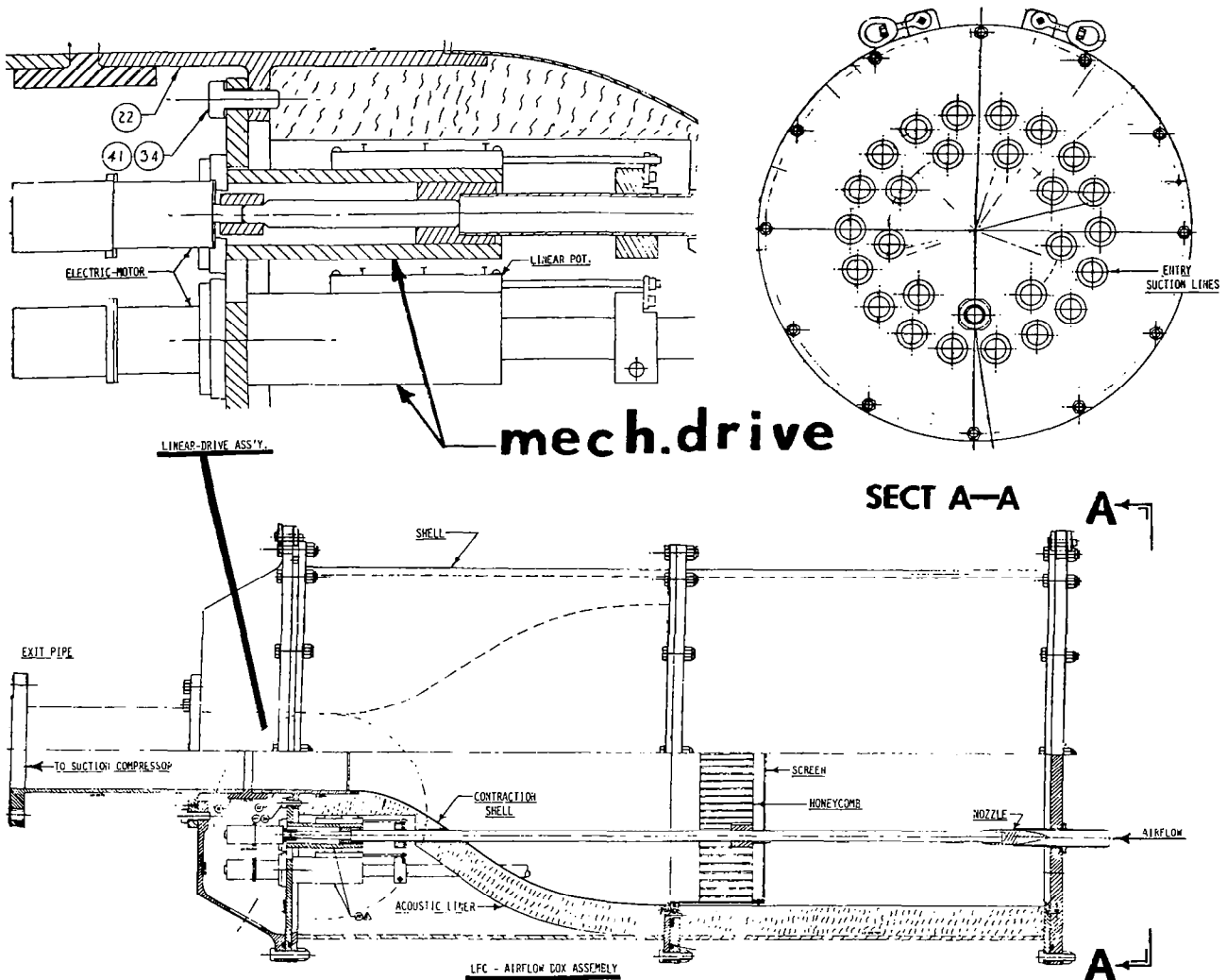


Figure 26

LFC VARIABLE SONIC NOZZLE ASSEMBLY

Figure 27 is a sketch of the sonic nozzles that are located just downstream of the individual suction control boxes. The nozzles provide for flow control to the suction compressor and feed back noise control through the system. In general, the sonic nozzles were designed based on the "sonic plug" principal and contain a motor-driven needle assembly very similar to those for the suction boxes. Sonic flow at the contraction is achieved by longitudinal adjustment of the needle with varying flow rates. The nozzle needle geometry and stroke are sized based on the suction box range of flow rates. The nozzle inlet is sized by the box exit piping. Exit flow from the sonic nozzles enters a collector manifold to the suction compressor.

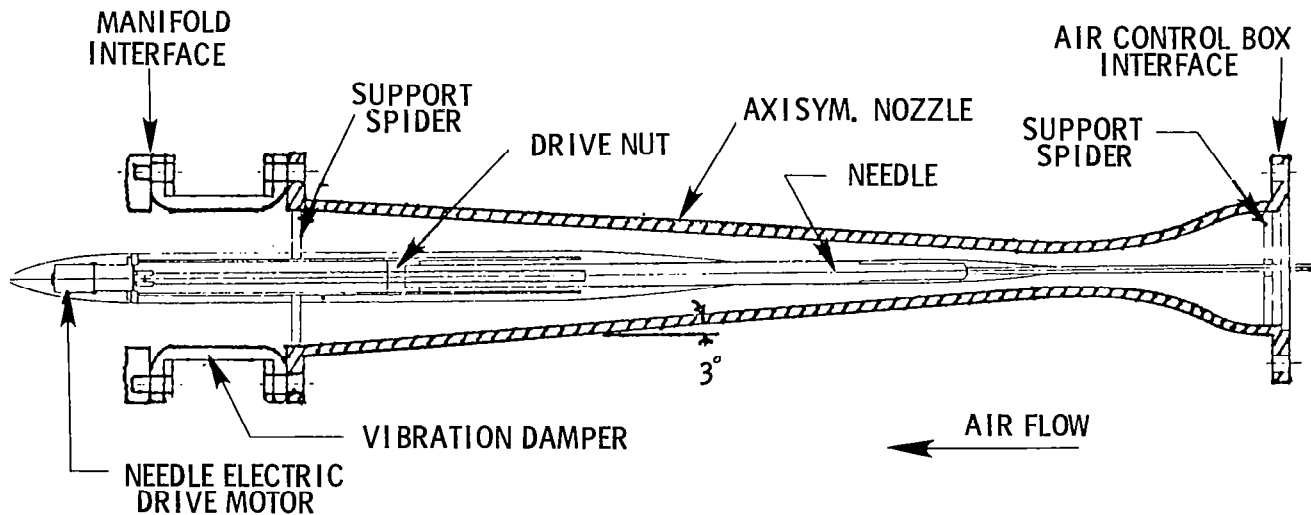


Figure 27

SKETCH OF LFC AIRFOIL SURFACE INSTRUMENTATION

Sketches of the LFC airfoil plan view with locations of the surface instrumentation are shown in figures 28(a) and 28(b) for the upper and lower surfaces, respectively. The solid dots are for static pressure orifices, open circles for thin-film gages and crosses for acoustic gages. A corresponding acoustic gage is located in the plenum opposite the indicated surface acoustic gages. The upper and lower surfaces contain a total of 300 orifices, 50 thin-films, and 26 acoustic.

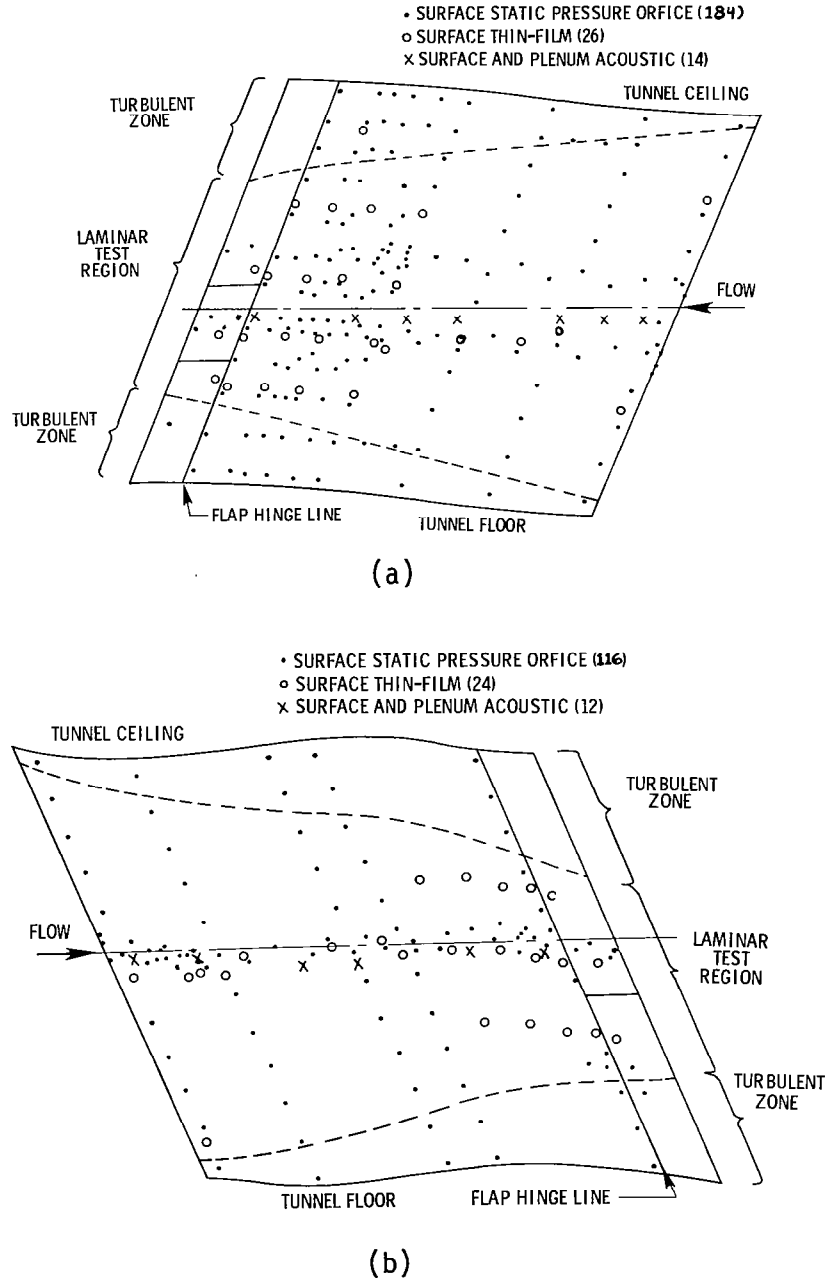


Figure 28

PERMISSIBLE AMPLITUDE RATIO h/λ OF MULTIPLE SPANWISE WAVES FOR FULL-CHORD LAMINAR FLOW ON SUPERCRITICAL AIRFOILS

Since the static pressure in the local supersonic zone of LFC airfoils varies proportional to the change in surface slope and to the Prandtl factor $(M^2 - 1)^{1/2}$ supercritical LFC airfoils may become particularly sensitive to surface waviness, especially for low supersonic Mach numbers with respect to sonic bubble. The possible adverse effects of critical waviness under such conditions may: (1) cause a decrease in local external pressure sufficient to induce outflow of suction air (2) change the pressure distribution such as to influence growth of boundary layer disturbance (3) generate a pressure wave that reflects to the airfoil surface from the sonic line and subsequent transition. Pfenninger (ref. 9) has performed some calculations of the effect of waviness on the pressure distribution over the Langley LFC airfoil with a 320-point inviscid Korn-Garabedian analysis. No known criterion exists for such supercritical LFC airfoils other than the analysis of Pfenninger (ref. 9) which arbitrarily introduces a local surface wave on the LFC airfoil by change of coordinates and subsequent pressure profile. Figure 29 shows the variation of permissible amplitude ratio h/λ for multiple spanwise waves on supercritical LFC airfoils as determined by the empirical expression derived from previously measured data (ref. 14) and represented by the solid lines at several Re_c 's. The dashed line represents the LFC airfoil fabrication goal based on Pfenninger's conservative analysis (ref. 9) and the symbols are from actual model upper surface measurements representing the worst case.

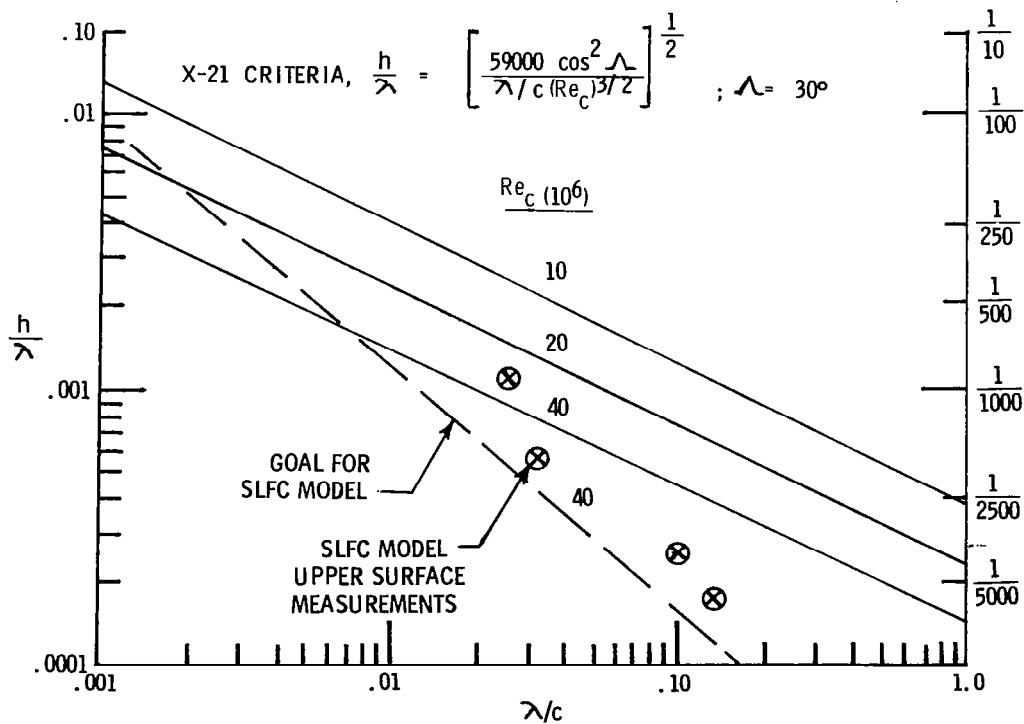


Figure 29

OUTLINE OF LINER DESIGN PROCEDURE

In order to produce a transonic wind-tunnel flow which simulates free-air flow about an infinite yawed wing, contouring of all nonporous boundary walls is required. The design procedure was developed and conducted by Perry Newman and Clay Anderson of NASA LaRC using several existing computation tools. Basically, the bounding streamlines in the desired flow field are determined in order to establish the inviscid test-section shape. The determined streamlines are then faired back into the existing tunnel walls. Then assessment is made of all viscous blockage corrections in the presence of the model pressure field and required suction control (fig. 30).

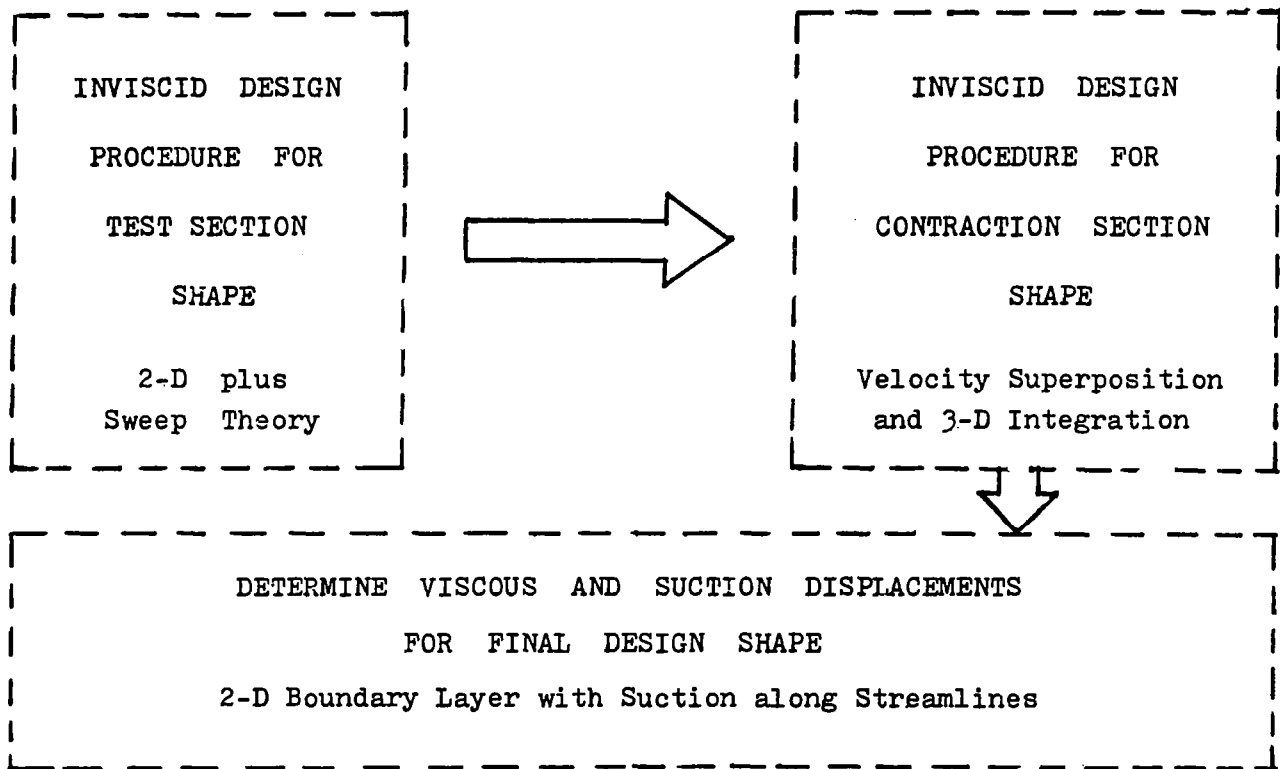


Figure 30

CALCULATED LINER CONTOURS AND SUPERCRITICAL FLOW NEAR MODEL

Many interactions were required of liner design procedure outlined previously in order to satisfy existing tunnel and flow, as well as other imposed constraints for the present liner. Figure 31 is a scaled illustration of the relative size of the LFC airfoil model, its embedded 3-D supersonic flow regions ($M > 1$), and the inviscid liner shape at the model. The contours shown are for the NASA LaRC 8-ft TPT wall liner and swept supercritical LFC model having the ratio of total tunnel height to chord of about unity.

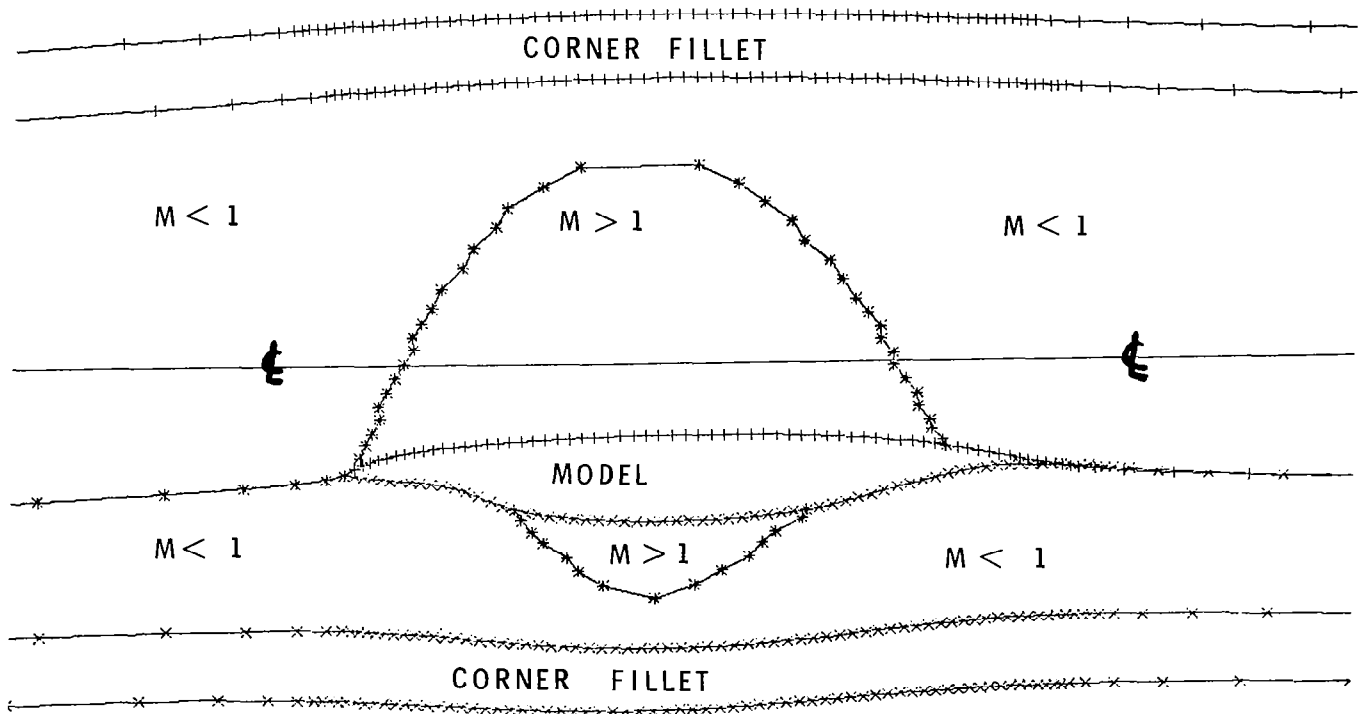


Figure 31

SCHMATIC OF CONTOURED LINER FOR LaRC 8-FT TPT

Figure 32 shows a side and top view of the 8-ft TPT LFC liner. The rapid contraction section shape changes from circular to rectangular with corner fillets and represents about 27% increase in the area ratio change. The increased tunnel liner contraction ratio and need for a wall choke at the downstream end of the test section lead to a very forward location of the model in the tunnel. The test-section liner contour extends downstream of the model and produces a smooth fairing into the existing diffuser by slowly changing the distorted liner cross-sectional shape streamwise. Streamlines for the swept LFC airfoil flow split at the leading edge and contact the upper and lower surfaces which are displaced from each other in the spanwise direction at the trailing edge. Thus the cross-sectional views shown illustrate steps (SHELF) in the liner floor and ceiling contour downstream of the model.

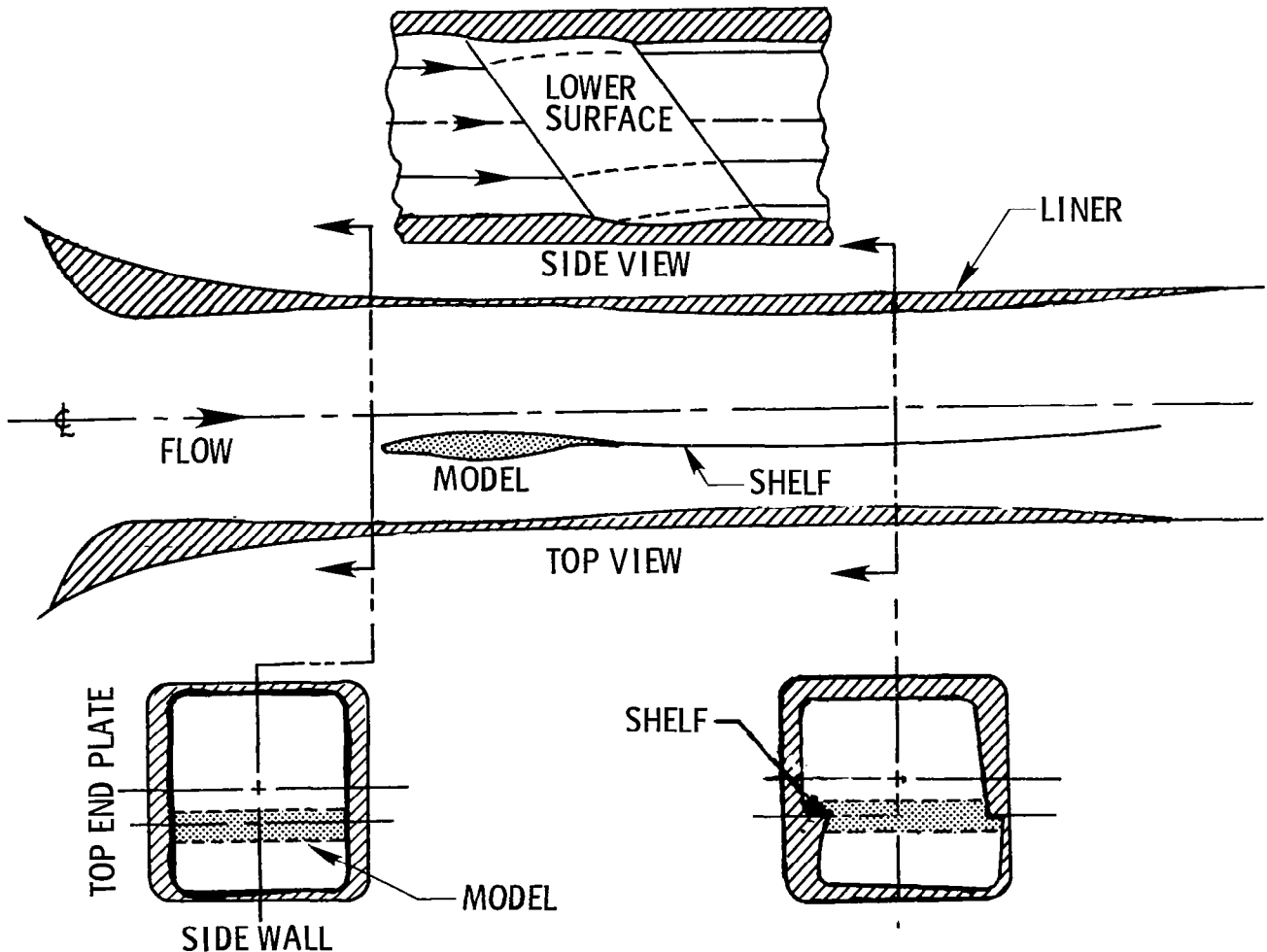


Figure 32

SUCTION DISTRIBUTION ON LINER ENDPLATE NEAR MODEL

Both viscous and suction displacement corrections were determined based on a 2-D stripwise analysis of the liner using a finite difference boundary-layer code (ref. 12) and in the presence of the model junctures and pressure field. Design suction levels were determined to prevent the liner turbulent wall boundary layer from separating in the juncture regions. Figure 33 shows a 3-D view of the calculated suction contours on the liner end walls above and below the LFC airfoil surface. The indicated contour lines are variations of the required suction coefficient C_Q , which peaks near the model forward and aft regions. Peak C_Q values shown occur on the liner wall opposite the model lower surface concave regions and then decrease away from the model.

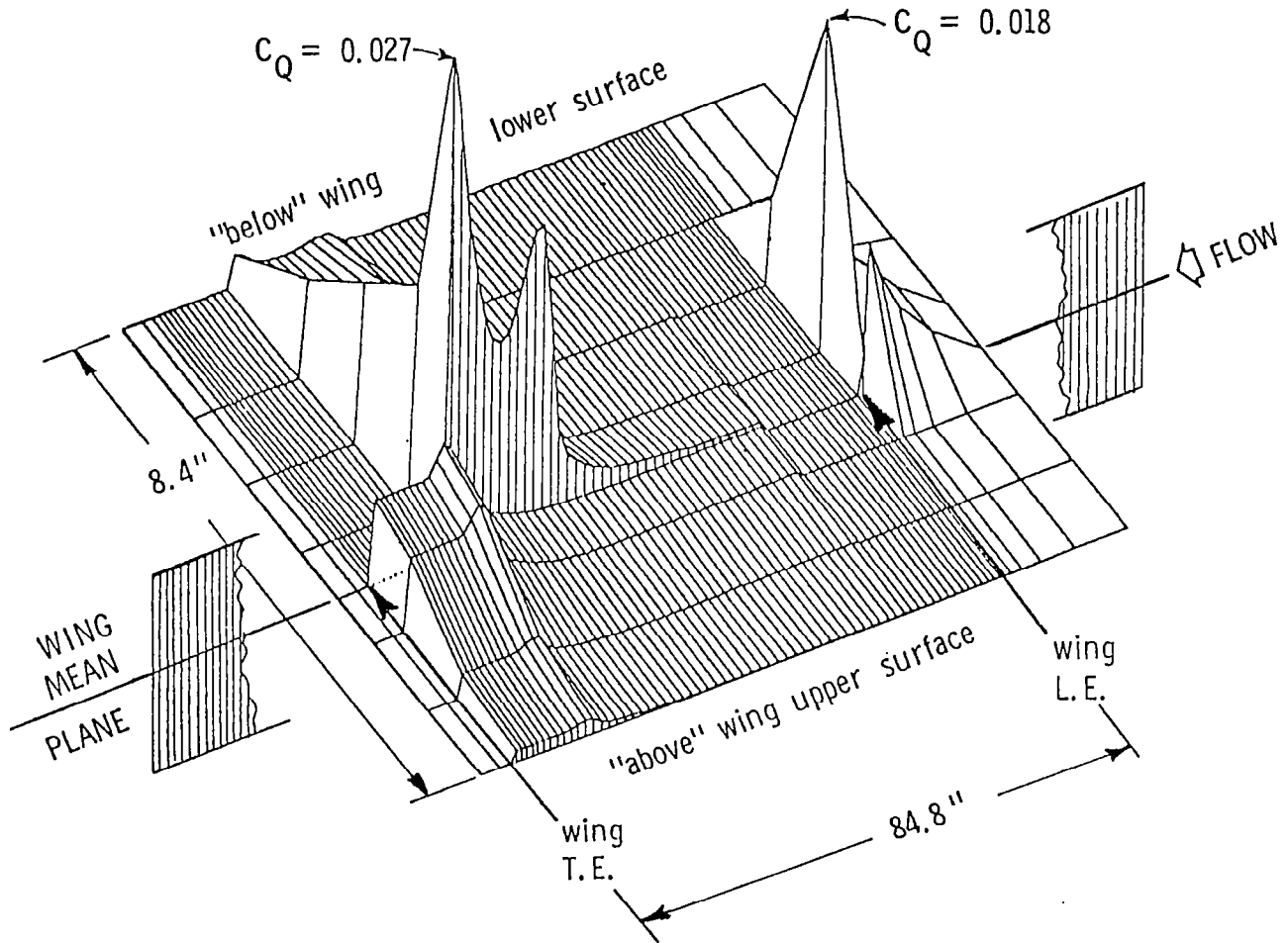


Figure 33

STREAMLINE LOCATION OF LINER WALL PRESSURE ORIFICES

Figure 34 illustrates the spatial location of static pressure orifices along theoretical streamlines determined for the LaRC 8-ft TPT wall liner contour. The indicated number and spacing of orifices along a given stream vary depending on whether the streamline was considered vital to the evaluation of the liner-model-choke performance during testing. Extent of orifice locations includes the upstream nozzle contraction section around the LFC airfoil model, downstream choke and diffuser. A total of 1016 orifices are on all four walls.

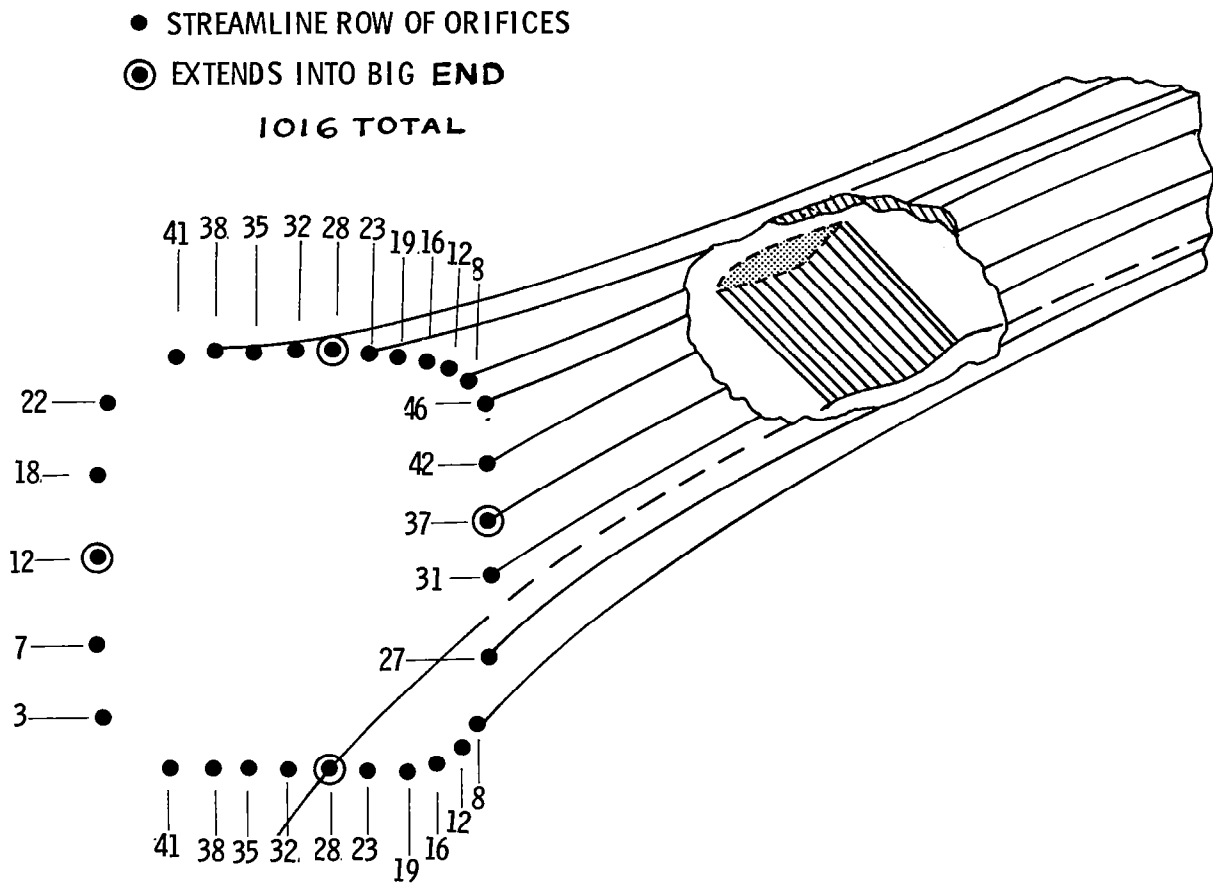


Figure 34

LFC LINER WALL PRESSURE ORIFICE LOCATIONS

Figure 35 further illustrates the contoured liner wall orifice locations around the model and sidewall mounted choke plates. The figure shows stream-wise orifice locations on the tunnel sidewall opposite the vertical-mounted model upper surface and the floor. This typical grid of orifice locations allows evaluation of model sonic bubble tunnel wall interference and model-wall juncture boundary layer flow.

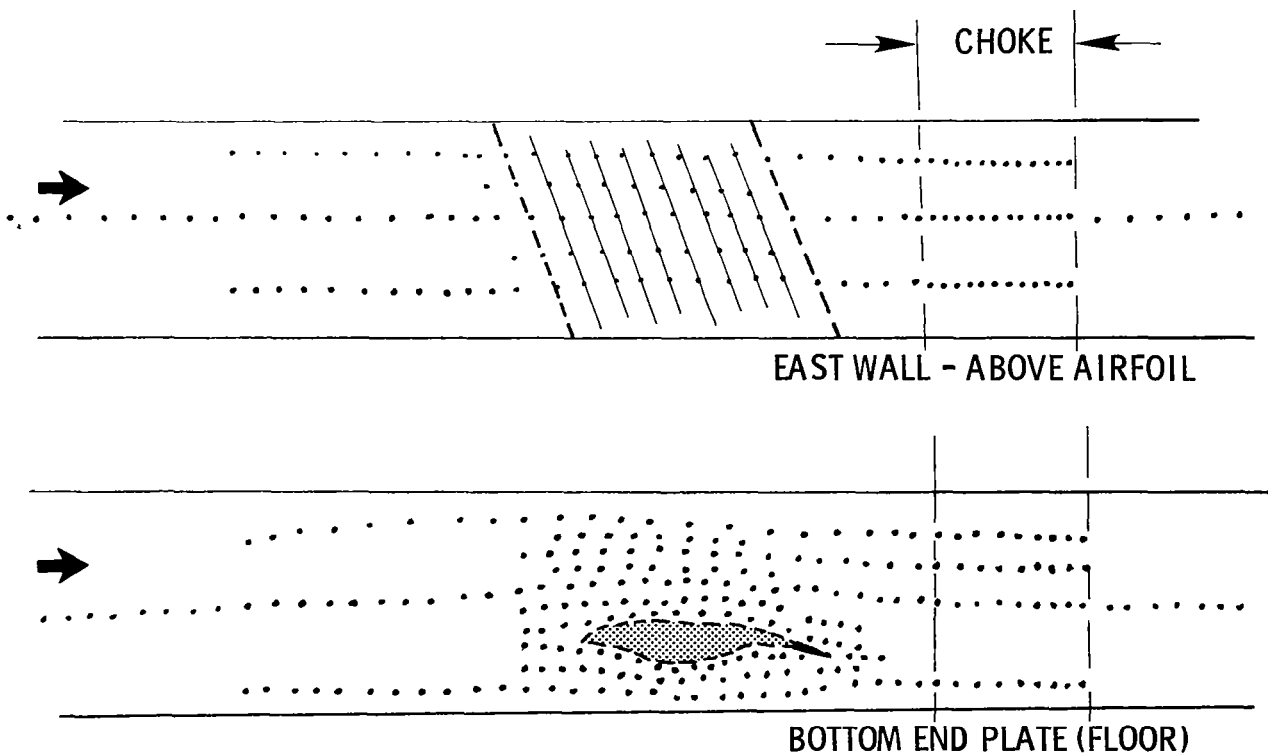


Figure 35

LaRC 8-FT TPT VARIABLE 2-WALL CHOKE AND PLENUM VENT

A sketch of the liner wall choke, shown in figure 36, is located about one choke chord length downstream of the LFC airfoil trailing edge and on the walls opposite the model upper and lower surfaces. The choke has been designed for variable deflection toward the tunnel centerline through a bell-crank having a 10:1 mechanical advantage. The resulting local area change, when deflected, allows a choke range of free-stream Mach number of $0.80 < M_{\infty} < 0.84$. A spanwise porous strip is located on the choke surface downstream of the maximum deflection point for venting of the flow for emergency shutdown requirements.

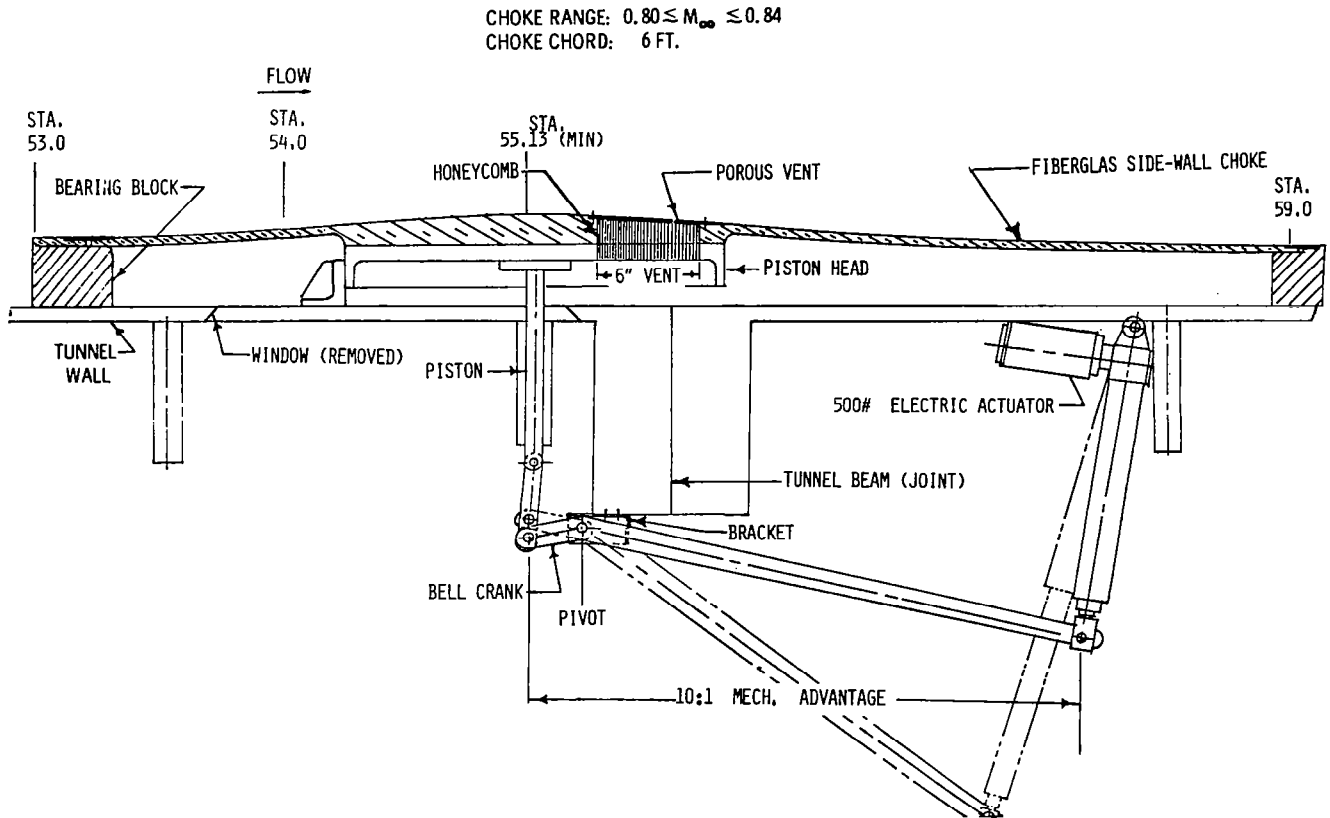


Figure 36

CONCLUSIONS

The most promising application of laminar flow control (LFC) is for future long-range transport aircraft where the percentage drag reduction appears to be the largest. In an effort to realize significant drag reduction and increased aircraft efficiency, the NASA Langley Research Center has designed and constructed a swept supercritical LFC airfoil with plans for testing to confirm performance and to establish a technology base for future long-range commercial transports. The developed airfoil has unique design optimization features and a suction system to establish laminar flow with minimum suction. The test facility to be used for conducting the LFC experiment has been modified to insure achievement of required flow quality and transonic free-air flow over the yawed LFC airfoil.

REFERENCES

1. Pfenninger, W.: Laminar Flow Control, Laminarization. AGARD-R-654, V. Karman Institute, Belgium, 1977.
2. Harvey, W. D.; Stainback, P. C.; and Owen, F. K.: Evaluation of Flow Quality in Two Large NASA Wind Tunnels at Transonic Speeds. NASA TP-1737, Dec. 1980.
3. Bauer, F.; Garabedian, P.; Korn, D.; and Jameson, A.: Supercritical Wing Sections II. Lecture Notes in Economics and Mathematical Systems, M. Beckman and H. P. Lunzi, eds., Springer-Verlag, 1975.
4. Kaups, Kalle; and Cebeci, Tuncer: Users Guide for Program Main to Calculate Compressible Laminar Boundary Layers with Suction on Swept and Tapered Wings. J. Aircraft, Vol. 14, No. 7, July 1977, pp. 661-667.
5. El-Hady, N. M.: On the Stability of Three-Dimensional Compressible Nonparallel Boundary Layers. AIAA Paper 80-1734, July 1980.
6. Srokowski, A. J.; and Orszag, S. A.: Mass Flow Requirements for LFC Wing Design. AIAA Paper 77-1222, 1977.
7. Mack, L. M.: On the Stability of the Boundary Layer on a Transonic Swept Wing. AIAA Paper 79-0264, Jan. 1979.
8. Dagenhart, John Ray: Amplified Crossflow Disturbances in the Laminar Boundary Layer on Swept Wings with Suction. NASA TP-1902, Nov. 1981.
9. Pfenninger, W.; Reed, H. L.; and Dagenhart, J. R.: Design Considerations of Advanced Supercritical Low Drag Suction Airfoils. Viscous Flow Drag Reduction, ed. by G. R. Hough, Vol. 72 of Progress in Astronautics and Aeronautics, 1980.
10. Smith, A. M. O.: On the Growth of Taylor-Goertler Vortices Along Highly Concave Walls. Quart. Appl. Math., vol. 13, 1955, pp. 233-262.
11. Kobayashi, R.: Taylor-Goertler Instability of a Boundary Layer with Suction on Blowing. AIAA J., vol. 12, 1974, pp. 394-395.
12. Anderson, E. C.; and Lewis, C. H.: User Guide for STRMLN: A Boundary Layer Program for Contoured Wind-Tunnel Liner Design. NASA CR-159058, 1979.
13. Raetz, G. S.: Appendix: Evaluation of the Profile Drag Coefficient of an Untapered Swept Suction Wing. Northrop Rept. BLC-93, NAI-57, 317, Feb. 1957.
14. Lachman, G. V. (ed.): Boundary Layer and Flow Control, Vol. 2, Pergamon Press, New York and London, 1961.
15. Pfenninger, W.; and Bacon, J. W.: About the Development of Swept Laminar Suction Wings with Full Chord Laminar Flow. Northrop Rept. BLC-130, NOR 60-299, 1960.

STATUS OF NASA ADVANCED LFC AIRFOIL HIGH-LIFT STUDY

Zachary T. Applin
NASA Langley Research Center

INTRODUCTION

Laminar flow over major portions of aircraft wings has long been known to have beneficial effects in terms of aerodynamic performance and fuel economy. However, due to the rigid constraints on the surface roughness of aircraft wings, this technology has not, to date, proved to be feasible for commercial operation. Discontinuities in the surface are also detrimental to the maintenance of laminar flow over the airfoil. High-lift devices cause discontinuities in the surface when in the stowed position. These devices also leave open pockets in the surface when deployed. In addition, the storage of these high-lift devices requires internal volume that could otherwise be used for the laminar flow control (LFC) system. Despite all of the difficulties associated with high-lift devices on LFC wings (especially on the leading edge), the benefits that can be obtained with their use merits research in this area.

This paper discusses the design of a high-lift system for the NASA advanced LFC airfoil designed by Pfenninger (see ref. 1). The high-lift system consists of both leading- and trailing-edge flaps. A 3-meter-semispan, 1-meter-chord wing model using the above airfoil and high-lift system is under construction and will be tested in the NASA Langley 4- by 7-Meter Tunnel. This model will have two separate full-span leading-edge flaps (0.10c and 0.12c) and one full-span trailing-edge flap (0.25c). The purpose of this model will be to study the leading-edge characteristics of this airfoil. A parametric study of the effects of variations in the leading-edge flap overlap, gap, deflection, and chord will be performed with this model. This will result in quantitative data on the improved aerodynamic performance afforded by this high-lift device. The design of this model was completed in January 1981, and construction is underway and is expected to be completed in time for a wind-tunnel test in March 1982.

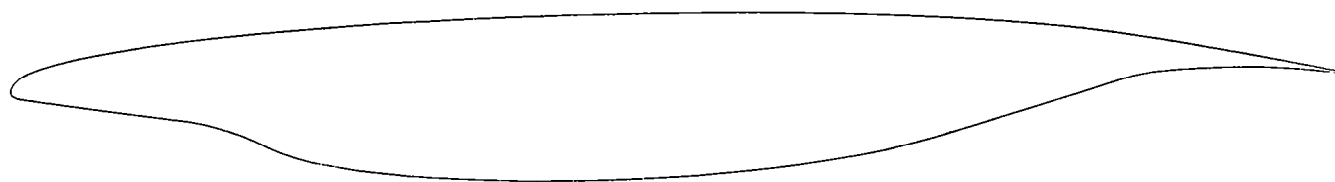
The performance of this high-lift system was predicted by the NASA two-dimensional viscous multi-component airfoil program. This program combines an inviscid potential-flow solution with an ordinary boundary-layer solution and a confluent boundary-layer solution (for multiple components) to obtain the viscous characteristics of the configuration.

This program was also used to predict the characteristics of the LFC airfoils developed by the Douglas Aircraft Company (DAC) and Lockheed-Georgia Aircraft Company (GELAC) (refs 2 and 3). The DAC LFC airfoil discussed in the paper uses both a leading- and trailing-edge high-lift device. This system maintains LFC on the upper surface only because of the leading-edge device. The GELAC LFC airfoil uses only a trailing-edge high-lift device. This design maintains LFC on both the upper and lower surfaces. Both of these designs gave sufficient performance for a commercial transport flight envelope.

Based on the data in this paper the addition of a leading-edge device for the NASA LFC airfoil is necessary for high angles of attack and increased lift. The data base for the influence of high-lift systems on LFC airfoils should be expanded. This will enable potential users of LFC technology to make judgements on the benefits or detriments of the various high-lift systems available. Finally, the theoretical data presented in this paper should be correlated with experimental values that will be obtained from the wind-tunnel model.

LEADING-EDGE FLAP STORAGE

Since the leading-edge region of the NASA advanced LFC airfoil is very thin, storage of a leading-edge flap and its mechanism may prove to be a difficult task using conventional technology. The basic airfoil has been modified by shifting the lower surface lobe rearward and increasing the camber. (See fig. 1.) This modification allowed enough length in the chord-wise direction for storage of a 0.12c leading-edge flap. However, no account has been made at this time for the thickness required for storing such a device.



LFC 989HL AIRFOIL SECTION

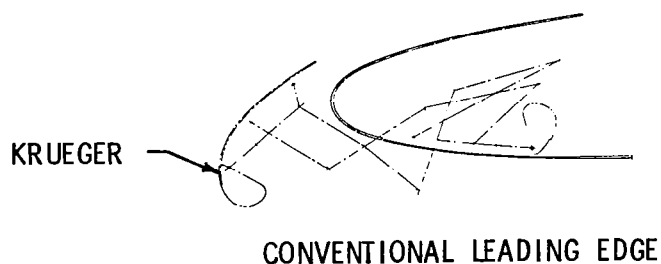


Figure 1

CRUISE PERFORMANCE

Figure 2 shows the lift-coefficient versus angle of attack in the upper chart and the percent separation on the upper surface of the airfoil in the lower chart for the cruise airfoil. The Mach number (0.2) and Reynolds number (4,660,000) used in the analysis are those that will be achieved in the wind-tunnel test of the semispan model. Since the program used to determine these characteristics is an attached flow program, the upper chart shows only the linear portion of the lift curve. The form factor based on boundary-layer quantities is used to predict the point of separation. The aerodynamic characteristics predicted by this program are considered valid only as long as the percent of separation remains below 5 percent of the airfoil chord. The cutoff point is indicated in the upper chart where the solid line stops and the dashed line starts. In addition, due to the rather slender leading edge of this airfoil, a very abrupt stall pattern is predicted. This is indicated by the percent separation going from almost no separation to almost full separation on the upper surface for a one degree increment in angle of attack.

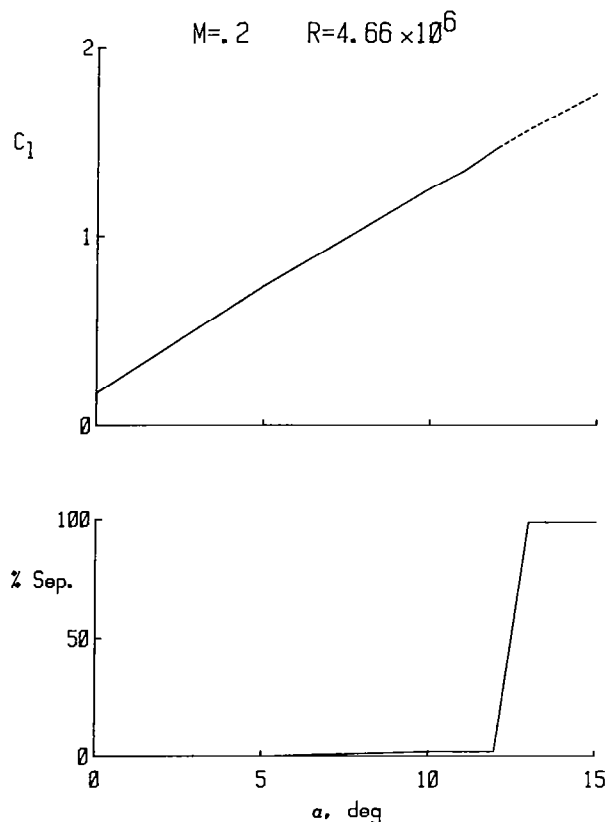


Figure 2

CRUISE PERFORMANCE

The pressure distribution over the upper and lower surface of the cruise airfoil is shown in figure 3. This configuration was predicted to have a maximum two-dimensional lift coefficient of 1.5 at about 12° angle of attack. As expected, this configuration does not provide sufficient performance ($C_L = 4.0$) for takeoff and landing.

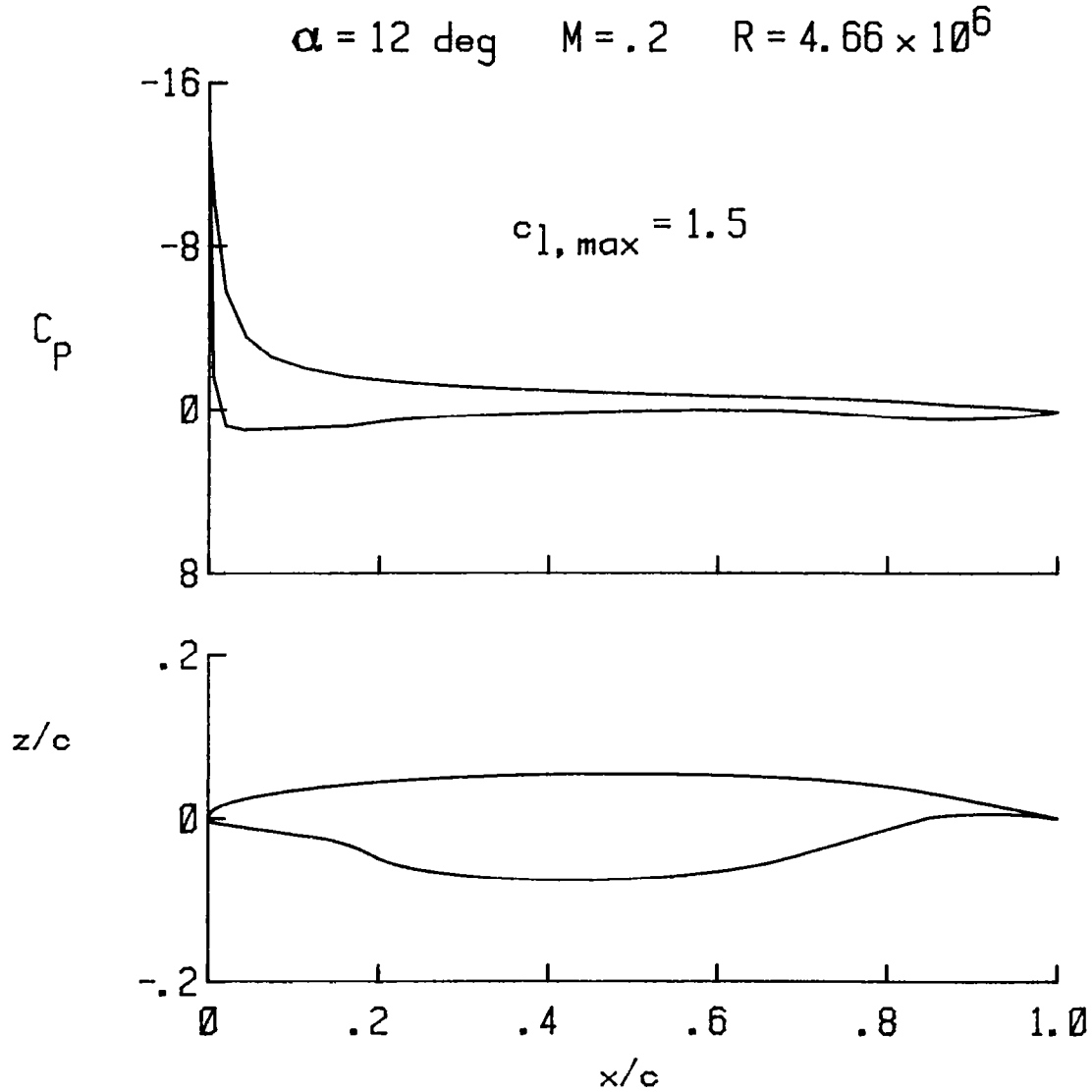


Figure 3

HIGH-LIFT TRAILING-EDGE FLAP PERFORMANCE

Adding a 0.25c trailing-edge flap to the cruise airfoil was the next step in designing a high-lift system for this airfoil. The lift coefficient and the percent separation on the upper surface of the wing versus angle of attack are shown in figure 4. Again, as indicated by the lower chart, an abrupt stall pattern is predicted. This indicates that a leading-edge device is needed for this airfoil to achieve higher angles of attack and increased lift.

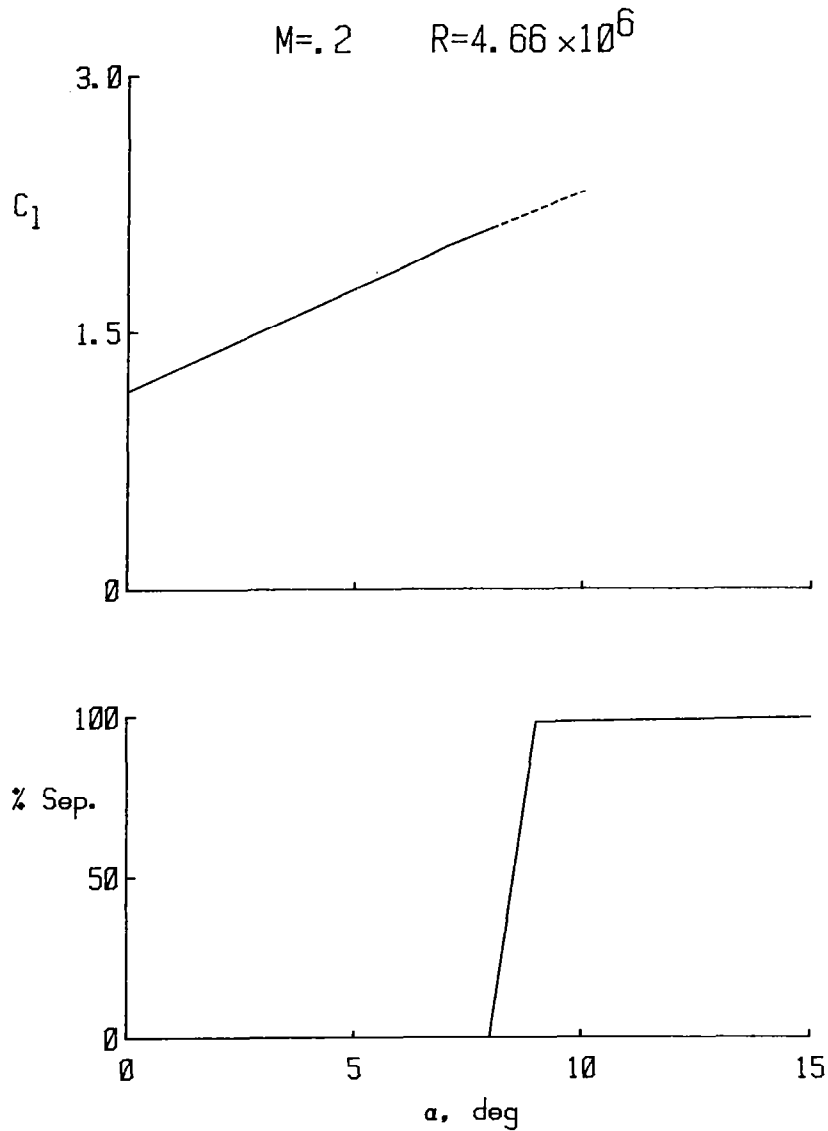


Figure 4

HIGH-LIFT TRAILING-EDGE FLAP PERFORMANCE

Figure 5 shows the pressure distribution over the trailing-edge flap configuration. This configuration separates between 8° and 9° for a flap deflection of 15° and between 7° and 8° for a flap deflection of 30° . These give a maximum two-dimensional lift coefficient between 2.0 and 2.9. This configuration has insufficient performance for takeoff and landing conditions for a commercial transport.

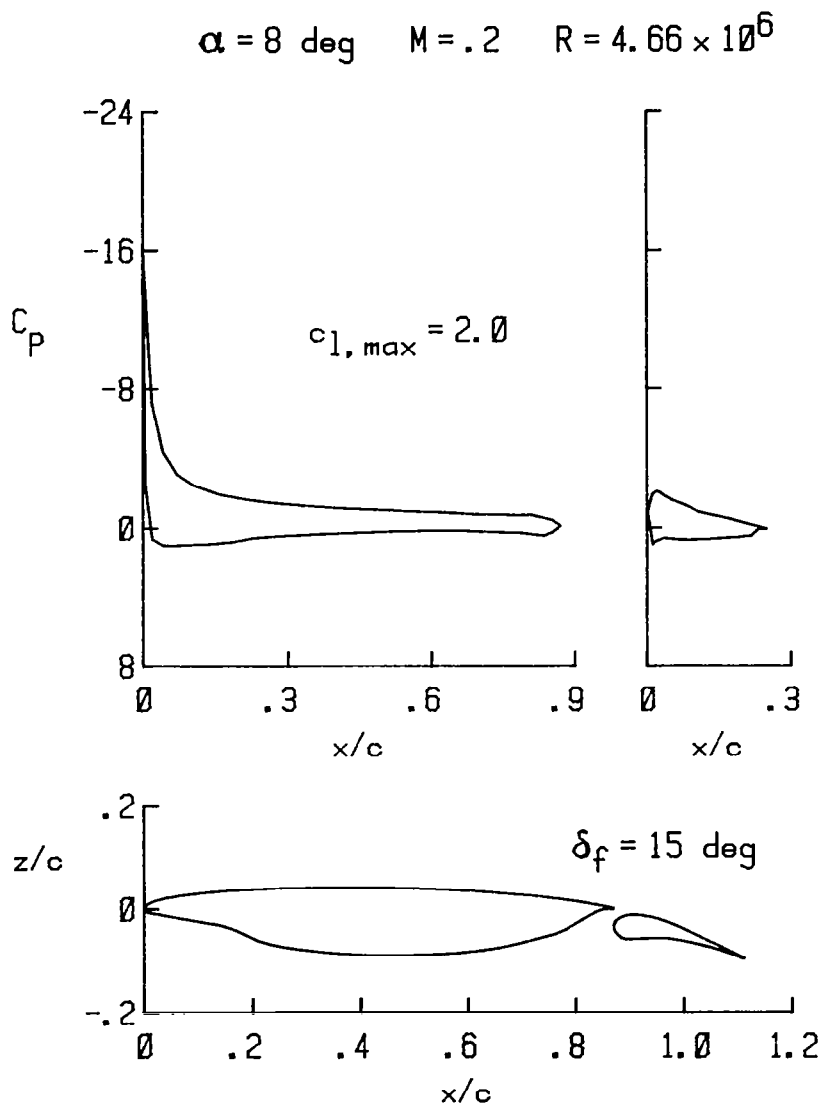


Figure 5

HIGH-LIFT LEADING- AND TRAILING-EDGE FLAP PERFORMANCE

The lift coefficient and percent separation versus angle of attack for the leading- and trailing-edge flap configurations are shown in figure 6. As expected, with the addition of the leading-edge flap on the airfoil, the stall pattern predicted is not as abrupt as for the trailing-edge flap and the cruise configurations. This is indicated by the percent separation increasing at a relatively slow rate as the angle of attack is increased.

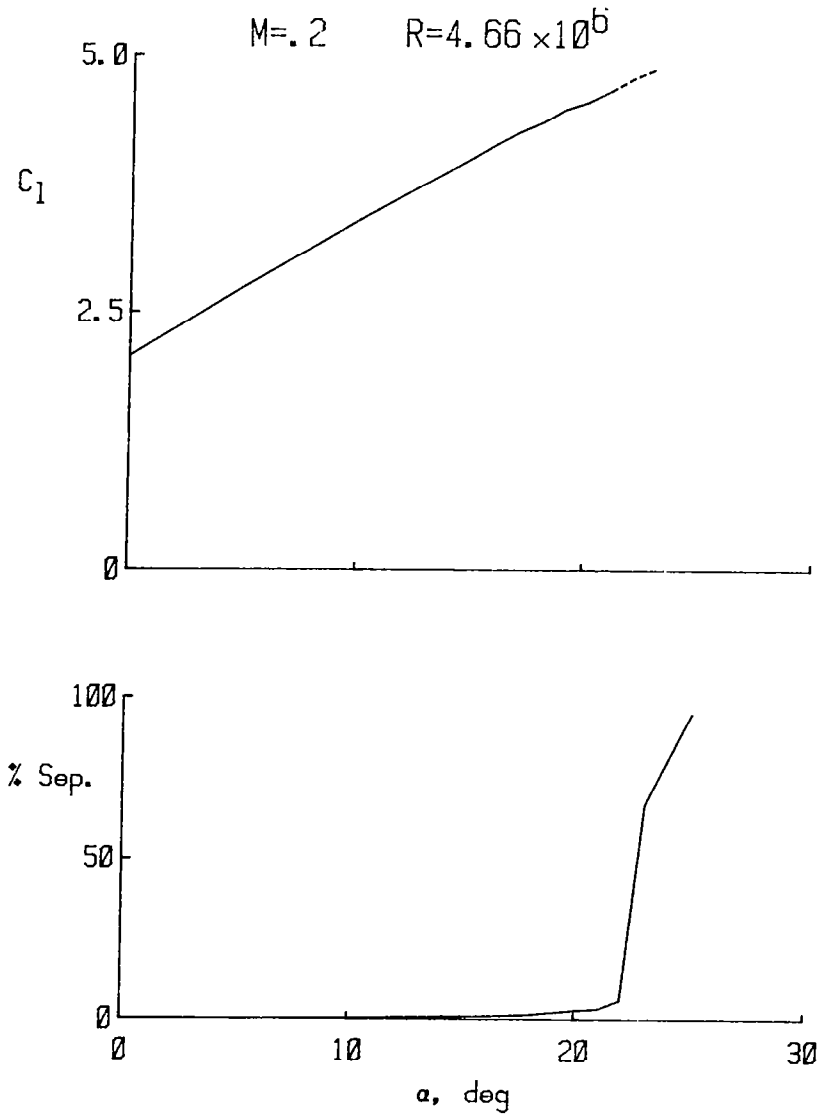


Figure 6

HIGH-LIFT LEADING- AND TRAILING-EDGE FLAP PERFORMANCE

Figure 7 shows the pressure distribution over the leading- and trailing-edge flap configuration. This configuration gives a maximum two-dimensional lift coefficient of from 3.1 to 4.7 depending on leading-edge flap size and deflection. This configuration provides the necessary performance required for takeoff and landing of a commercial transport.

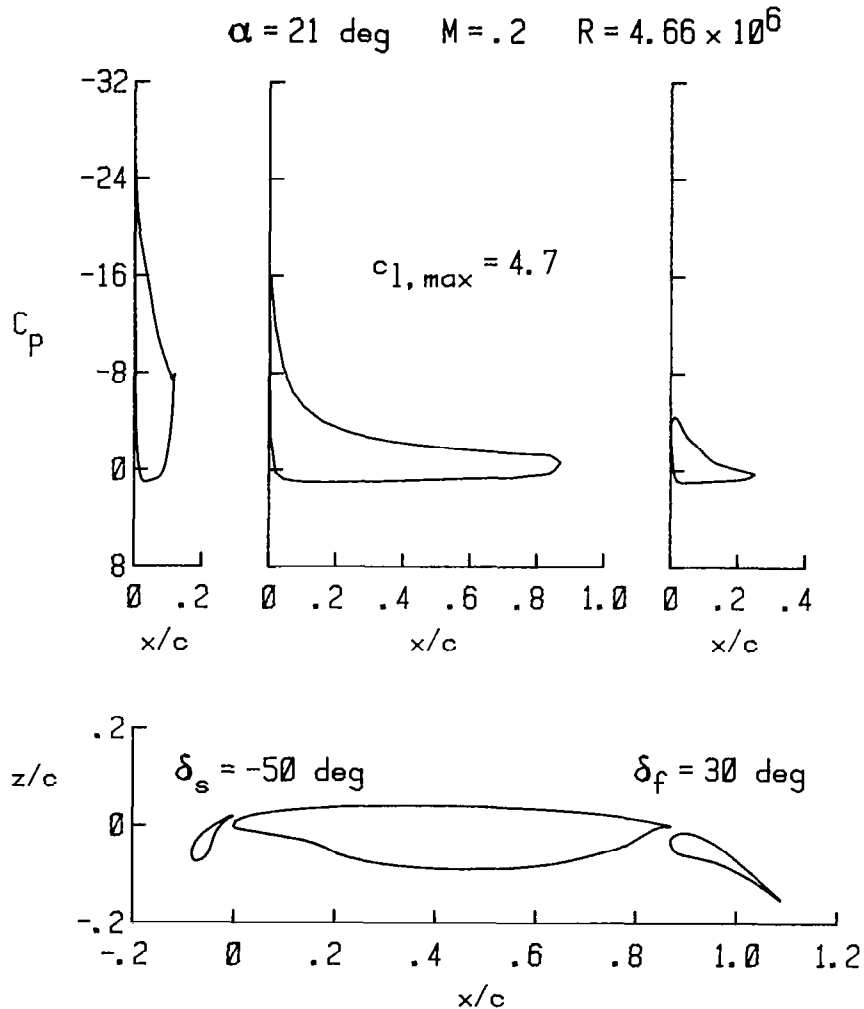


Figure 7

DEFINITION OF OVERLAP, GAP, AND DEFLECTION

The definition of overlap, gap, and deflection used in this study are the same as described in reference 4. Basically, the overlap is defined as the distance, parallel to the longest chord line of the forward component, from the lower surface trailing edge of the forward component to the most forward point on the aft component. The gap is defined as the distance from the lower surface trailing edge of the forward component to the closest point on the aft component. The deflection angle is defined as the angle between longest chord lines of the two components (fig. 8).

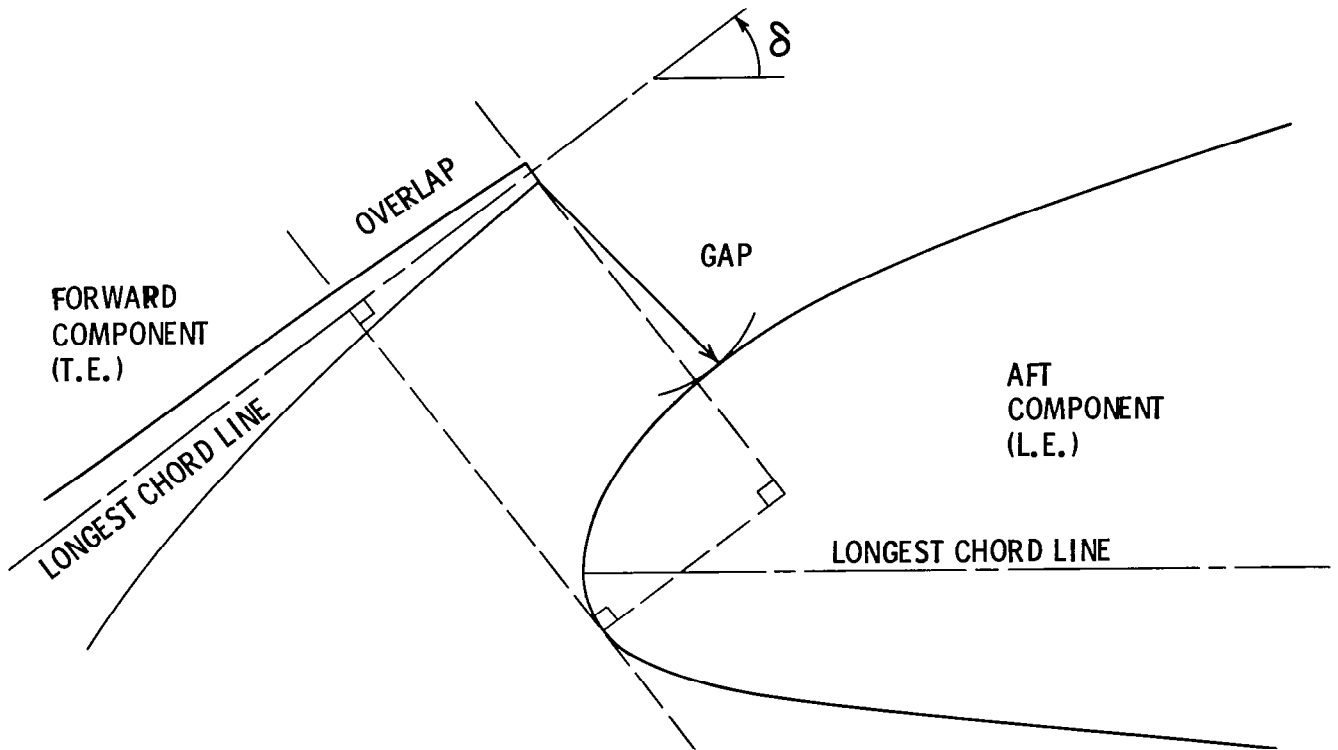


Figure 8

C_p DISTRIBUTION

Figure 9 shows the pressure coefficient plotted against the chordwise station for the leading-edge flap, the wing, and the trailing-edge flap. The overlap of the leading-edge flap is held constant while the gap is varied. The relative levels of the pressure peaks on the leading-edge flap and the wing are used to determine which settings of overlap and gap are optimum. In order to maintain attached flow on both components the relative levels of the pressure peaks should be about equal to avoid the premature separation of one component.

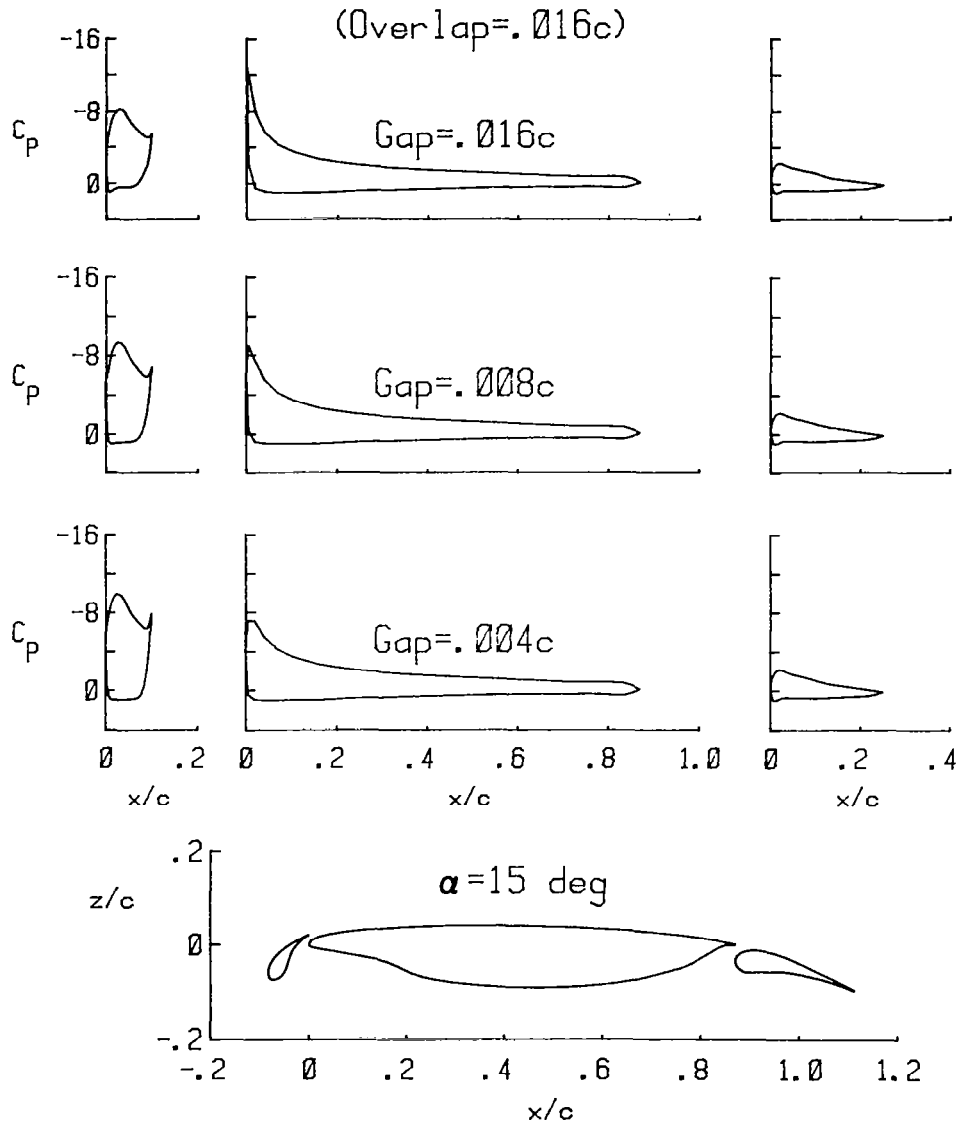


Figure 9

EFFECT OF OVERLAP VARIATION

Figure 10 shows the variation of the pressure peak with leading-edge flap overlap holding the gap constant at 0.012c. These data indicate that for small overlaps the peak pressure levels on the leading-edge flap and the wing show little change with changes in overlap. A baseline overlap of 0.16c was chosen for the wind-tunnel model. The mounting brackets will allow variations about this value to compare with the theoretical results shown in figure 10.

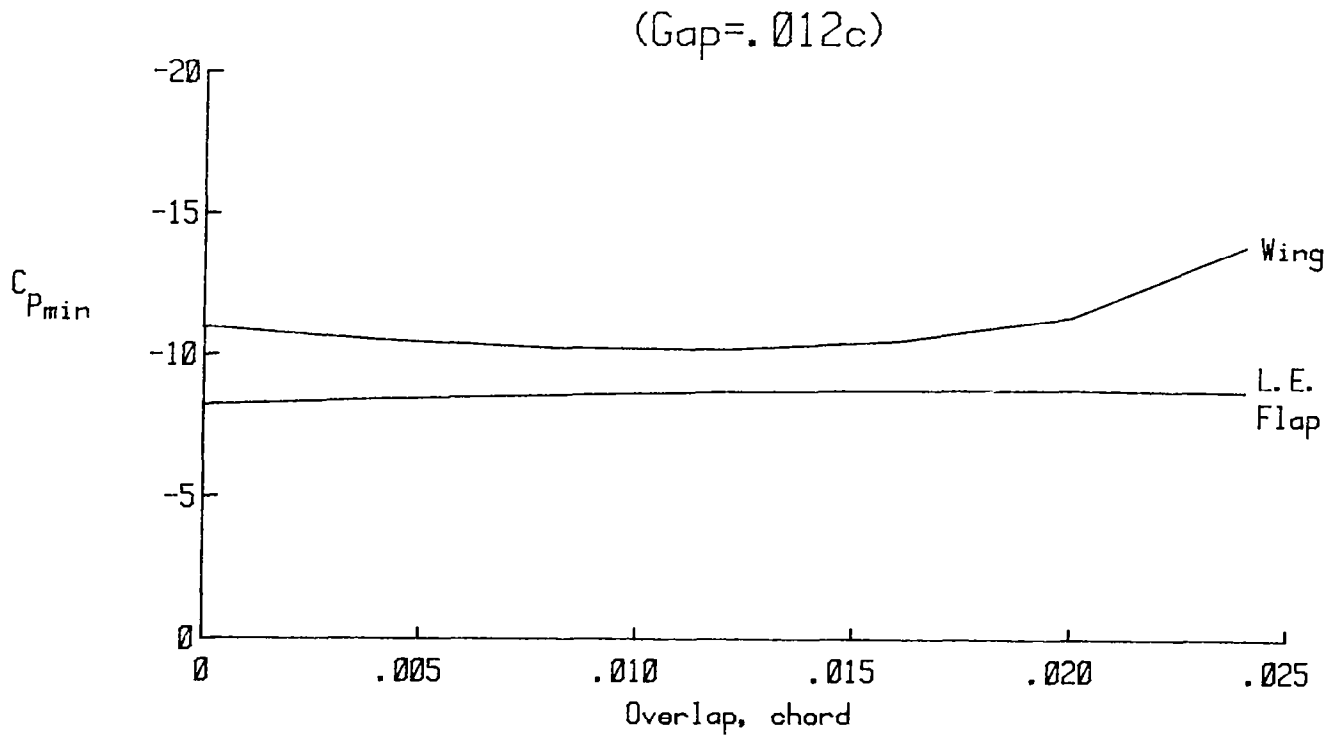


Figure 10

EFFECT OF GAP VARIATION

Figure 11 shows the variation of the pressure peaks with leading-edge flap gap holding the overlap constant at 0.016c. These data indicate significant variations in the peak pressure levels on the leading-edge flap and the wing with changes in gap. The point where both components have the same pressure peak level occurs at a gap of approximately 0.012c. A baseline gap of 0.012c was chosen for the wind-tunnel model. Again, mounting brackets will allow variations to compare with the theoretical results shown in figure 11.

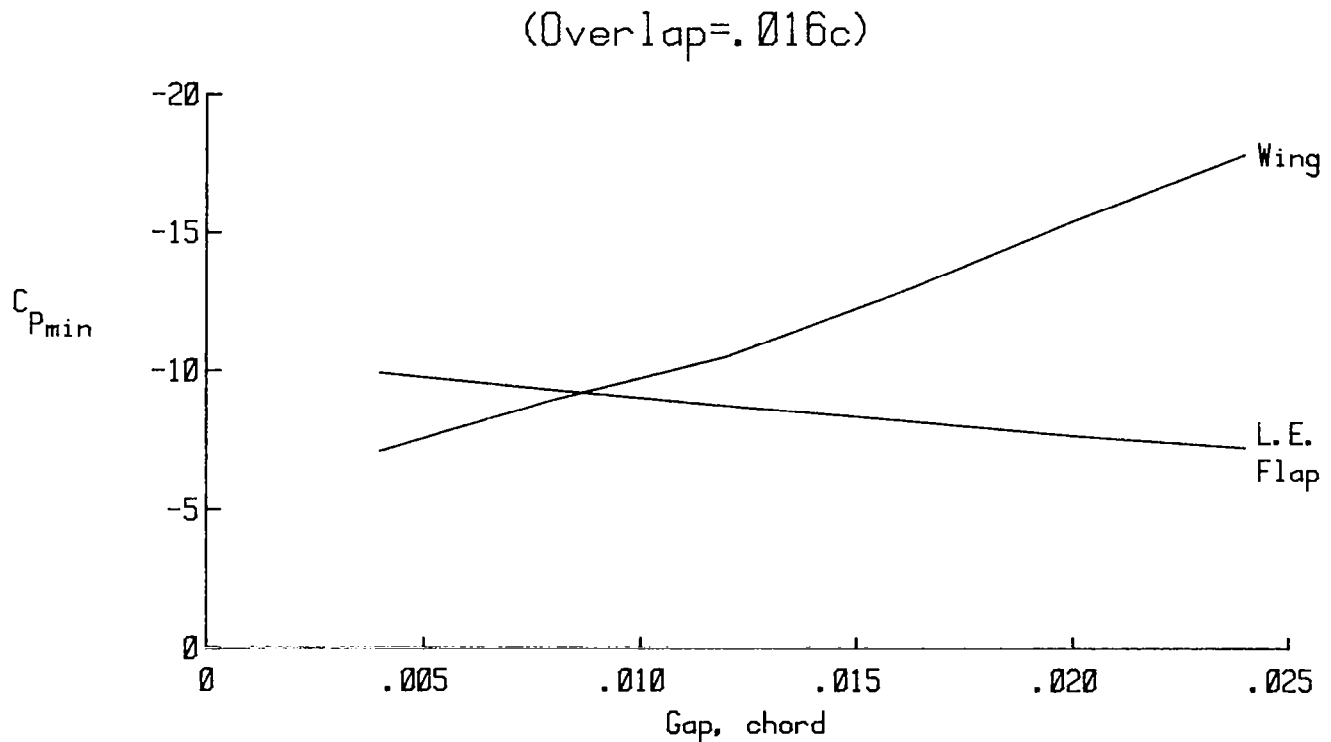


Figure 11

SELECTION OF LEADING-EDGE FLAP DEFLECTION AND CHORD

With the baseline leading-edge flap overlap and gap chosen, a study was done to determine the smallest chord and best deflection angle that would yield the necessary performance. Three sizes for the leading-edge flap were evaluated (0.08c, 0.10c, and 0.12c). The deflection of each size was varied from 40° to 60° in 5° increments (fig. 12). The 8-percent-chord leading-edge flap proved to be insufficient for maintaining attached flow at high angles of attack. The 10-percent-chord leading-edge flap maintained attached flow and provided the necessary performance characteristics for deflections from 50° to 60°. The 12-percent-chord leading-edge flap provided the desired performance in addition to maintaining attached flow for all deflections between 40° and 60°. The five configurations indicated were selected as baseline configurations for the wind-tunnel model. This will result in quantitative data on the effects on aerodynamic performance of leading-edge flap size and deflection.

L.E. FLAP: GAP = .012c OVERLAP = .016c

T.E. FLAP: GAP = .02c OVERLAP = 0c $\delta_F = 15^\circ \text{ \& } 30^\circ$

L.E. FLAP, DEG	C _{L.E. FLAP} c		
	.08	.10	.12
40			
45			
50		X	X
55		X	X
60		X	

Figure 12

LFC HIGH-LIFT SEMISPAN MODEL

The cruise and high-lift planforms of the 1- by 3-meter semispan model are shown in figure 13. This model has two chordwise rows of pressure taps near the mid-span. One row is designed to be streamwise for 0° sweep and the other row streamwise for 20° sweep. These pressure taps will be used to measure quasi-two-dimensional pressure distributions over the model. In addition, there are six spanwise pressure taps near the leading and trailing edge to measure the amount of crossflow over the model. The model will be mounted on a six-component balance to measure forces and moments.

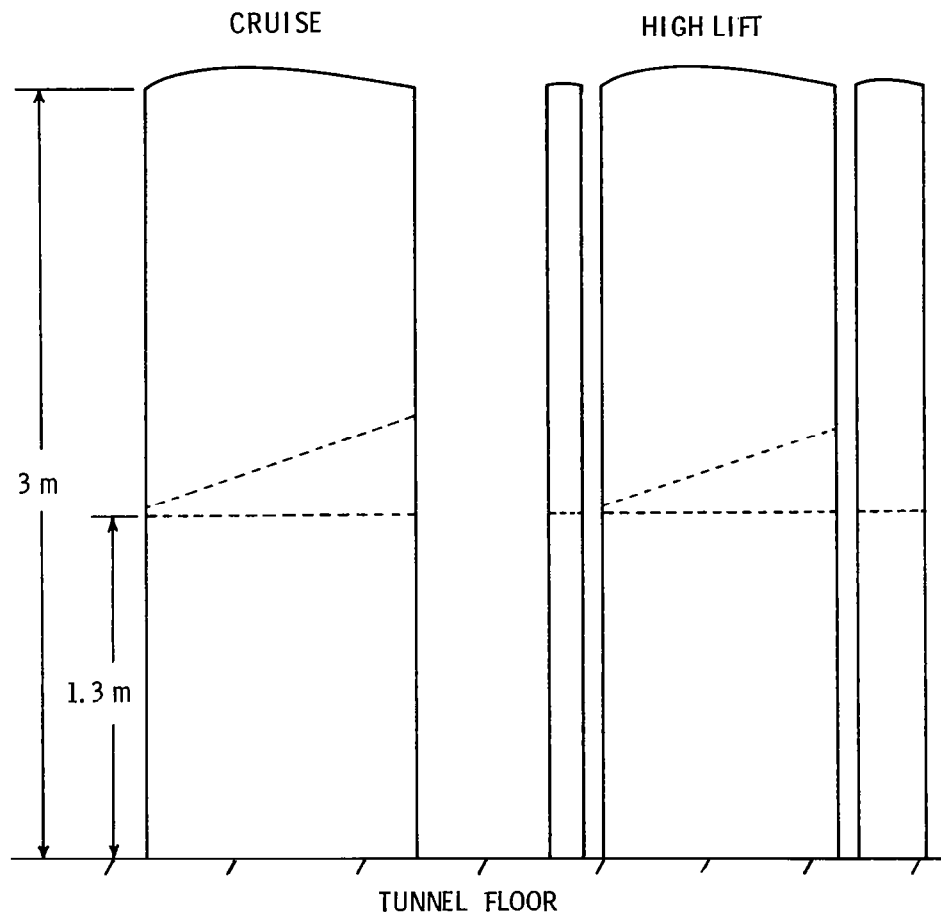


Figure 13

DAC LFC AIRFOIL

After defining the high-lift system for the NASA LFC airfoil the final task was to evaluate existing high-lift configurations for LFC airfoils. The designs of the Douglas Aircraft Company (DAC) and the Lockheed-Georgia Company (GELAC) were selected for this study. These were selected because of the two different approaches to a LFC high-lift system. The DAC design uses both a leading- and trailing-edge device while maintaining LFC only on the upper surface of the airfoil. The GELAC design uses only a trailing-edge device and maintains LFC on both upper and lower surfaces of the airfoil.

The predicted performance of the DAC LFC high-lift configuration is shown in figure 14. A maximum two-dimensional lift coefficient of 4.5 at about 24° angle of attack is predicted. However, for this configuration, this lift coefficient is possible only at the expense of losing LFC on the lower surface of the airfoil.

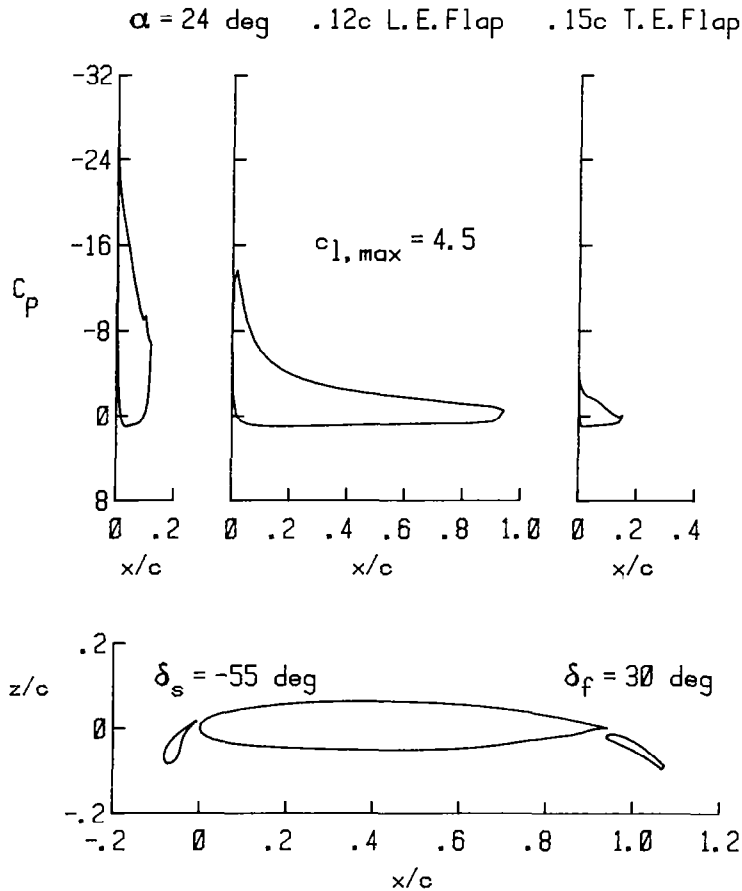


Figure 14

GELAC LFC AIRFOIL

The GELAC LFC high-lift airfoil is predicted to have a maximum two-dimensional lift coefficient of 2.9 at about 9° angle of attack (fig. 15); this configuration would require a wing larger than one with a leading-edge flap. However, LFC on both upper and lower surfaces is possible. The airfoil leading-edge shape produces an adverse pressure gradient on the upper surface and a neutral pressure gradient on the lower surface. As a result, a very smooth surface is required to prevent boundary-layer transition on either surface. This requirement makes it unreasonable to store a leading-edge device in the lower wing surface.

In contrast, the NASA LFC airfoil attempts to shape the pressure distribution such that the maintenance of laminar flow over the discontinuity caused by the stowed leading-edge flap will be possible. This will allow LFC on both surfaces to improve the overall performance of the LFC airfoil.

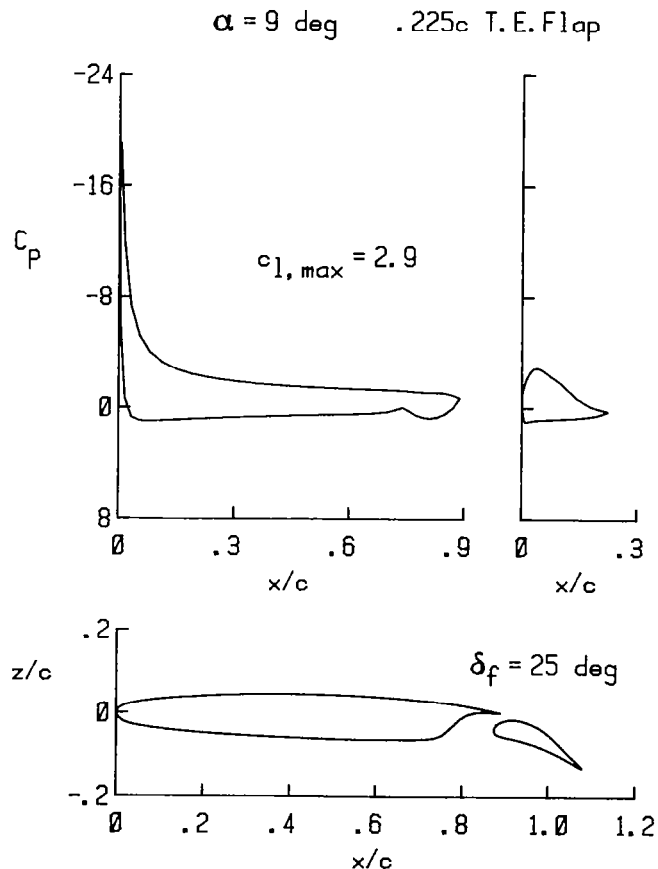


Figure 15

NASA ADVANCED LFC HIGH-LIFT SEMISPAN MODEL STATUS

DESIGN COMPLETED (JANUARY 1981)

CONSTRUCTION STARTED (FEBRUARY 1981)

SCHEDULED COMPLETION (MARCH 82)

CONCLUDING REMARKS

- THE DATA BASE FOR HIGH-LIFT SYSTEMS (BOTH LEADING AND TRAILING EDGE) ON LFC AIRFOILS SHOULD BE EXPANDED
- FURTHER STUDY OF THE OPTIMUM POSITIONS OF HIGH-LIFT DEVICES ON THE NASA LFC AIRFOIL SHOULD BE DONE
- THEORETICAL DATA PRESENTED IN THIS PAPER SHOULD BE CORRELATED WITH EXPERIMENTS

REFERENCES

1. Pfenninger, W.; Reed, Helen L.; and Dagenhart, J. R.: Design Considerations of Advanced Supercritical Low Drag Suction Airfoils. Viscous Flow Drag Reduction, Progress in Astronautics and Aeronautics, vol. 72, 1980, pp. 249-271
2. Anon: Evaluation of Laminar Flow Control System Concepts for Subsonic Commercial Transport Aircraft. McDonnell Douglas Rep. ACEE-01-PM-9891, Interim Review, Sept 11-12, 1979, NASA Langley Research Center
3. Anon: Evaluation of Laminar Flow Control System Concepts for Subsonic Commercial Transport Aircraft. NASA CR-159,254, September 1980
4. Morgan, Harry L., Jr.; and Paulson, John W., Jr.: Low-Speed Aerodynamic Performance of a High-Aspect-Ratio Supercritical-Wing Transport Model Equipped With Full-Span Slat and Part-Span Double-Slotted Flaps. NASA TP-1580, 1979.



STABILITY OF BOUNDARY LAYERS WITH POROUS SUCTION STRIPS:
EXPERIMENT AND THEORY*

G. A. Reynolds, W. S. Saric, H. L. Reed, and A. H. Nayfeh

Department of Engineering Science and Mechanics
Virginia Polytechnic Institute and State University
Blacksburg, Virginia

ABSTRACT

This report states the progress made on NASA Grants NSG-1608 and NSG-1255. During this last year, experiments were performed in the VPI & SU low-turbulence tunnel on the stability and transition of 2-D boundary layers on flat plates with and without suction. A number of general suction cases were tried and they are given in this report. Of particular interest was the work directed toward optimization of suction distribution. In the optimization tests the overall suction mass-flow rate was kept constant while different slot configurations were evaluated. The results of the July 1981 test series showed that the maximum stabilization occurred when the suction was moved toward the Branch I neutral point.

An analytical study of the stability of two-dimensional, incompressible boundary-layer flows over plates with suction through porous strips has been performed. The mean flow is calculated using linearized triple-deck, closed-form solutions. The stability results of the triple-deck theory are shown to be in good agreement with those of the interacting boundary layers. An analytical optimization scheme for the suction configuration has been developed. Moreover, numerical calculations were performed corresponding to the experimental configurations. In each case, the theory correctly predicts the experimental results.

*Prepared under NASA Grants NSG-1608 and NSG-1255 and ONR Contract No. N00014-75-C-0381

DESCRIPTION OF THE EXPERIMENT

The boundary-layer suction experiments are performed on a 6-foot x 12-foot flat-plate model which is equipped for the application of continuous suction at the four panel locations shown in Figure 1. Porous panels are inserted in two of the four locations on the flat plate where dimensions are given in centimeters from the leading edge. These suction panels were constructed by McDAC-Long Beach using a Dynapore porous material. This is a woven stainless steel which undergoes a calendaring process to provide uniform porosity with very good surface finish. The Dynapore material is laminated to a backing structure which, in addition to providing structural support, provides ducting for air removal. Figure 2 shows this porous-panel construction. The spanwise flutes shown in the figure are independent of one another and can be turned on or off by appropriate closing of the exit holes on the back of the panel. In this way the desired suction distribution can be obtained. The suction distribution can be varied from continuous suction over 10 inches to discrete suction over one 5/8-inch-wide flute.

Air removal from the porous panel is provided by a vacuum pump and plenum tank which is connected to the metering system shown in Figure 3. The plenum tank provides continuous running capabilities even at relatively high volume flow rates and requires little investment in pumping facilities. As presently configured, the system operates at a constant mass flow rate determined by the sonic choking nozzle. The sonic nozzle also eliminates propagation of sound upstream to the porous panels from the pumps and the primary air-removal piping. Because of the large pressure ratio between the tunnel and the vacuum tanks, choked flow is easily maintained. In the secondary section, the flow is divided and the volume flow rate to each of the porous panels is measured. The secondary manifold is fed by eight lines which supply suction to the eight subsections of the primary suction manifold on the flat plate. Provision has been made for eight metering valves in the secondary manifold to correct for possible spanwise non-uniformities, but this has not been necessary.

The data processing and computer controller system is diagramed in Figure 4. The primary elements of this system include four channels of constant temperature anemometry, the associated analog and digital signal processing, and the computer controller. The computer controls the 40-channel data-acquisition system, the spectrum analyzer, and the traverse motor controllers.

MEASUREMENTS

The flat plate suction experiment, the control system, and the data processing facilities, all developed in the last few years, now allow the careful, accurate, and high speed measurements of the mean flow and disturbance behavior under the influence of various suction configurations. Initial verification of the mean flow has shown that the flow is in fact a zero-pressure-gradient flow. Measurements across the boundary layer provide accurate determination of the mean-velocity profile and disturbance profile simultaneously. Input and output processing also provides the capability of simultaneous measurement of multiple-frequency or broad-band disturbances. The influence of suction on the mean flow is most readily observed through changes in the displacement thickness, δ^* , and momentum thickness, θ , obtained by integration of the velocity profile. Extent of the streamwise influence of suction on the mean flow can then be determined. Changes in the mean flow due to a single porous strip are barely discernible since the scatter in the

data corresponds to errors on the order of ≈ 0.05 mm. However, the downstream influence appears to be on the order of 15δ at these suction levels. In addition to boundary-layer disturbance profiles at the ribbon frequency, the total disturbance spectrum is obtained with and without suction. For example, consider the case of continuous suction over one porous panel (10 inches chordwise extent). The suction is applied near the second neutral point. Figure 5 shows a reduction in the fundamental and its harmonics as well as the broad-band background disturbances by at least an order of magnitude. In order to more precisely determine how these effects depend on the suction intensity and the streamwise extent of the suction, discrete suction strips were used. Suction was applied through just two flutes, each 5/8-inch wide and separated by 32 inches, shown as lines 1 and 2 in Figure 1. Disturbances were introduced at a dimensionless frequency, $F = \frac{2\pi v f}{U_\infty^2}$, near 50×10^{-6} as shown in Figure 6. The ribbon was located at $R = 415$ and the two suction strips were located at $R = 840$ and $R = 945$. Measurements here were carried out between the *. Measurements were taken at the maximum of the disturbance profile yielding the plot shown in Figure 7. The results of the experiment shown in Figure 6 were also interpreted by integration of the disturbance profile. This result is shown in Figure 8. The measurement of Figure 8 is more desirable than that of Figure 7 because errors due to improper selection of the $|u|_{\max}$ location are eliminated, and errors due to fluctuations in a single point measurement are minimized. Integration of the profile is also insensitive to changes in the profile shape which cause errors in some measurement techniques. In short, integration of the disturbance profile provides a very accurate determination of the disturbance amplitude and of the influence of suction.

COMPARISON OF THEORY WITH EXPERIMENT

Laminar viscous flow over a flat plate with porous strips exhibits a triple deck structure in the neighborhood of each strip. Using linearized triple deck theory with the dimensionless suction level at each strip as the small parameter, Reed and Nayfeh¹ proposed closed-form solutions describing this flow. The solutions consisted of a mean Blasius flow with corrections due to each strip linearly superposed. Upstream influence was accounted for in this theory.

Using the linearized triple deck closed-form solutions for the streamwise velocity components, Reed and Nayfeh¹ performed stability calculations and predicted that optimal strip configurations occur for a given frequency when suction is concentrated close to the streamwise position corresponding to the first neutral point of the stability curve. The next seven figures show comparisons between the linear triple deck theory and the experiments for different strip configurations as indicated below. All figures show the integrated disturbance amplitude versus $\sqrt{\text{Re}_x}$.

The following is a summary of the suction strip configurations tested. All porous strips are 5/8-inch wide. Figures 9-11 indicate results for a dimensionless frequency of 20×10^{-6} and a square root of the unit Reynolds number per meter of $R_u = 987$. In Figure 9, one suction strip on Panel II at $x = 248$ cm. is open with a suction level of $v_0 = 5.5 \times 10^{-3} U_\infty$. In Figure 10, two suction strips are open, one on

Panel I at $x = 194.3$ cm. with $v_0 = 2.6 \times 10^{-3} U_\infty$ and one on Panel II at $x = 247.6$ cm. with $v_0 = 3.0 \times 10^{-3} U_\infty$. Figure 11 shows one porous strip open on Panel I at $x = 194.3$ cm. with $v_0 = 5.5 \times 10^{-3} U_\infty$. Figures 12-15 indicate results for a dimensionless frequency of 25×10^{-6} . The square root of the unit Reynolds number per meter in Figures 12-14 is $R_u = 961$. In Figure 15, $R_u = 877$. Figure 12 shows one strip on Panel I at $x = 194.3$ cm. with $v_0 = 5.7 \times 10^{-3} U_\infty$. Three strips are open on each of Panels I and II in Figure 13, each strip having a suction level of $v_0 = 1.0 \times 10^{-3} U_\infty$. The locations of the six strips are $x = 184.8, 194.3, 203.8, 238.1, 247.6,$ and 257.1 cm. In Figure 14, there is suction through seven strips on Panel I and three on Panel II, the first seven strips having $v_0 = 4.2 \times 10^{-4} U_\infty$ and the next three having $v_0 = 1.1 \times 10^{-3} U_\infty$. The locations of the ten strips are $x = 184.8, 187.9, 191.1, 194.3, 197.5, 200.6, 203.8, 238.1, 247.6,$ and 257.1 cm. Finally, Figure 15 has the same configuration as Figure 14 except at a lower unit Reynolds number. In all cases the theory has predicted the experimental results well. The experimental results indeed show that maximum stabilization occurs when suction is moved forward toward the Branch I neutral point.

Figure 16 shows one last case of continuous area suction on Panels I and II for a dimensionless frequency of 25×10^{-6} . However, the corresponding theoretical results are unavailable at this time.

REFERENCE

- ¹Reed, H. L.; and Nayfeh, A. H.: Stability of Flow over Plates with Porous Suction Strips. AIAA-81-1280, 1981.

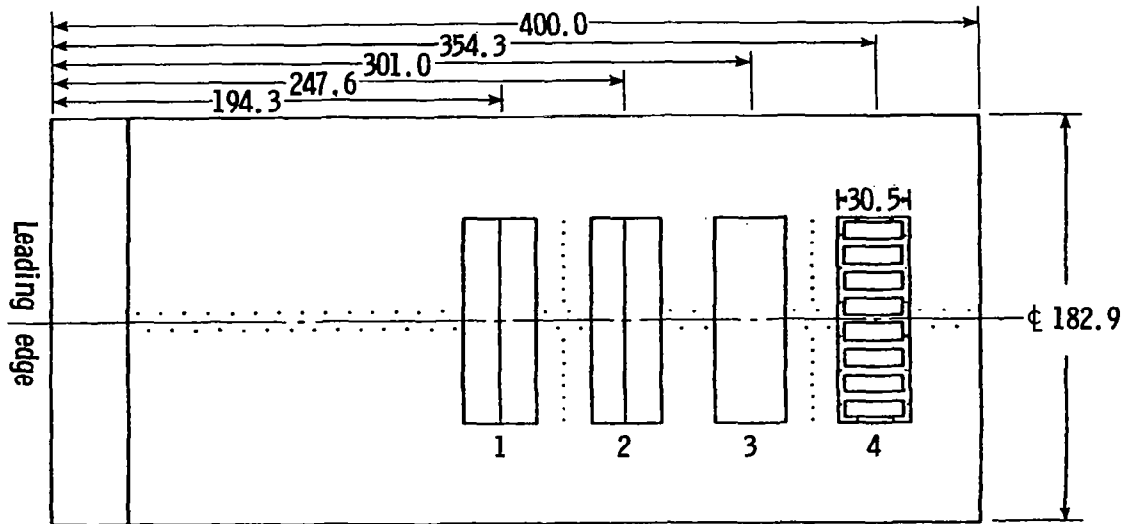


Figure 1

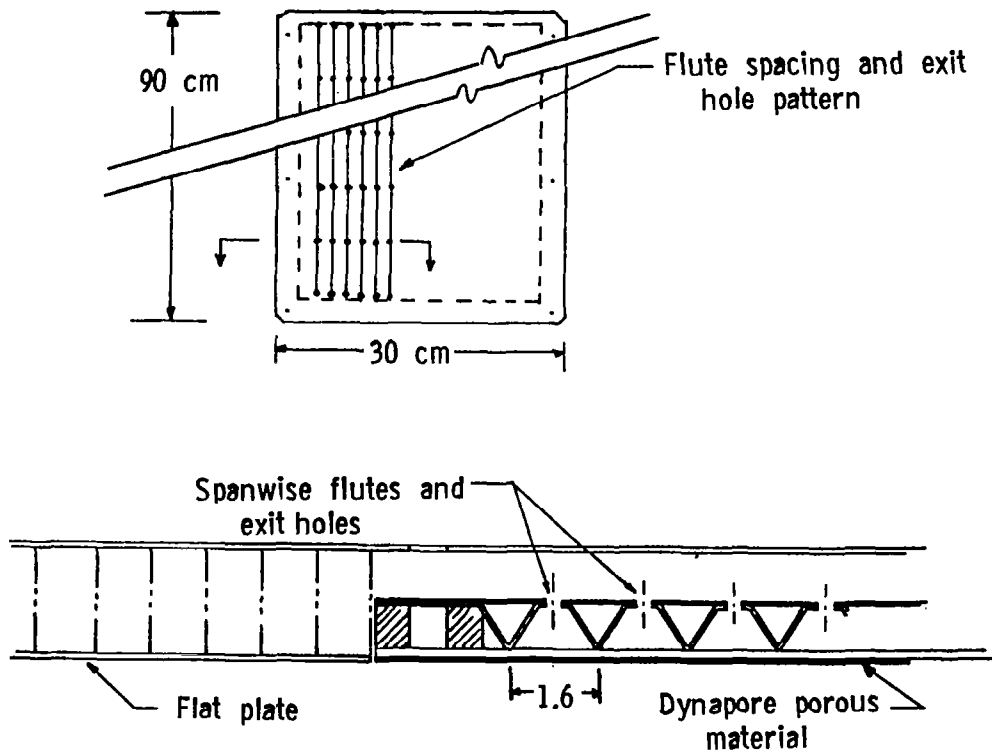


Figure 2

Suction Control System

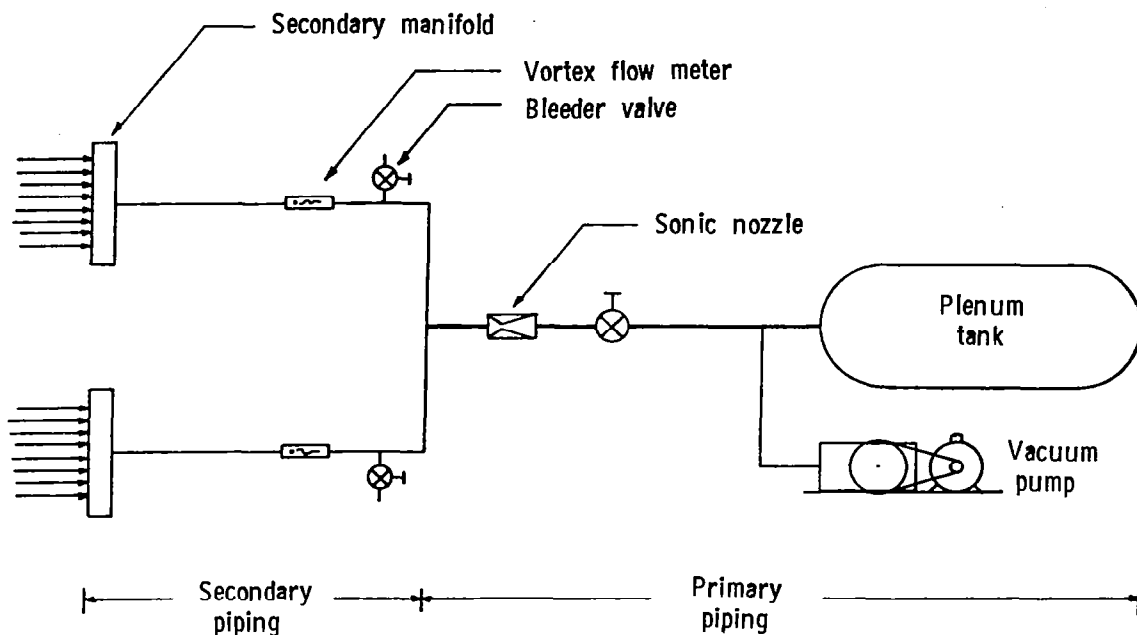


Figure 3

Instrumentation flow chart

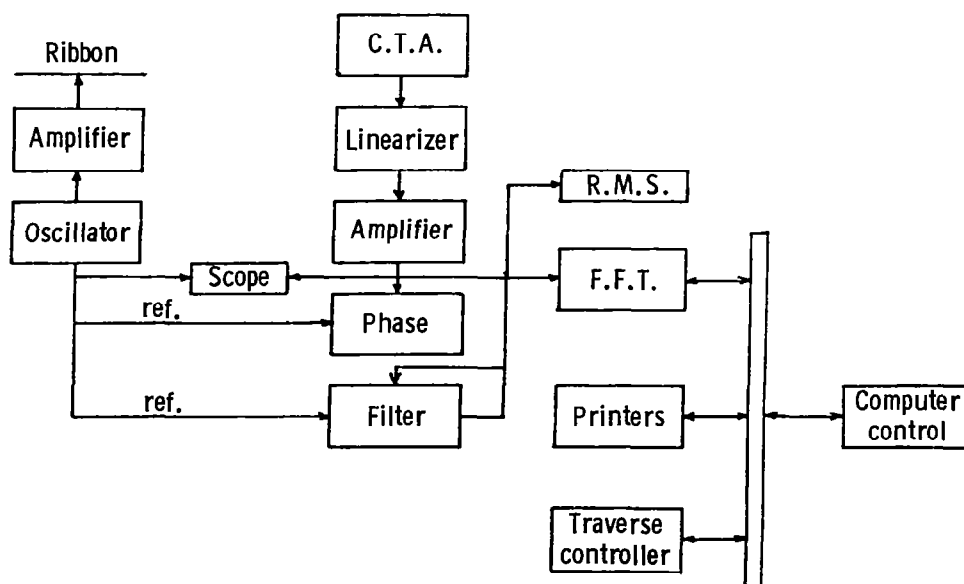


Figure 4

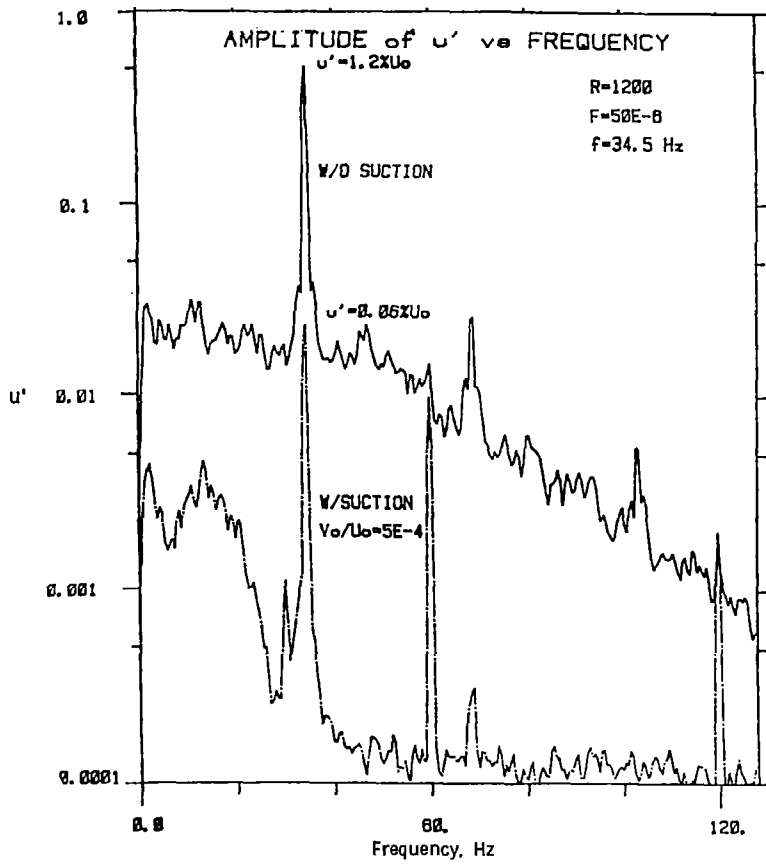


Figure 5

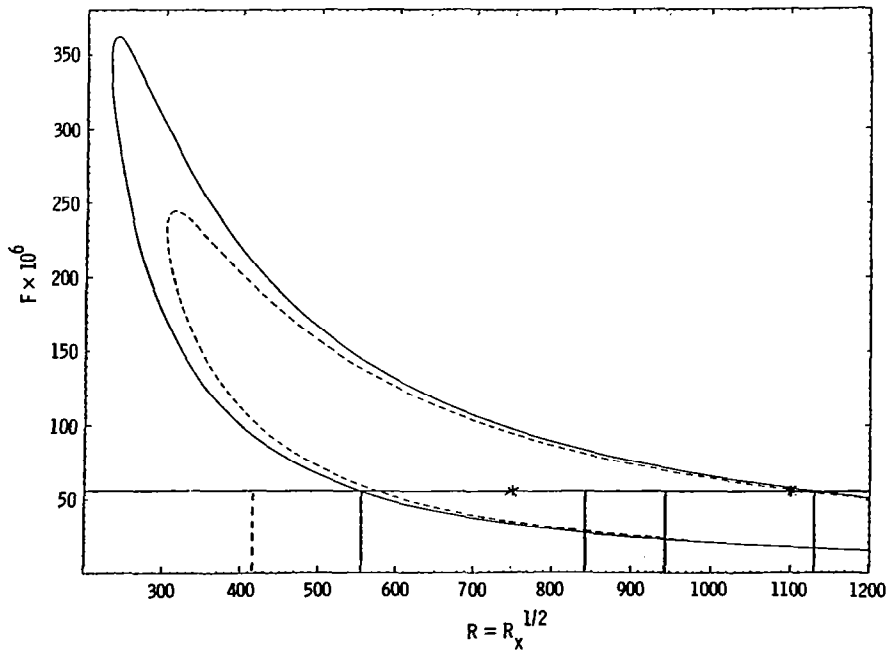


Figure 6

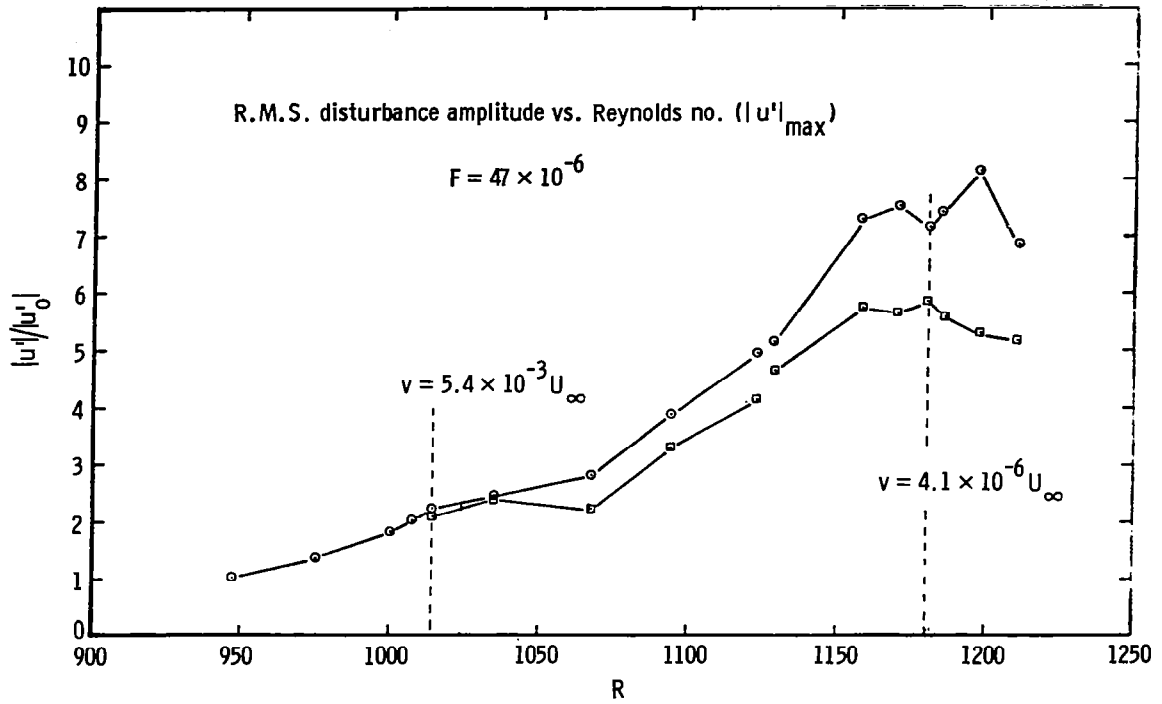


Figure 7

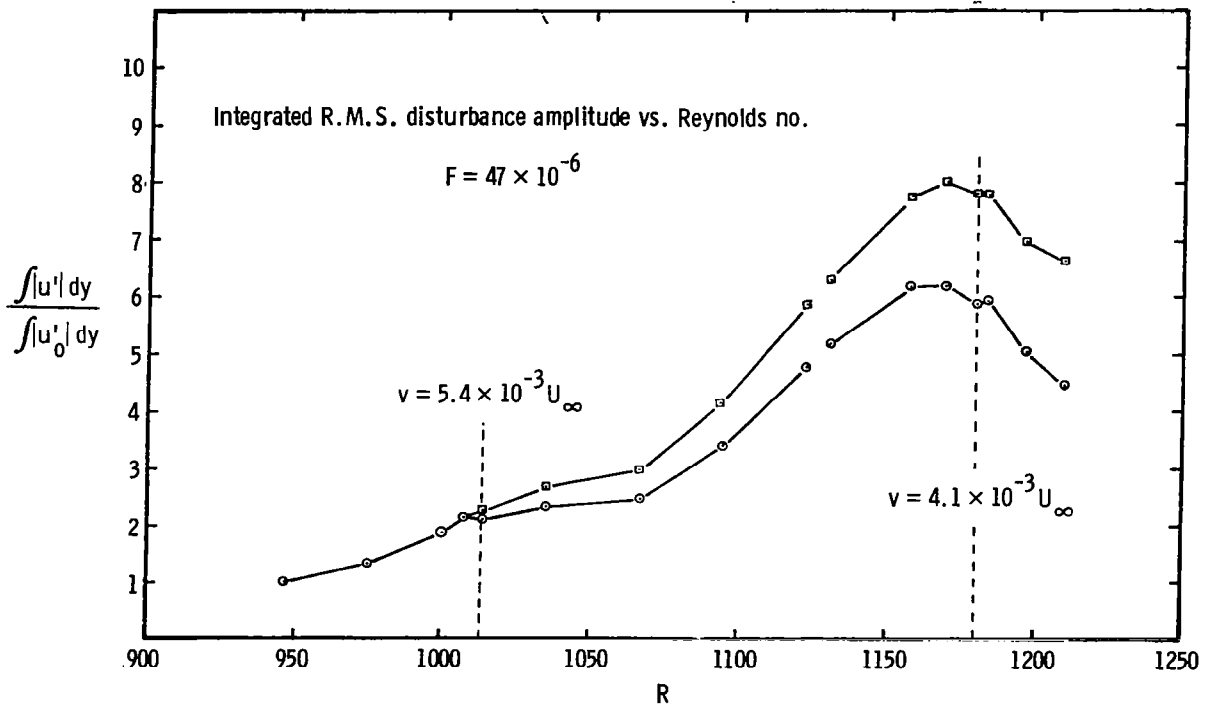


Figure 8

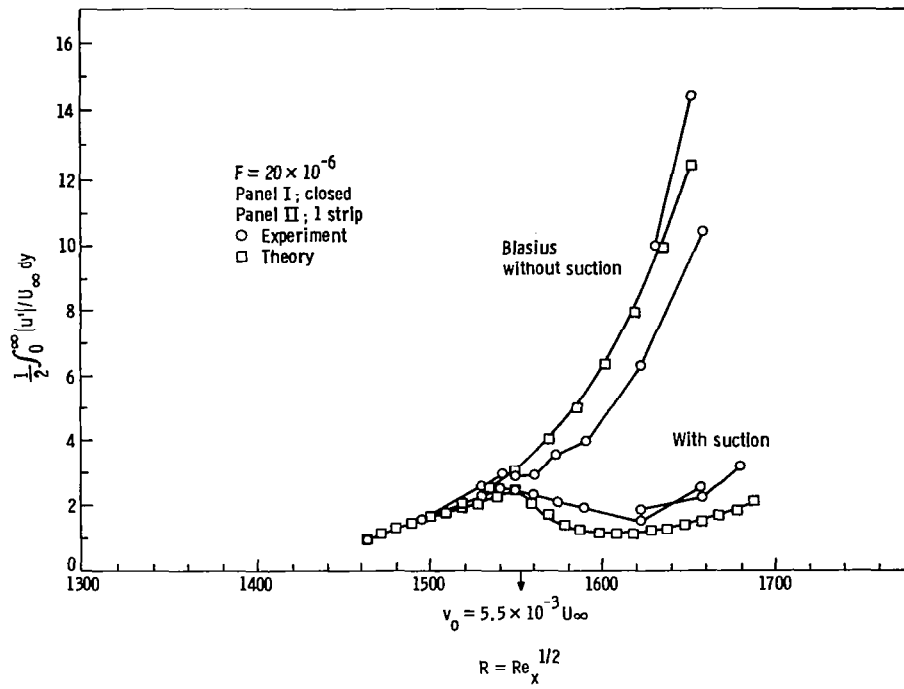


Figure 9

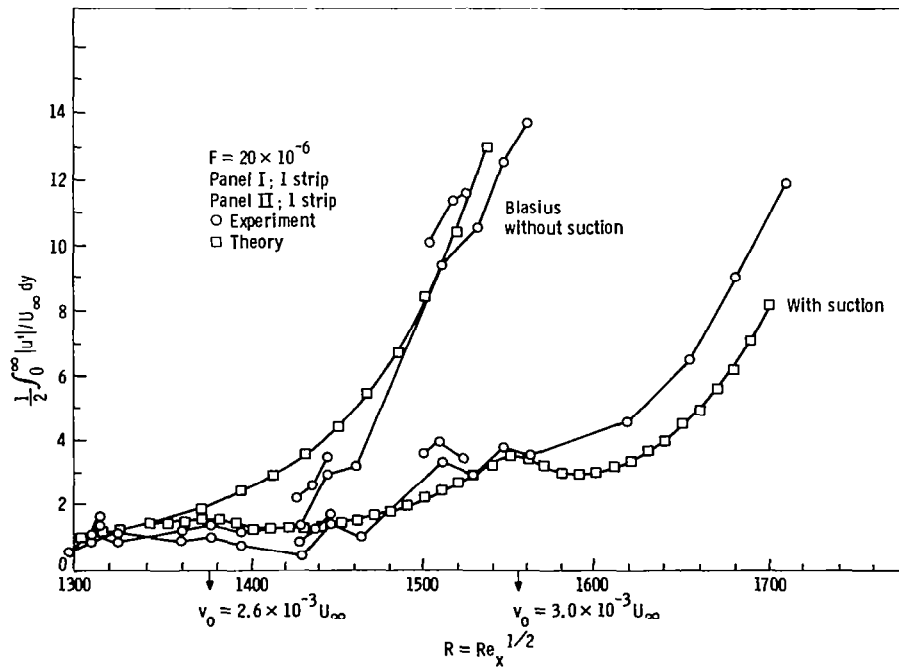


Figure 10

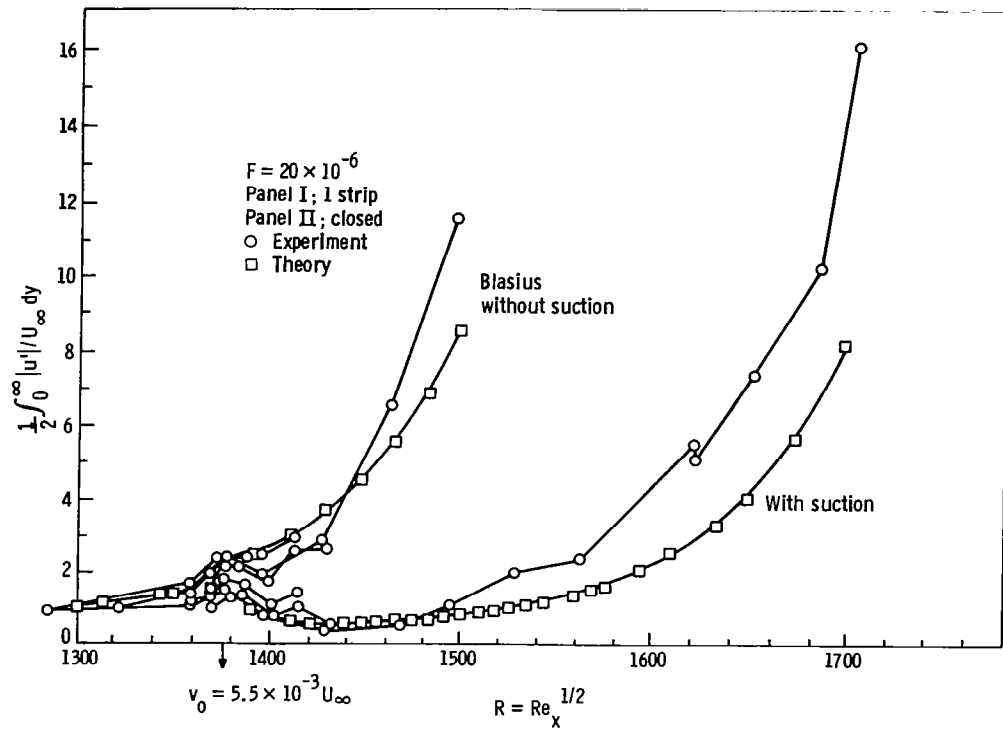


Figure 11

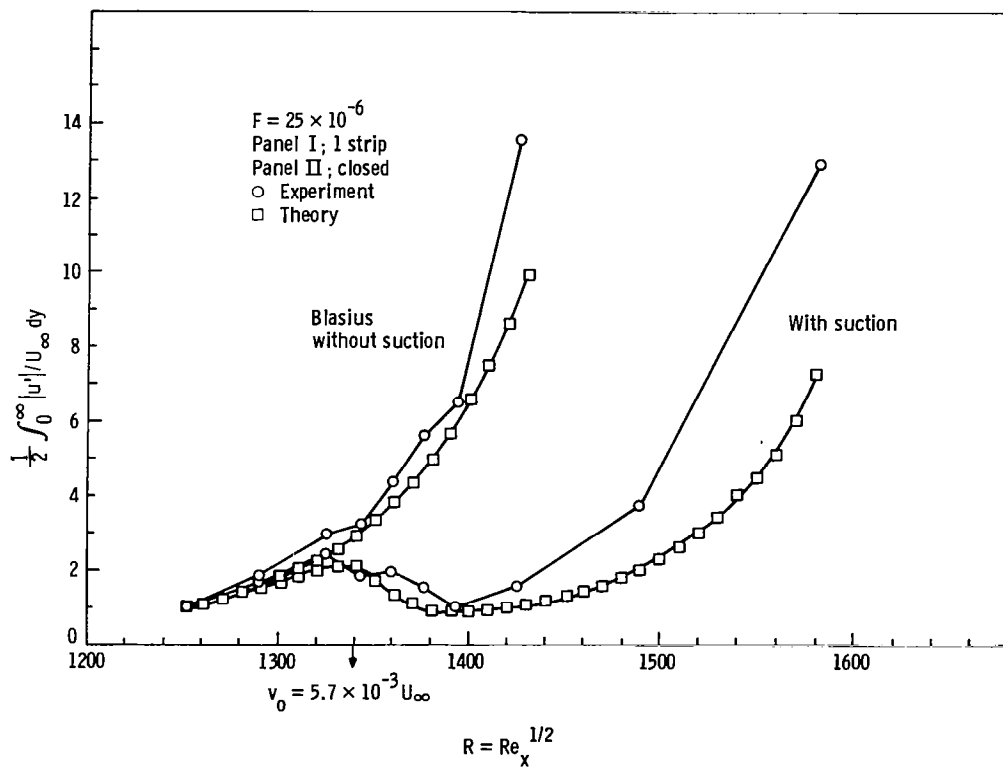


Figure 12

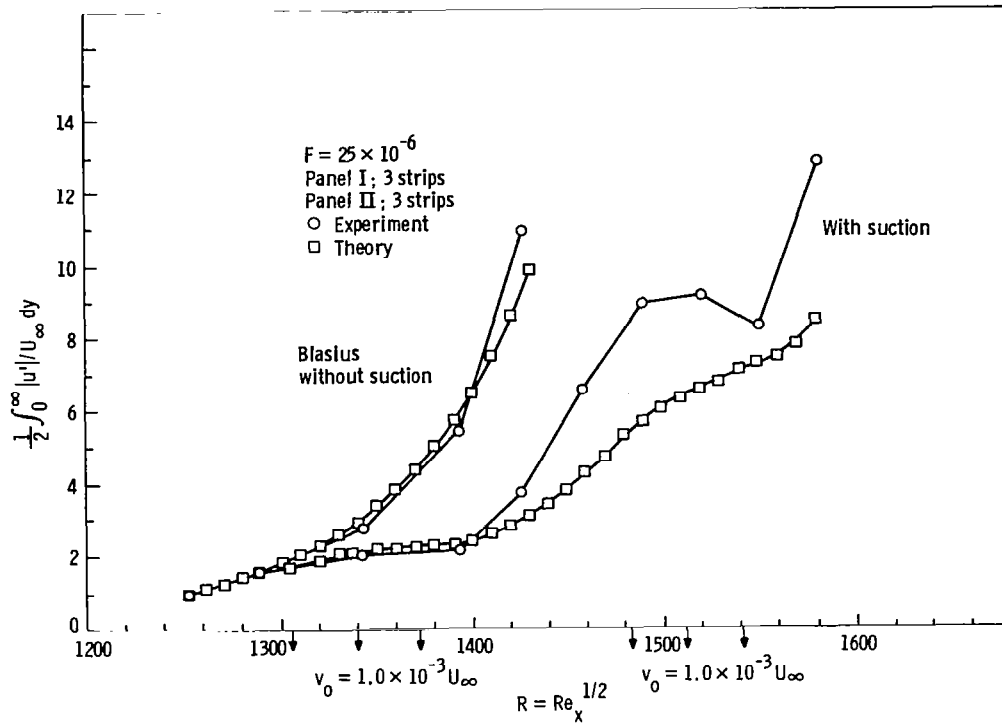


Figure 13

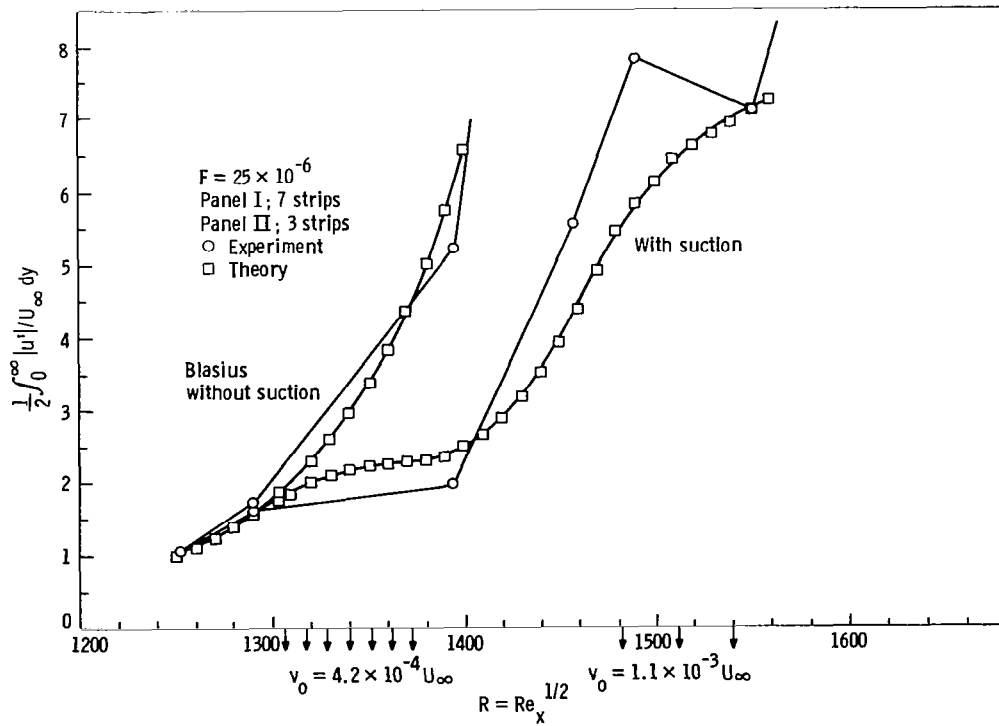


Figure 14

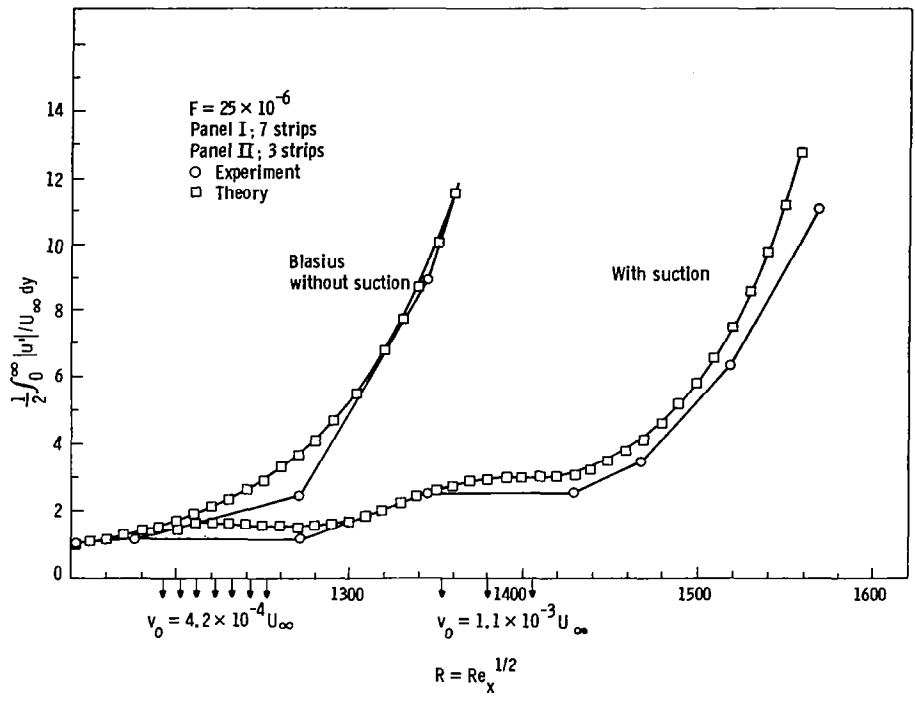


Figure 15

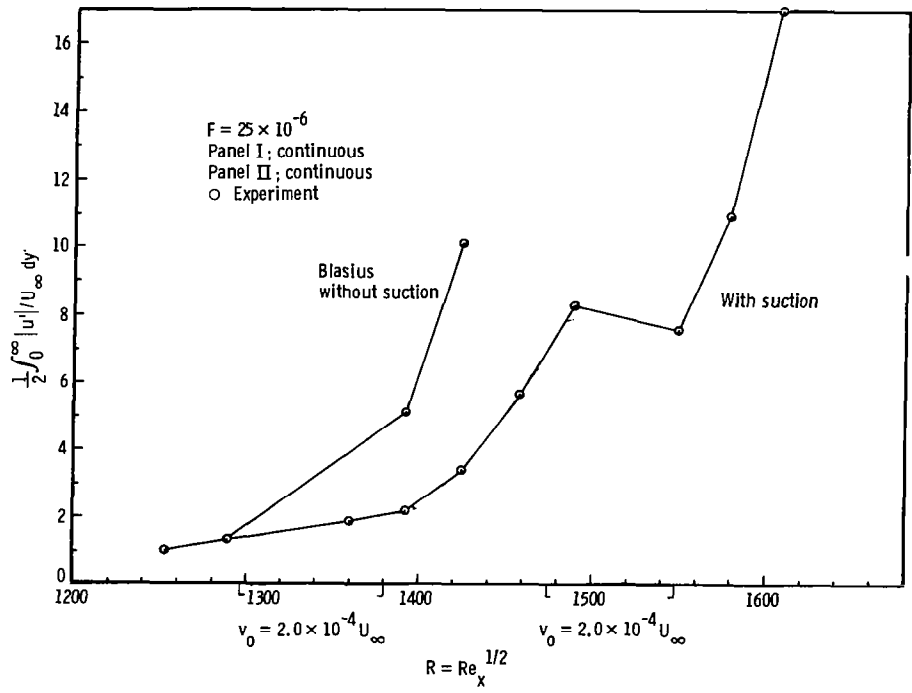


Figure 16

PROBABILITY OF LAMINAR FLOW LOSS
BECAUSE OF ICE CRYSTAL ENCOUNTERS

Richard E. Davis
NASA Langley Research Center
Hampton, Virginia

ABSTRACT

A method has been developed for combining the cloud detector observation results from the NASA Global Atmospheric Sampling Program (GASP) with Knollenberg probe observations of cloud particle concentration from other programs to derive estimates of the ambient concentration of particles larger than a given size. The method has been applied to estimate the probability of encountering particle concentrations which would degrade the performance of laminar flow control (LFC) aircraft. It is concluded that LF loss should occur only about one percent of the time in clear air and that flight within clouds should always result in a significant (≥ 26 percent) loss of LF, with 90 percent LF loss occurring about one percent of the time. Preliminary estimates of cloud encounter probability are presented for four airline routes, and conclusions are presented as to the best altitudes for cloud avoidance in extratropical and tropical latitudes.

BACKGROUND AND PROBLEM DEFINITION

USAF X-21 flights in early 1960's experienced laminar flow (LF) loss within clouds and within "haze". Theoretical analysis by Hall (ref. 1) supports LF loss within cloud particle concentrations. This raises the following two questions:
 1. What is the probability of LF loss because of meteorological factors along various candidate ACEE transport routes/altitude profiles? and its corollary, 2. What is the optimum design altitude profile for acceptable probability of LF loss with ACEE transport?

ASSUMPTIONS

These two assumptions can be made:

1. A route may be described in terms of the following route variables:

- La latitude
- Lo longitude
- H height (i.e., aircraft altitude)
- S season
- M meteorological condition (e.g., jet stream, monsoon, cyclone, anticyclone, etc.)
- T tropopause location

2. The altitude regime of interest for the "ACEE transport" is 25 kft to 45 kft (7.62 - 13.71 km) MSL.

EQUATION FOR PROBABILITY OF LF LOSS

$$P \left\{ \begin{array}{l} \text{LF LOSS} \\ \text{ROUTE} \\ (L_a, L_o, H, S, M, T) \end{array} \right\} = P \left\{ \begin{array}{l} \text{LF LOSS} \\ \text{CLEAR} \\ \text{AIR} \end{array} \right\} * P \left\{ \begin{array}{l} \text{(CLEAR AIR)} \\ \text{ROUTE} \end{array} \right\} \\
 + P \left\{ \begin{array}{l} \text{LF LOSS} \\ \text{HAZE} \end{array} \right\} * P \left\{ \begin{array}{l} \text{(HAZE)} \\ \text{ROUTE} \end{array} \right\} \\
 + P \left\{ \begin{array}{l} \text{LF LOSS} \\ \text{CLOUD} \end{array} \right\} * P \left\{ \begin{array}{l} \text{(CLOUD)} \\ \text{ROUTE} \end{array} \right\}$$

THUS, IT IS NECESSARY IN PRINCIPLE TO DETERMINE OR ESTIMATE THESE SIX PROBABILITY COMPONENTS FOR EACH ROUTE OF INTEREST.

PLAN OF ATTACK

The following steps constitute Stage I of the LaRC/LeRC/contractor effort to characterize LF loss:

1. Assume LF is lost only within clouds
2. Derive cloud encounter statistics from NASA Global Atmospheric Sampling Program (GASP)
3. Analyze for dependence on route variables
4. Obtain initial estimate of cloud encounter probability along routes of interest
5. Determine overall magnitude of cloud encounter problem

If results of Stage I are favorable, then Stage II is implemented:

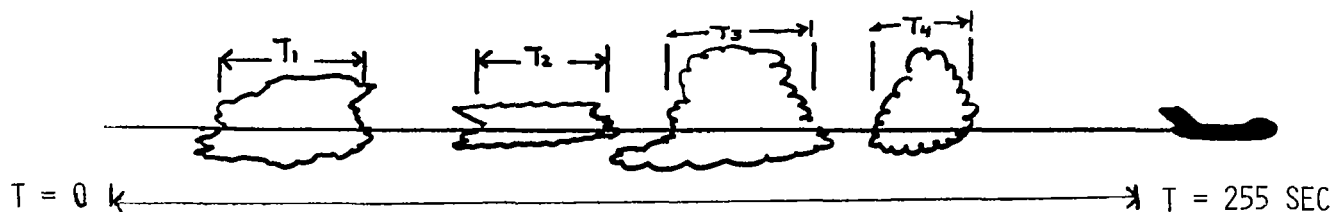
1. Develop method for scaling GASP particle encounter statistics to obtain LF loss statistics
2. Determine probability of LF loss in clear air, haze, and clouds

GASP CLOUD DETECTOR DATA

Each second, a measurement of the concentration (no./m³) of particles larger than 3 μm is taken. If the concentration $> 6.6 \times 10^4/\text{m}^3$, the measurement is defined as a cloud. Measurements are grouped by 255-sec time segments. (At 500 knots, this is a horizontal distance of about 64 km.) For each 255 second segment (schematic below), compute the following:

$$\text{TIC} = \text{percentage time-in-cloud} = \sum_{i=1}^N T_i / 255 \times 100$$

N = number of clouds encountered



STAGE I - DISCUSSION OF GASP CLOUD ENCOUNTER RESULTS

GASP data from 12/75 to 12/77 have been analyzed to date. The remaining 1-1/2 yrs. of GASP data will be analyzed during CY 82. Therefore, the statistics presented here should be regarded as representative, but not final.

The sample to date includes 960 flights and 52 164 cloud encounter observations, 7647 of which were within or near clouds, at an altitude range of 25 to 45 kft MSL. The number of flights along each route having cloud detector observations is presented in table 1. As expected, the preponderance of observations are derived from the principal airline routes.

ROUTE SUMMARY OF FLIGHTS WITH CLOUD ENCOUNTER DATA

Route	1976												1977											
	D	J	F	M	A	M	J	J	A	S	O	N	D	J	F	M	A	M	J	J	A	S	O	N
Chicago - Calif.		5	5	6	8	13																		
Calif-Hawaii	4	5	26	4	16	10				3			10	2	4									
Calif-NE U.S.	2	1	6	1		2							5		1	1	4			1		1	2	4
Hawaii-Chicago	2			6	12	6												12		6	2	12	2	3
NE U.S.-Europe		11			4	13				31									1	6	2	12	2	3
Calif-Tokyo		1		2	1					1			3			1	14		1	6	8	12	8	2
Western U.S.-Europe				2	3														30				1	4
Seattle-Calif				2	2														2					4
Seattle-Hawaii				4	6																			2
New York-S. Amer					1											6								
Calif-S. Amer					3	1				2														
New York-Tokyo													3			1	15	1	3	9	9	11	4	1
S. Asia-Europe		1		2	1				14	1	4		7	8	4								2	
Austr.-S. Asia									14		4		12	10	5									
Hawaii-S. Pacific			2							3	16	2	4	2	4	2	6							4
S. Pacific-																								
Austr/N. Zea			2							3	10	2	4											2
Calif-Austr/N. Zea											10	2	1			1	6	1	3		2			
E. Austr/W. Austr							4			1	3	6	3											
N - above flights	8	24	42	33	66	33			32	35	18		73	38	26	6	35	29	37	25	19	38	22	20
N - all flights	8	30	49	50	86	45	0	0	66	50	0	29	120	60	51	13	36	54	38	29	21	42	37	30

Total flights in table 666
 Total all flights 960
 % of total flights in table 69%

Table 1

DISTRIBUTION OF CLOUD ENCOUNTER OBSERVATIONS

The next four figures, taken from reference 2, show the distribution of the observations used in this study as follows:

Figure 1: By latitude

Figure 2: By season

Figure 3: By altitude band

Figure 4: By distance from the tropopause

As an example, consider figure 1, which gives the distribution by latitude. Considering only the band 40°N to 50°N, note the following:

1. There were approximately 11 300 observations in this band.
2. This comprised 23 percent of the total number of observations.
3. The hatched bars denote observations in the vicinity of clouds. Note that there were 2000 such observations making up 4 percent of the total.
4. The (16) above the hatched bar denotes that for 16 percent of the observations, clouds were noted (civ ≡ clouds-in-vicinity).

Perhaps of most interest here are the numbers above the bars, indicating that the highest probability of cloud encounter occurs near the equator. Recall that all seasons and altitudes have been included.

DISTRIBUTION OF CLOUD DETECTOR OBSERVATIONS BY LATITUDE

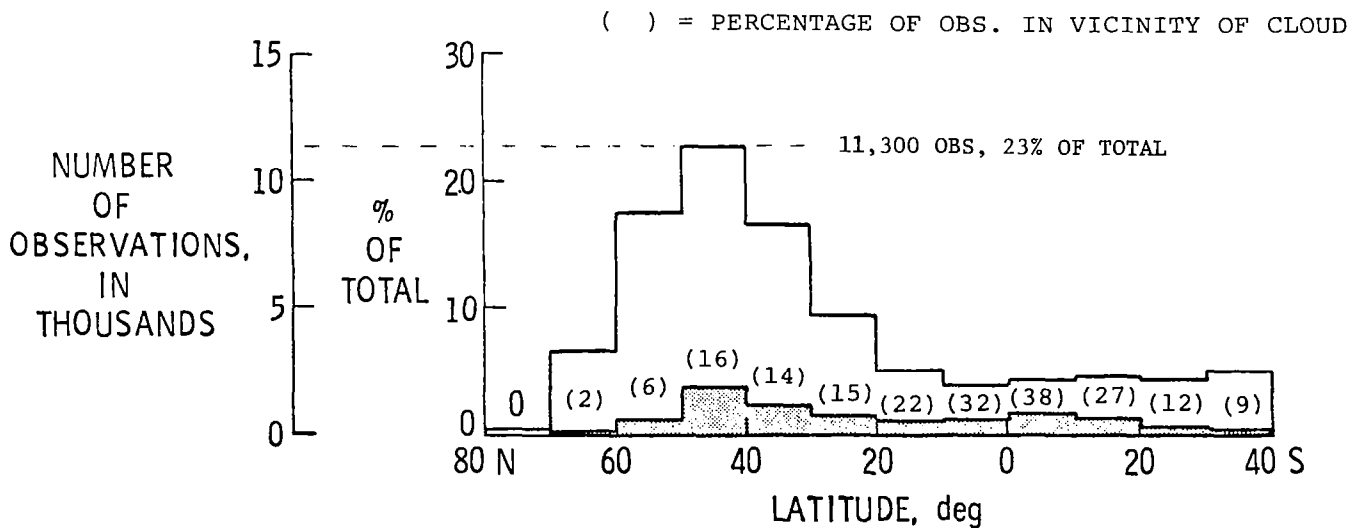


Figure 1

DISTRIBUTION OF OBSERVATIONS BY SEASON

Figure 2 shows the seasonal distribution of observations. Note that there is a higher percentage of cloud encounters in winter. As all altitudes and latitudes have been included, the reason for this is not totally clear, but this probably merely indicates a higher proportion of tropical routes in winter.

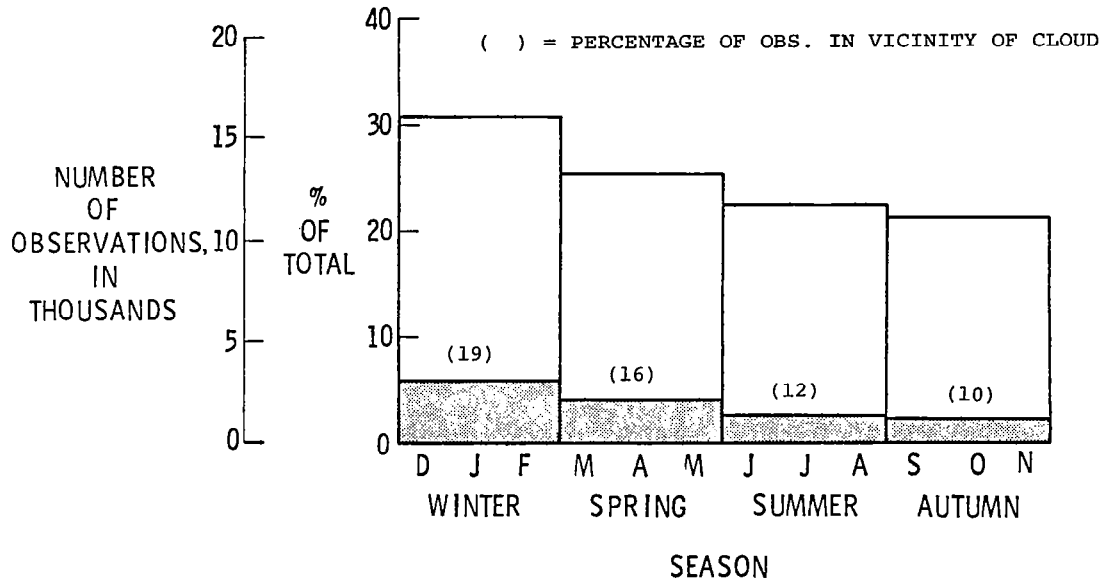


Figure 2

DISTRIBUTION OF OBSERVATIONS BY ALTITUDE

Figure 3 shows, as expected, that the preponderance of data was gathered in these three altitude bands: 28.5-33.5, 33.5-38.5, and 38.5-43.5 kft. Therefore, these three bands were chosen for statistical analysis in the study. Note that the percentages of cloud encounter in these three bands are 20, 16, and 9 percent, respectively. Recall that all latitudes and seasons are included here.

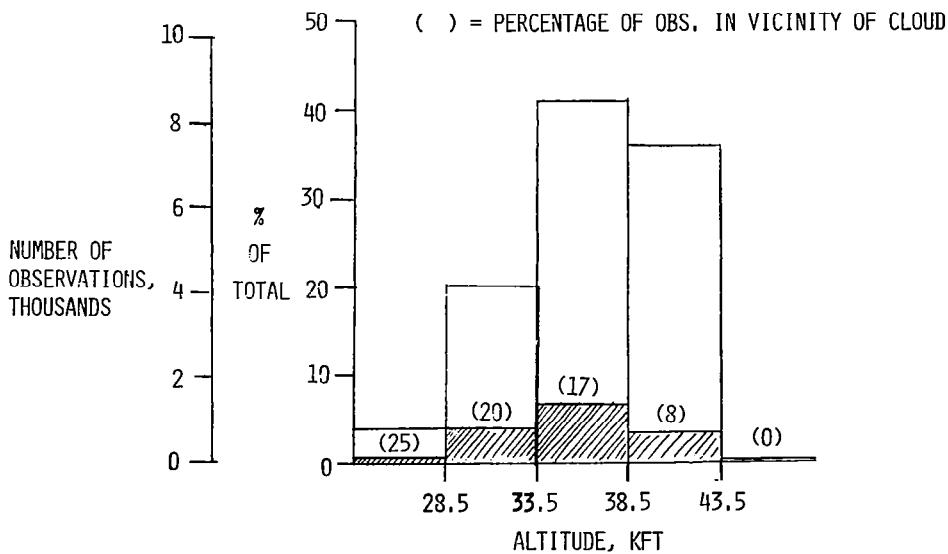


Figure 3

DISTRIBUTION OF OBSERVATIONS BY DISTANCE FROM TROPOPAUSE

Figure 4 shows the distribution of observations by distance from the tropopause. Roughly 2/3 of the observations were taken in the troposphere and 1/3 in the stratosphere. The percentage of cloud encounters decreases markedly above the tropopause. The quick conclusion is to operate in the stratosphere (i.e., above tropopause) everywhere, but the tropopause is > 50 kft in tropics, above the ACEE altitude constraints. Therefore, further statistical study is needed to identify the best altitude within the 25-45 kft constraint.

() = PERCENTAGE OF OBS. IN VICINITY OF CLOUD

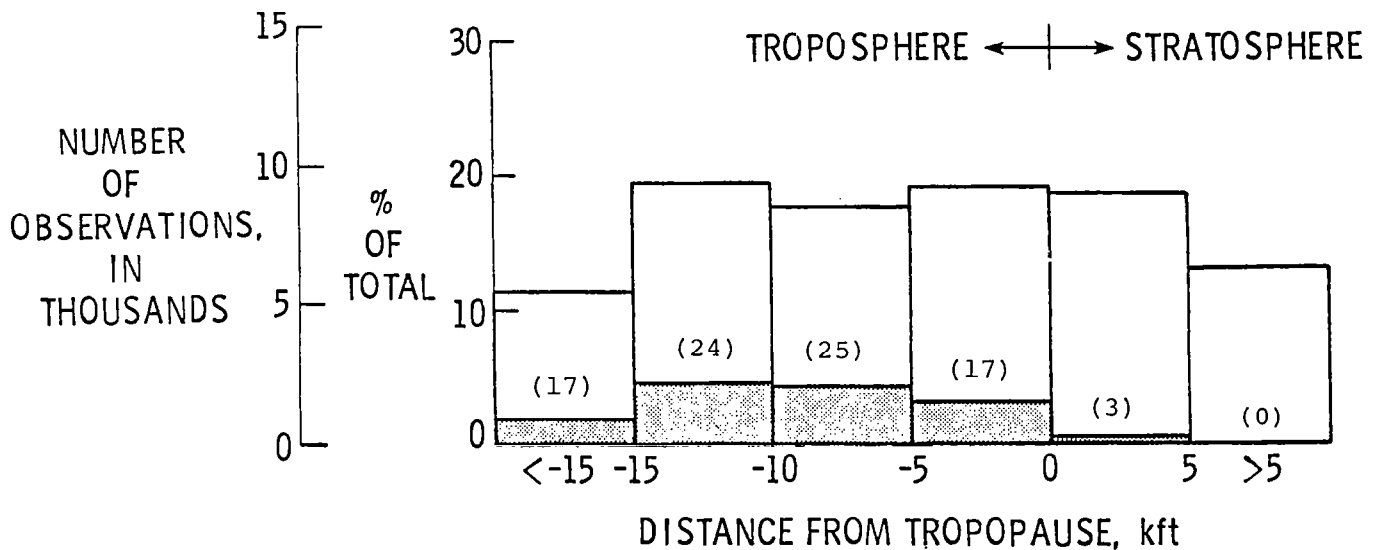


Figure 4

CLOUD ENCOUNTER STATISTICS

Statistics are presented in table 2 for cloud encounter probability during winter over a range of latitudes. An example is presented within the box in the table. We see that, for 35° latitude (band 30-40°N), the following are true:

(A) The probability of cloud encounter ($P(TIC > 0)$) is:

- 2.5 percent in the 38.5-43.5 kft altitude band
- 20.5 percent in the 33.5-38.5 kft altitude band
- 21.8 percent in the 28.5-33.5 kft altitude band

(B) The probability of being in clouds > 10 percent of time ($P(TIC \geq 10\%)$) is:

- 1.1 percent in the 38.5-43.5 kft altitude band
- 16.3 percent in the 33.5-38.5 kft altitude band
- 17.6 percent in the 28.5-33.5 kft altitude band

(C) See table 2 for $P(TIC \geq 25\%)$ and $P(TIC \geq 50\%)$.

Tables 3, 4, and 5 present the same type of data for spring, summer, and autumn, respectively. All these statistics are taken from reference 2.

CLOUD ENCOUNTER STATISTICS - WINTER

WINTER													
LATITUDE:	75.	65.	55.	45.	35.	25.	15.	5.	-5.	-15.	-25.	-35.	
ALT. (KFT)													
					A								
$P(TIC > 0)$													
38.5-43.5		0.0	0.0	12.2	2.5	3.7	15.0	24.9	40.7	54.3	12.5	2.1	
33.5-38.5	0.0	0.0	17.2	20.9	20.5	21.8	10.2	34.6	33.6	25.5	12.2	4.5	
28.5-33.5		1.0	15.8	31.7	21.8	16.0	10.2	24.6	46.8	20.8	17.3	14.9	
					B								
$P(TIC \geq 10\%)$													
38.5-43.5		0.0	0.0	10.8	1.1	2.7	8.6	20.1	34.5	43.8	6.6	1.6	
33.5-38.5	0.0	0.0	14.2	15.8	16.3	17.2	7.8	26.1	24.7	20.1	8.5	6.3	
28.5-33.5		1.0	14.0	25.2	17.6	13.6	9.2	18.3	34.2	14.2	12.5	13.9	
					C								
$P(TIC \geq 25\%)$													
38.5-43.5		0.0	0.0	10.1	1.0	1.5	5.7	16.1	29.1	32.2	5.1	.8	
33.5-38.5	0.0	0.0	12.3	13.5	13.8	11.7	6.5	21.6	18.2	16.5	6.6	4.6	
28.5-33.5		0.0	11.0	20.1	13.6	10.7	8.1	14.1	26.7	9.5	10.7	10.1	
					D								
$P(TIC \geq 50\%)$													
38.5-43.5		0.0	0.0	9.3	.6	.9	1.8	10.8	18.6	19.9	2.9	.5	
33.5-38.5	0.0	0.0	10.1	9.7	10.2	7.1	3.0	13.9	11.6	11.7	4.8	3.6	
28.5-33.5		0.0	6.1	16.7	9.8	7.3	5.7	7.7	15.5	3.9	7.9	7.1	

Table 2

CLOUD ENCOUNTER STATISTICS - SPRING

SPRING												
LATITUDE:	75.	65.	55.	45.	35.	25.	15.	5.	-5.	-15.	-25.	-35.
ALT. (KFT)												
P(TIC>0)											A	
38.5-43.5	0.0	.5	10.1	10.8	8.5	40.9	41.3	53.5	36.6	4.8	9.0	
33.5-38.5	4.0	2.4	10.9	15.8	17.1	23.8	29.2	54.4	36.3	13.3	25.0	
28.5-33.5	0.0	26.8	20.6	26.9	25.2	24.8	13.6	16.0	30.0	29.2	7.7	34.8
P(TIC ₂ 10%)											B	
38.5-43.5	0.0	0.0	7.0	7.9	4.6	32.1	29.6	39.2	27.2	0.0	0.0	
33.5-38.5	0.0	0.0	7.1	11.1	10.4	11.3	14.8	25.0	42.7	22.1	10.0	0.0
28.5-33.5	0.0	22.0	14.2	19.2	12.9	14.0	5.1	4.0	30.0	16.7	0.0	30.4
P(TIC ₂ 25%)											C	
38.5-43.5	0.0	0.0	5.4	6.6	3.3	20.2	25.4	30.4	19.4	0.0	6.0	
33.5-38.5	0.0	0.0	5.8	8.5	7.6	8.7	11.7	18.3	25.2	14.2	10.0	0.0
28.5-33.5	0.0	22.0	10.1	17.4	7.7	10.1	3.4	4.0	10.0	16.7	0.0	24.1
P(TIC ₂ 50%)											D	
38.5-43.5	0.0	0.0	3.9	4.5	1.9	14.5	14.8	18.9	13.3	0.0	5.0	
33.5-38.5	0.0	0.0	3.5	4.9	4.3	4.5	7.6	10.8	14.6	7.1	3.3	0.0
28.5-33.5	0.0	19.5	6.0	8.4	4.1	4.2	1.7	0.0	10.0	8.3	0.0	21.7

Table 3

CLOUD ENCOUNTER STATISTICS - SUMMER

SUMMER												
LATITUDE:	75.	65.	55.	45.	35.	25.	15.	5.	-5.	-15.	-25.	-35.
ALT. (KFT)												
P(TIC>0)												A
38.5-43.5	0.0	.6	1.0	9.6	8.6	4.3	17.9	50.0	73.4	26.8	5.4	2.4
33.5-38.5	7.1	2.7	9.1	30.3	14.4	0.0	58.9	27.1	20.2	2.1	4.5	.7
28.5-33.5			33.8	20.0	4.5	22.6	54.4	44.4	17.8	4.5	4.5	15.7
P(TIC ₂ 10%)												B
38.5-43.5	0.0	.1	.4	5.8	5.3	2.1	10.3	39.1	65.6	22.0	0.0	0.0
33.5-38.5	0.0	1.0	4.7	21.3	10.1	0.0	46.1	18.6	17.6	.7	2.8	.4
28.5-33.5			10.8	11.9	3.4	16.4	44.0	31.6	13.5	4.5	1.1	11.8
P(TIC ₂ 25%)												C
38.5-43.5	0.0	.1	.1	4.0	2.5	2.1	5.1	34.4	53.1	17.1	0.0	0.0
33.5-38.5	0.0	.5	2.9	15.3	7.3	0.0	39.0	14.4	13.4	.7	1.1	0.0
28.5-33.5			6.2	11.1	2.4	12.4	37.9	24.1	7.6	1.3	1.1	6.9
P(TIC ₂ 50%)												D
38.5-43.5	0.0	.1	0.0	2.1	.8	0.0	5.1	28.1	39.1	7.3	0.0	0.0
33.5-38.5	0.0	.2	1.1	8.9	4.1	0.0	24.1	7.6	7.6	.7	0.0	0.0
28.5-33.5			3.1	5.2	1.8	8.6	23.1	9.8	2.2	1.3	0.0	2.9

Table 4

CLOUD ENCOUNTER STATISTICS - AUTUMN

AUTUMN												
LATITUDE:	75.	65.	55.	45.	35.	25.	15.	5.	-5.	-15.	-25.	-35.
ALT. (KFT)												
					A							
P(TIC>0)												
38.5-43.5	0.0	.3	2.4	8.3	8.3	14.5	25.4	7.1	8.3	9.1	2.7	1.9
33.5-38.5	0.0	6.0	6.8	14.8	14.6	6.7	15.7	39.8	22.1	21.4	6.0	4.7
28.5-33.5		62.5	9.8	17.9	12.0	8.3	13.7	36.9	50.0	9.3	27.5	13.9
					B							
P(TIC≥10%)												
38.5-43.5	0.0	.3	1.4	4.7	6.1	4.8	17.5	6.0	4.2	4.5	0.0	0.0
33.5-38.5	0.0	4.1	4.7	9.9	9.2	4.0	12.4	30.1	16.9	13.6	5.2	0.0
28.5-33.5		56.3	7.0	10.6	8.3	7.1	10.7	23.1	34.8	9.3	25.0	12.7
					C							
P(TIC≥25%)												
38.5-43.5	0.0	0.0	.7	3.1	4.6	3.6	11.1	4.8	4.2	2.3	0.0	0.0
33.5-38.5	0.0	2.3	3.4	6.8	6.5	1.8	7.8	22.6	16.9	10.4	5.2	0.0
28.5-33.5		56.3	4.0	8.3	5.3	5.8	7.6	20.0	19.6	9.3	25.0	11.4
					D							
P(TIC≥50%)												
38.5-43.5	0.0	0.0	.1	1.4	3.6	2.4	6.3	2.4	2.8	2.3	0.0	0.0
33.5-38.5	0.0	0.0	1.9	4.2	4.4	.4	5.9	14.0	10.3	5.8	4.3	0.0
28.5-33.5		50.0	3.0	4.6	3.0	5.8	5.6	10.8	8.7	4.7	17.5	10.1

Table 5

PRELIMINARY ESTIMATES OF CLOUD ENCOUNTER PROBABILITY FOR THREE ROUTES

In table 6, the routes JFK-LHR, JFK-LAX, and LAX-HNL are described for summer and winter. As an example, consider only the route JFK-LAX, using the format of the code block. For the summer, in the 33.5-38.5 kft altitude band, there were 14 observations (NOBS). The probability of cloud encounter is 50 percent; the probability of being in clouds for over 10 percent of the route is 21.4 percent; the probability of being in clouds more than 25 percent of the route is 7.1 percent; and the probability that more than 50 percent of the route is in clouds is 0. For the winter, there are more observations (277) and higher confidence. There is a 23.1 percent probability of cloud encounters and a 12.3 percent probability that 50 percent of the route will be within clouds.

For winter (same route), it is interesting to compare the probability of cloud encounter for the 3 altitude bands. In the 28.5-33.5 kft band there is a 34.7 percent probability of encountering clouds. In the middle altitude band, we have 23.1 percent, as discussed earlier. In the highest altitude band, there is only a 0.8 percent probability of cloud encounter. The marked superiority of the uppermost altitude band is also apparent in the statistics for the JFK-LHR and LAX-HNL routes.

The sample sizes in some of the blocks are too small for statistical confidence. In the next phase of the study all GASP data will be included and higher statistical confidence will result.

CODE:

ALT. BAND

	NOBS
ROUTE	P(TIC > 0%)% P(TIC ≥ 10%)%
	P(TIC ≥ 25%)% P(TIC ≥ 50%)%

SUMMER

WINTER

ROUTE	ALTITUDE BAND (Kft)						LAT. /LONG. CELL ON ROUTE	ALTITUDE BAND (Kft)					
	28.5 - 33.5		33.5 - 38.5		38.5 - 43.5			28.5 - 33.5		33.5 - 38.5		38.5 - 43.5	
JFK-LHR	NO DATA		17 0 0 0 0	262 0.8 0.8 0.8 0.8		30-75 W/ 50-60 N	50 20.0 16.0 6.0 2.0		89 31.5 27.0 25.8 23.5		12 0 0 0 0		
JFK-LAX	4 25.0 25.0 0 0	14 50.0 21.4 7.1 0		17 5.9 5.9 0 0			30-40 N/ 75-120 W	72 34.7 29.2 25.0 18.1		277 23.1 19.1 17.0 12.3		262 0.8 0.4 0.4 0.4	
LAX-HNL	7 0 0 0 0	29 0 0 0 0		41 0 0 0 0		20-30 W/ 120-165 W		259 20.8 17.0 12.7 9.3		869 20.0 15.5 10.9 6.8		320 3.8 2.8 1.6 0.9	

Table 6

PRELIMINARY ESTIMATES OF CLOUD ENCOUNTER PROBABILITY ON LOS ANGELES - TOKYO ROUTE

In table 7, the long Los Angeles-Tokyo (LAX-HND) route is simulated by the statistics of several adjacent latitude/longitude cells from the grid in reference 2. The superiority of the uppermost altitude band over this latitude range is again apparent. For this route, just as in the preceding example, there is generally less chance of cloud encounters in winter than in summer. (This is probably due to less convective activity in winter.) Intercomparison of the lower two altitude bands is difficult due to sample size problems and meteorological effects. It is planned to repeat this analysis for this and several other routes in the next phase of the study.

	NOBS			
CODE:	P(TIC > 0%)%	P(TIC ≥ 10%)%		
	P(TIC ≥ 25%)%	P(TIC ≥ 50%)%		

ROUTE SEGMENT (APPROX) AND LAT./LONG. CELL	SUMMER						WINTER					
	ALTITUDE BAND (KFT)						ALTITUDE BAND (KFT)					
	28.5 - 33.5		33.5 - 38.5		38.5 - 43.5		28.5 - 33.5		33.5 - 38.5		38.5 - 43.5	
1. LAX - 35 N/120 W 30-40 N/75 - 120 W	4 25.0 0 0	14 25.0 21.4 7.1 0	17 5.9 5.9 0 0	72 34.7 29.2 25.0 18.1	277 23.1 19.1 17.0 12.3	262 0.8 0.4 0.4 0.4						
2. 35 N/120 W - 40 N/125 W 30-40 N/120-165 W	30 23.3 16.7 6.7 6.7	130 9.2 5.0 4.2 1.7	173 6.4 3.5 1.2 0	267 22.8 17.6 12.0 8.2	682 21.3 16.6 13.8 10.3	351 4.6 2.0 1.7 0.9						
3. 40 N/125 W 50 N-145 W 40-50 N/120-165 W	7 14.3 0 0 0	206 33.5 22.8 15.5 5.8	317 14.2 8.2 4.4 1.3	16 37.5 25.0 12.5 6.3	63 25.4 20.6 17.6 4.8	29 3.4 0 0 0						
4. 50 N/145 W-55 N/165 W 50-60 N/120-165 W	NO DATA	113 18.6 8.8 5.3 0.8	143 0 0 0 0	14 0 0 0 0	43 0 0 0 0	42 0 0 0 0						
5. 55 N/165 W-50 N/165 E 50-60 N/165 W-150 E	NO DATA	111 9.9 4.5 0.9 0	366 2.5 1.1 0.5 0	NO DATA	39 0 0 0 0	85 0 0 0 0						
6. 50 N/165 E-40 N/150 E 40-50 N/165 W-150 E	NO DATA	352 38.6 26.7 18.8 12.2	384 9.6 6.0 3.9 1.8	NO DATA	33 0 0 0 0	46 0 0 0 0						
7. COMPOSITE 3-6 35 N/ 120 W-40 N/150 E 40-60 N/120 W-150 E	INSUFF. DATA	782 30.3 19.9 13.4 7.2	1210 7.5 4.4 2.6 0.9	INSUFF. DATA	178 9.0 7.3 6.2 1.7	196 0.5 0 0 0						
8. 40 N/ 150 E - HND 30-40 N/150-105 E	28 28.6 25.0 25.0 17.9	117 40.2 29.9 23.1 15.4	103 15.5 8.7 3.9 2.9	13 0 0 0 0	20 0 0 0 0	18 0 0 0 0						

Table 7

PRELIMINARY CONCLUSIONS FROM STAGE 1

An analysis of 2 years of GASP cloud encounter measurements yields the following conclusions:

1. On the average, cloud encounters occur on about 15 percent of the data samples available worldwide (25-45 kft, all seasons and latitudes).
2. Cloud encounter frequency varies with season, latitude, synoptic weather situation, and, especially, distance from the tropopause.
3. Cloud encounter frequency for various routes may be estimated from the data. As demonstrated, some routes should present no LF problems, others some LF degradation.
4. Poleward of 25° latitude, flight in the 38.5-43.5 kft altitude band gives best probability of cloud avoidance.
5. Within 25° of the equator, the 33.5-38.5 kft band appears to be the best.

STAGE II - ESTIMATION OF DEGREE OF LF LOSS IN CLOUDS AND CLEAR AIR:
 "THE HALL CRITERIA"

Hall (ref. 1) performed the only known analytical investigation of LF loss in clouds. The problem is treated as one of particles in a gas flow. A particle imbedded in laminar boundary layer gas flow generates a wake vortex. If the particle concentration is high enough, the laminar boundary layer is destroyed and LF is lost. The degree of LF loss is greater for larger particles and at higher particle concentrations.

An example of the Hall curve for 40 kft and Mach 0.75 is shown in figure 5. Note the following characteristics:

1. The curve for threshold of LF loss (seperates partial loss and no-loss areas)
2. The curve for total LF loss (seperates total loss and partial loss areas)
3. There is no loss of LF for particles $< 33 \mu\text{m}$ diameter, regardless of particle concentration
4. There is no loss of LF loss if particle concentration $< 350/\text{m}^3$, regardless of particle size
5. There is total loss of the LF if the concentration of particles $> 33 \mu\text{m}$ is $\geq 1.9 \times 10^5/\text{m}^3$ or, for example, if the concentration of particles $> 60 \mu\text{m}$ is $\geq 1.3 \times 10^5/\text{m}^3$, and so forth
6. Between conditions 4 and 5, partial loss of LF is experienced

PREDICTED LFC PERFORMANCE WITHIN CLOUDS AT 40,000 FT (12.19 KM) AND 0.75 MACH

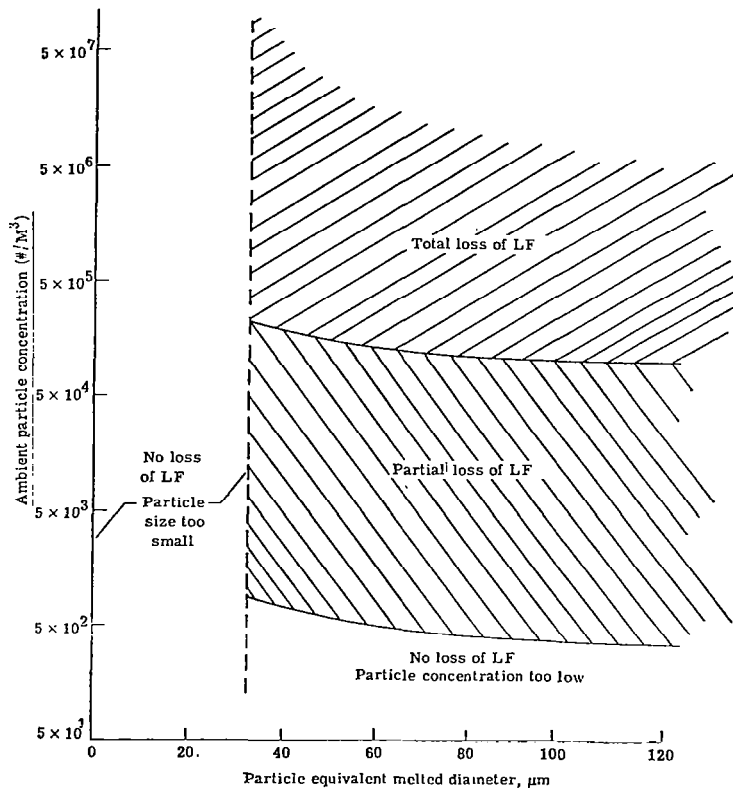


Figure 5

REMARKS ON USE OF HALL MODEL

The following cautions should be applied to use of the Hall model:

1. The model was developed based on 5:1 aspect ratio elliptical airfoil cross section.
2. The model was derived assuming all ice-cloud particles are hexagonal prisms with 2.5:1 aspect ratio. It has since been found that other shapes are more commonly encountered in ice crystal clouds.
3. The model was never verified in LFC operation, as no cloud particle spectrometers were flown (or even available).

However, Hall's is the only model known. Therefore, we will use it with caution in making preliminary estimates. The first verification of the Hall criteria awaits the NASA ACEE LEFT (Leading-Edge Flight Test) Program, to begin in 1983.

SCALING OF GASP RESULTS

The GASP particle counter registers the total concentration for all particles larger than $3 \mu\text{m}$ in diameter. Yet we have seen from Hall's work that only particles larger than $33 \mu\text{m}$ at 40 kft and $18 \mu\text{m}$ at 25 kft would cause LF problems. Therefore, it was necessary to develop a method for scaling each GASP observation to derive the number of particles within the observation that were of sufficient diameter to affect LFC. A method for doing this is described hereinafter.

SCALING CONCEPT

The following steps are used in this scaling concept:

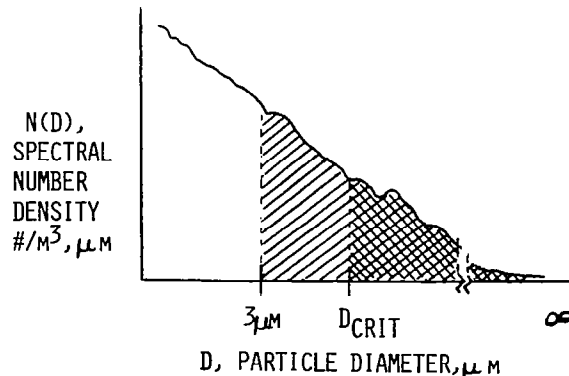
1. Consider cloud particle spectra, derived from Knollenberg probe measurements, as in the figure.
2. Derive scaling factor R (defined as ratio of areas in the accompanying fig.)
3. Repeat derivation for as many measurements as can be obtained from subsets for a similar season, latitude, longitude, altitude, and cloud type.
4. Obtain statistical data on R for each subset.
5. Results:

$$R_{\min} \cong 10 \text{ (cloud bases)}$$

$$R_{\max} \cong 1000 \text{ (very thin cirrus)}$$

$$\bar{R} \approx 100$$

$$R_{\text{mode}} \cong 30$$



APPLICATION OF SCALING FACTOR R TO GASP DATA

The crucial assumption is that the R values derived from the comparatively few Knollenberg probe data (source is refs. 3-10) are representative and can be used to scale the abundant GASP data to derive statistics meaningful for LF impact studies. The method is the following:

1. Obtain GASP measurement ($= \int_{3\mu\text{m}}^{\infty} N(D)dD$)
2. Divide by an R value appropriate for cloud type, latitude, season, etc.
3. Result = $\int_{\text{LF crit. size}}^{\infty} N(D)dD$, the number of particles affecting LFC
4. Study statistics of this result
5. Estimate percentage LF loss (percentage of wing area which loses LF when encountering this particle concentration) from Hall curves

PRELIMINARY CONCLUSIONS FROM STAGE II - GASP PARTICLE CONCENTRATION STATISTICS
AND PERCENTAGE LF LOSS

Statistics of ambient particle concentrations, in clear air and haze + clouds, were derived. Concentrations were divided by the scaling factor R (R = 10 and R = 30 were used for conservatism). Conclusions for R = 30 are the following (see table 8):

1. In clear air, LF is lost \approx 1 percent of the time.
2. In clouds and haze, LF loss is always significant:

100 percent prob. of \geq 26 percent LF loss
 28 percent prob. of \geq 65 percent LF loss
 55 percent prob. of \geq 51 percent LF loss
 1 percent prob. of \geq 89 percent LF loss

Note that these statistics could be used to convert cloud encounter probabilities to LF loss probabilities.

CUMULATIVE PROBABILITY DISTRIBUTIONS OF PARTICLE CONCENTRATIONS N
IN CLOUDS AND CLEAR AIR, DERIVED FROM GASP DATA,
TOGETHER WITH ESTIMATED DEGREE OF LF LOSS

(ALL SEASONS, ALTS., LATS. INCLUDED)

N_0 #PARTICLES/M ³ ($>3\mu\text{M}$ DIAM.)	$P(N \geq N_0)$ IN "CLEAR AIR," %	EST. DEGREE OF LF LOSS (R = 10), %	EST. DEGREE OF LF LOSS (R = 30), %	$P(N \geq N_0)$ IN CLOUD, %
10	32.0	0	0	100.
10^2	12.0	0	0	100.
3×10^2	5.8	0	0	100.
10^3	2.6	0	0	100.
3×10^3	1.3	0	0	100.
10^4	0.3	12.1	0	100.
3×10^4	0	30.4	12.1	100.
5×10^4	0	38.9	20.7	100.
7×10^4	0	44.5	26.4	100.
10^5	0	50.4	32.4	90.
3×10^5	0	68.7	50.8	55.
7×10^5	0	82.8	65.1	27.2
10^6	0	88.7	71.1	16.8
3×10^6	0	100.0	89.6	1.3

Table 8

WORK REMAINING AND TENTATIVE SCHEDULE

Analyses of complete GASP data archive (late 1983) will provide:

Better statistical base

More routes analyzed for probability of cloud encounter

More extensive meteorological analysis

Completion of LF impact assessment studies (late 1983) will provide:

More analysis of R values for various cloud types

Development of LF loss estimates for a wide variety of routes

Recommendation of optimal LF altitude structure for different geographic regimes

Comprehensive error analysis of GASP-Knollenberg-R value technique

Validation of Hall criteria with flights of Knollenberg probes aboard ACEE-LEFT research missions

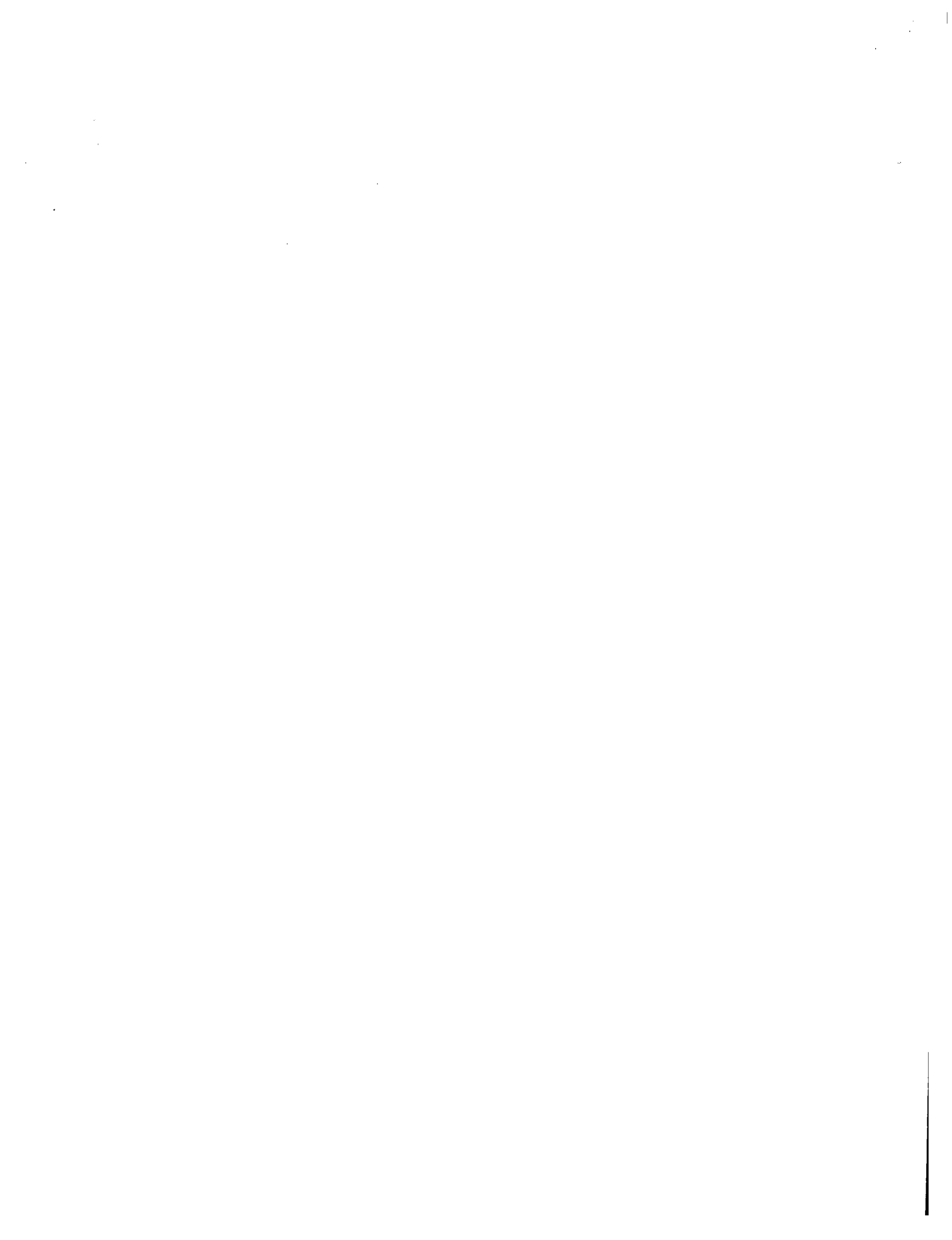
RESEARCH AND REPORTING

NO.	STEP	DATA SOURCE	RESEARCHERS	REFERENCES
1	Determine probability of cloud encounter (route, alt., season, etc.)	GASP	Nastrom Holdeman Davis	2
2	Determine total particle concentrations in clouds, clear air, haze	GASP	Nastrom Holdeman	2
3	Determine typical particle spectra in clouds*	USAF, Aeromet Corp.	Varley, Cohen, Barnes, Brooks, and Plank	3-10
4	Determine scaling relationships	USAF	Davis	This Conf.
5	Apply scaling relationships to GASP data	USAF	Davis	This Conf.
6	Estimate degree of LFC loss	All above + Hall report	Davis	This Conf., 1

*Independent of NASA research

REFERENCES

1. Hall, G. R.: On the Mechanics of Transition Produced by Particles Passing Through an Initially Laminar Boundary Layer and the Estimated Effect on the LFC Performance of the X-21 Aircraft. Northrop Corp., Oct. 1964.
2. Nastrom, G. D.; Holdeman, J. D.; and Davis, R. E.: Cloud Encounter and Particle Concentration Variabilities From GASP Data. NASA TP-1886, 1981.
3. Varley, D. J.: Cirrus Particle Distribution Study, Part 1. AFGL-TR-78-0192, Air Force Surveys in Geophysics, No. 394, Aug. 1978.
4. Plank, V. G.: Hydrometeor Parameters Determined from the Radar Data of the SAMS Rain Erosion Program - AFCRL/SAMS Report No. 2. AFCRL-TR-0249, Environmental Research Papers, No. 477, Jun. 1974.
5. Varley, D. J.; and Brooks, D. M.: Cirrus Particle Distribution Study, Part 2. Air Force Surveys in Geophysics, No. 399, AFGL-TR-78-0248, October 10, 1978, pp. 108.
6. Varley, D. J.: Cirrus Particle Distribution Study, Part 3. Air Force Surveys in Geophysics, No. 404, AFGL-TR-78-0305, December 11, 1978.
7. Varley, D. J.; and Barnes, A. A.: Cirrus Particle Distribution Study, Part 4. Air Force Surveys in Geophysics, No. 413, AFGL-TR-79-0134, June 18, 1979, pp. 91.
8. Cohen, I. D.: Cirrus Particle Distribution Study, Part 5. Air Force Surveys in Geophysics, No. 414. AFGL-TR-79-0155, July 13, 1979, pp. 81.
9. Cohen, I. D.; and Barnes, A. A.: Cirrus Particle Distribution Study, Part 6. Air Force Surveys in Geophysics, No. 430, AFGL-TR-80-0261, September 4, 1980, pp. 106.
10. Varley, D. G.; Cohen, I. D.; and Barnes, A. A.: Cirrus Particle Distribution Study, Part 7. Air Force Surveys in Geophysics, No. 433, AFGL-TR-80-0324, October 16, 1980, pp. 78.



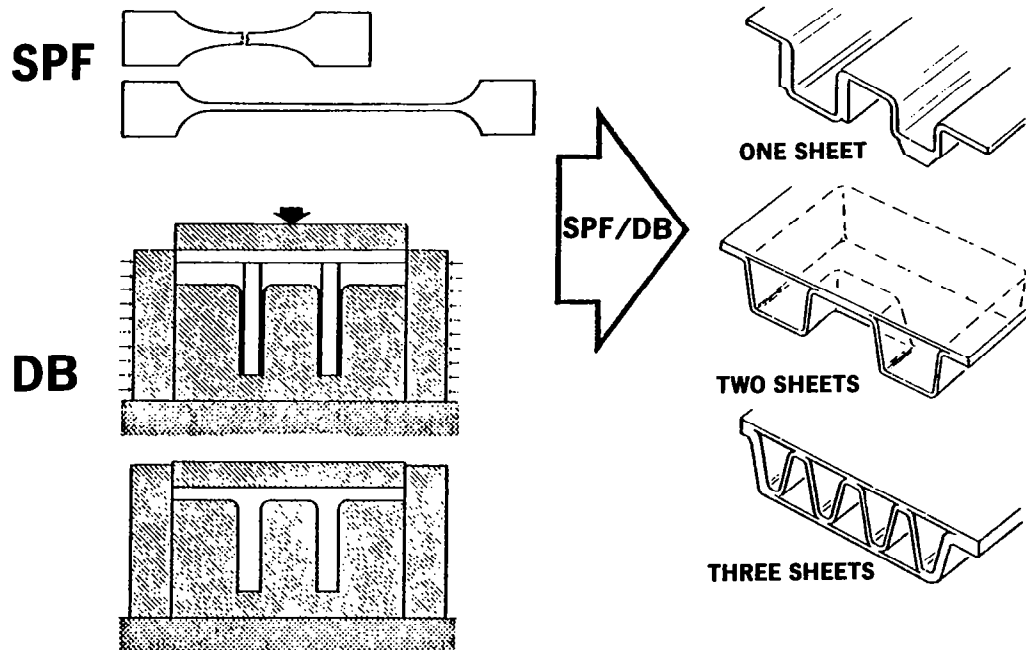
SPF/DB TITANIUM CONCEPTS
FOR STRUCTURAL EFFICIENCY

V. E. Wilson
North American Aircraft Division
Rockwell International Corp.
Los Angeles, California

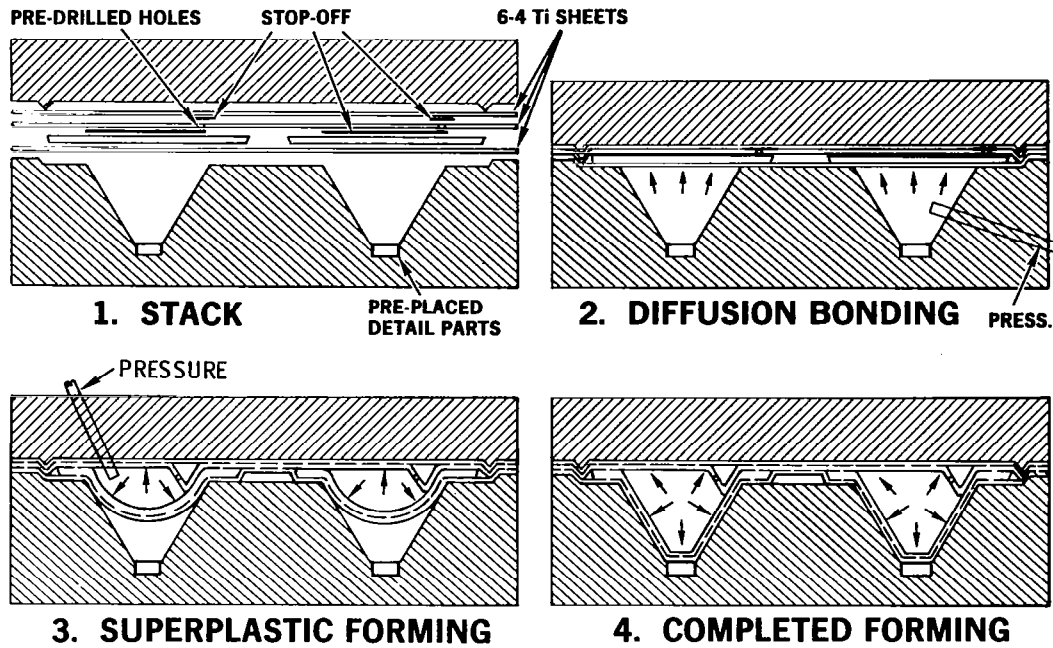
OBJECTIVES

- Determine applicability of SPF/DB Ti to LFC
 - Design concepts
 - Sub-scale fabrication
- Optimize approach to:
 - Design
 - Fabrication
 - Maintenance
- Demonstrate feasibility
 - LFC surface quality
 - Replaceable LFC strips

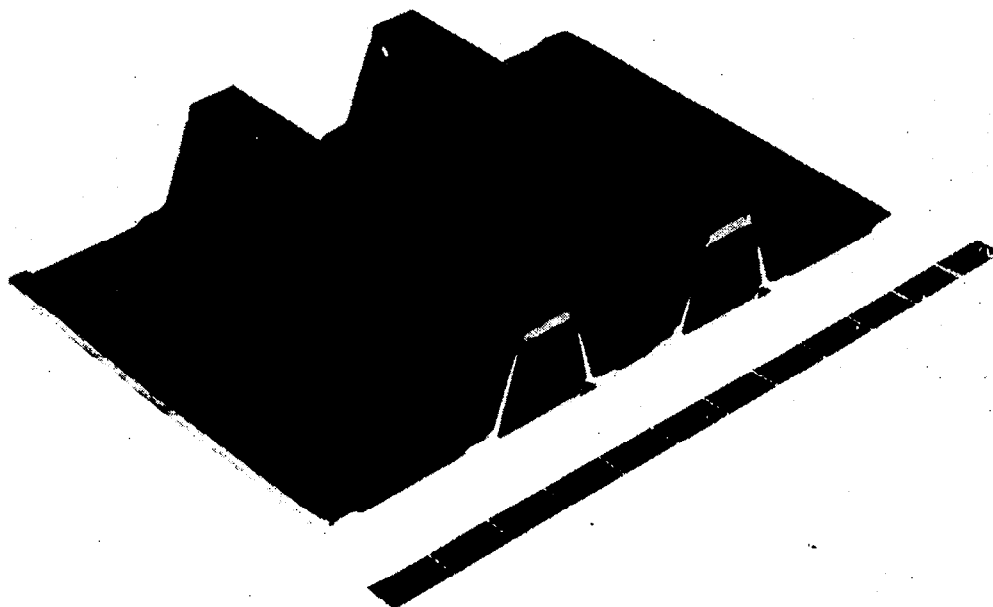
WHAT IS SUPERPLASTIC FORMING/ DIFFUSION BONDING (SPF/DB)?



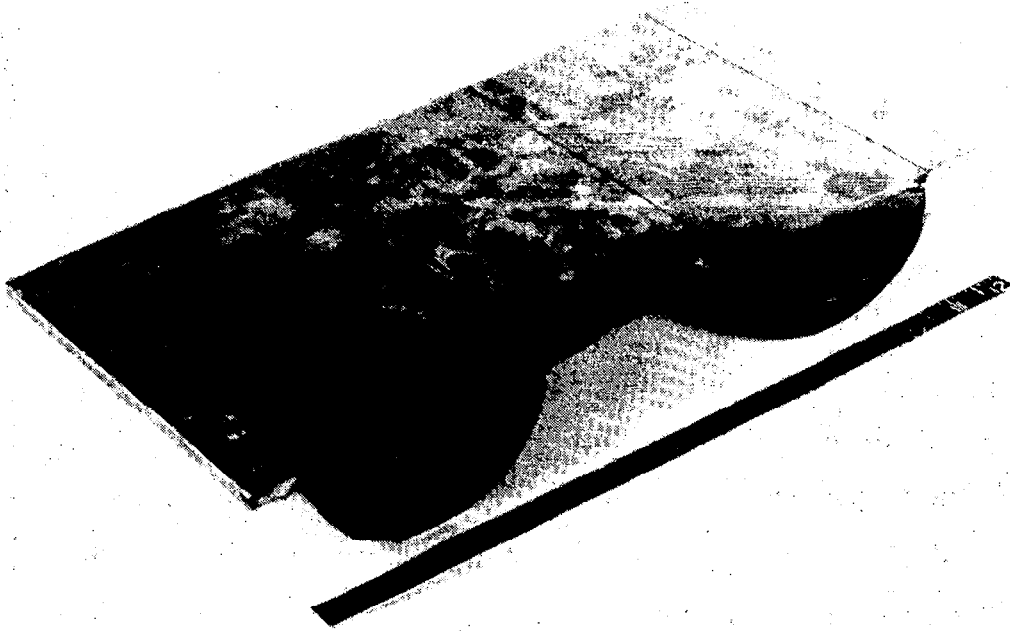
HAT SECTION STIFFENED SKIN PANEL FORMING PROCESS



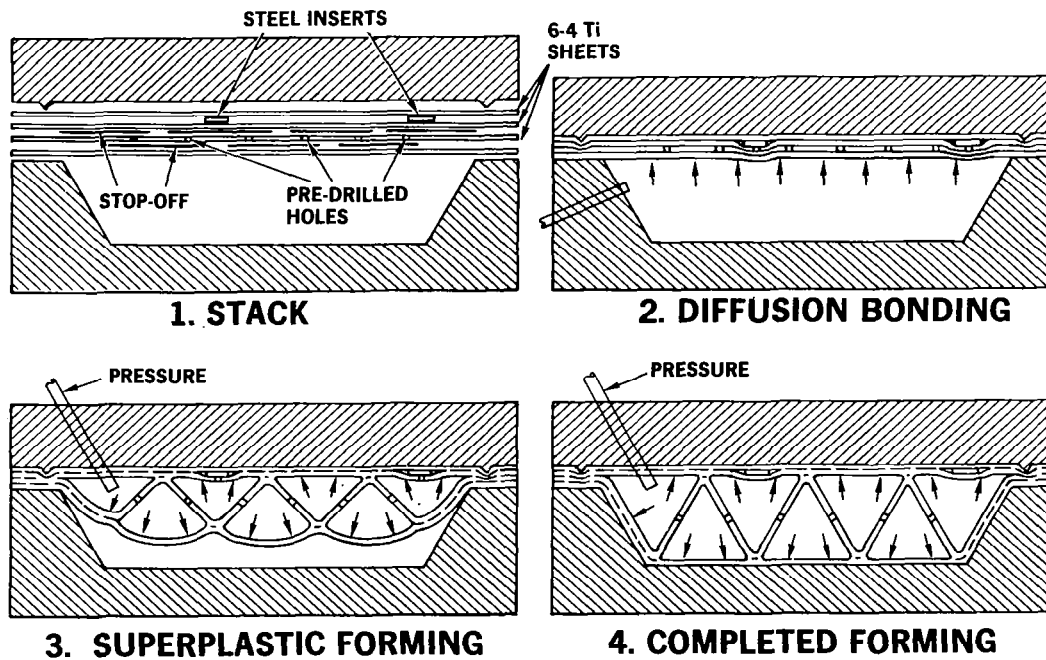
HAT SECTION STIFFENED SKIN PANEL



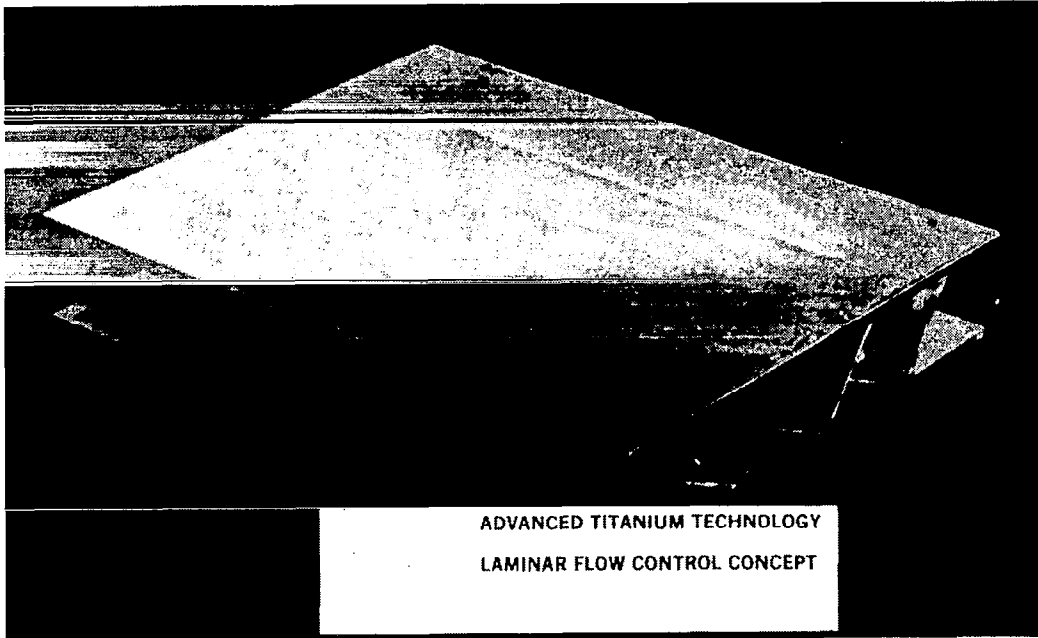
SEMI-CIRCULAR CORRUGATION STIFFENED SKIN CONCEPT




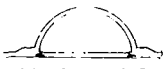

SINE WAVE TRUSS CORE SANDWICH PANEL FORMING PROCESS



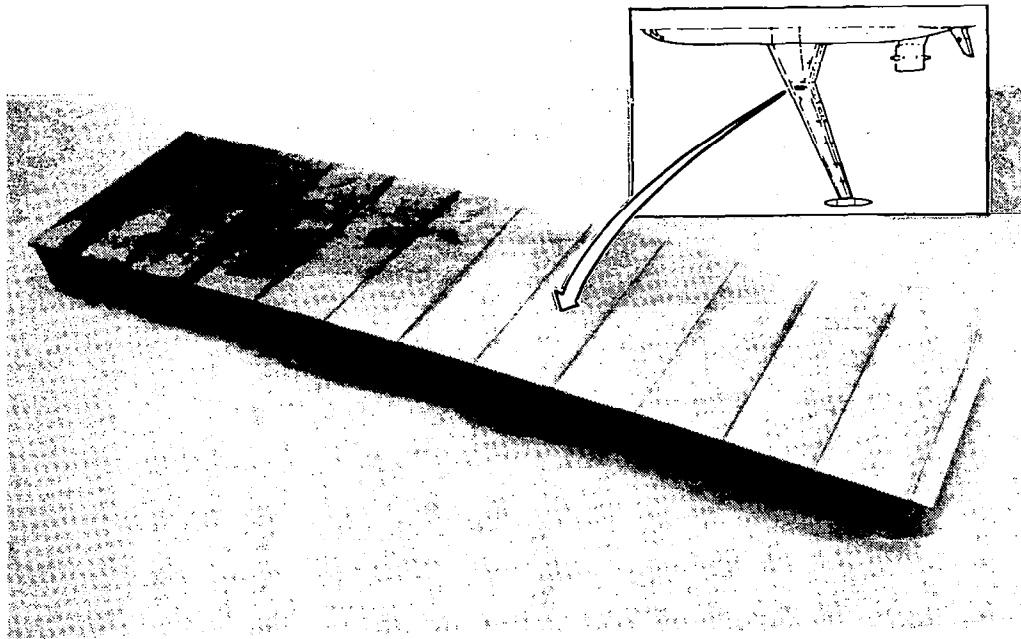
SINE WAVE TRUSS CORE SANDWICH PANEL



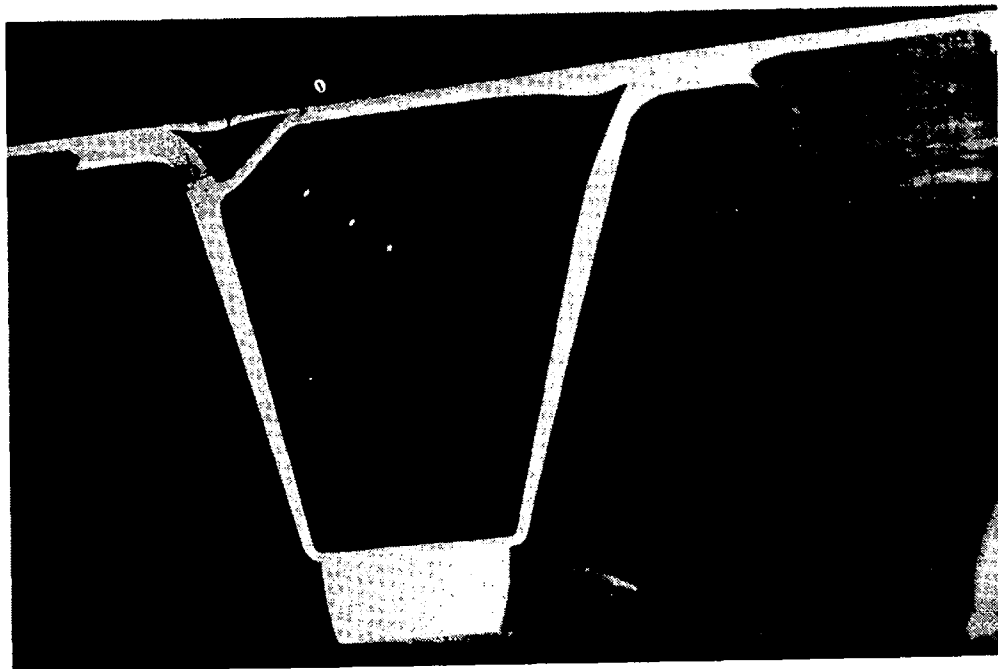
COMPARISON OF LFC DESIGN CONCEPTS

	HAT SECTION SEMI-SANDWICH	SEMI-CIRCULAR SEMI-SANDWICH	SINEWAVE TRUSS SANDWICH
			
Area / CM (t)	.622 CM ² / CM	.665 CM ² / CM	.703 CM ² / CM
Weight	LOW	LOW	HIGHER
Production cost	LOW	LOWEST	LOW
Visual inspection	YES	YES	SOME
Maintenance	GOOD	GOOD	MORE DIFFICULT
Airload rib Attachment	GOOD	MORE DIFFICULT	GOOD
Panel splice	GOOD	MORE DIFFICULT	MORE DIFFICULT
Tailorable geometry	GOOD	FAIR	FAIR
Duct area / CM	2.26 CM ² / CM	2.01 CM ² / CM	2.59 CM ² / CM

FEASIBILITY PANEL, MOLDLINE SURFACE

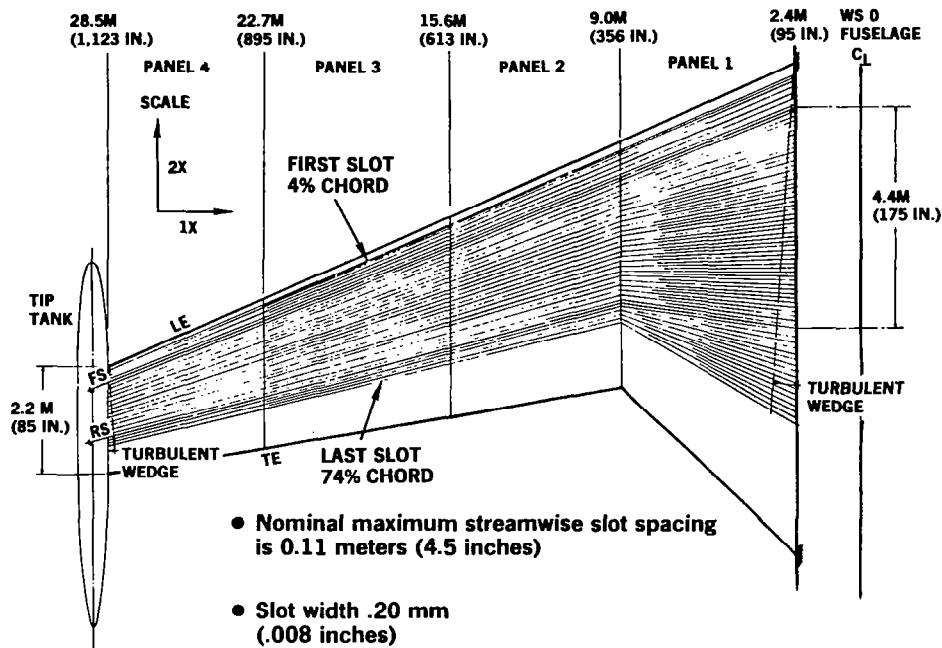


PLENUM AND METERING HOLES IN FEASIBILITY PANEL

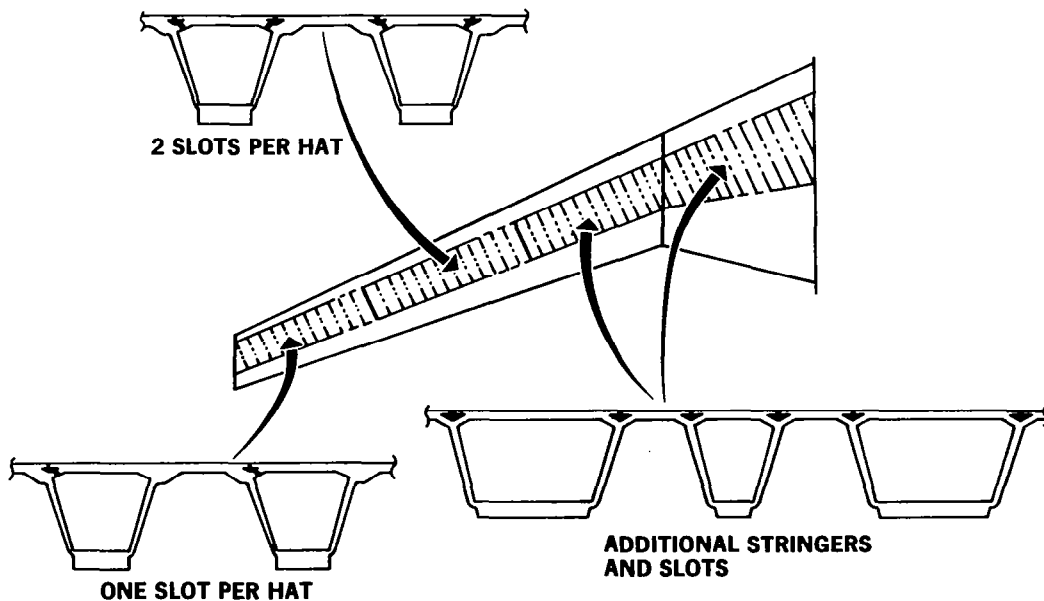


UPPER WING SURFACE SLOT SPACING

MAX 4.5 INCHES

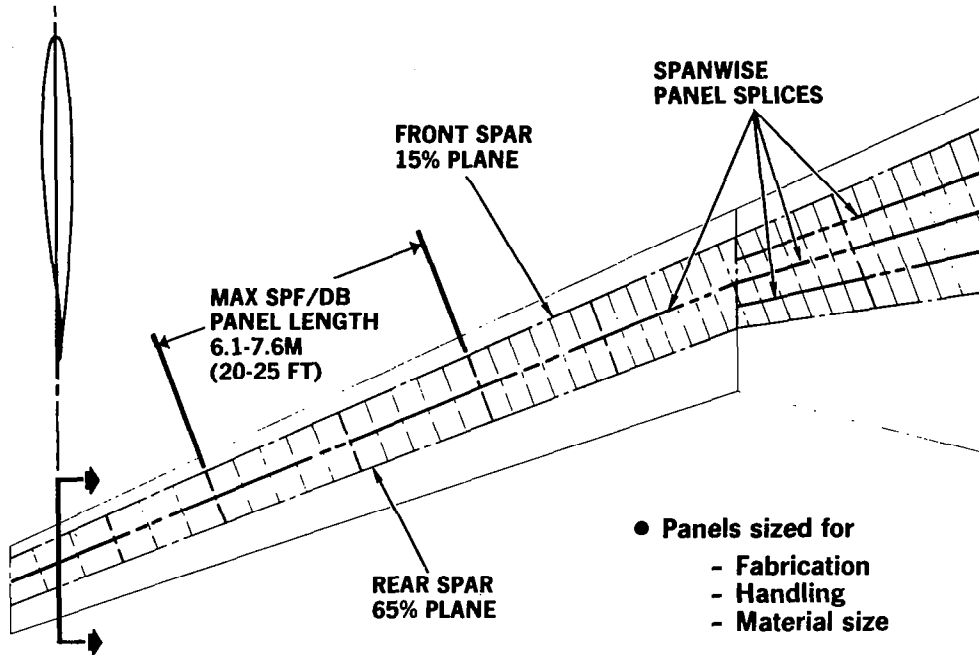


WING STRINGERS CHANGE TO MEET LFC REQUIREMENTS

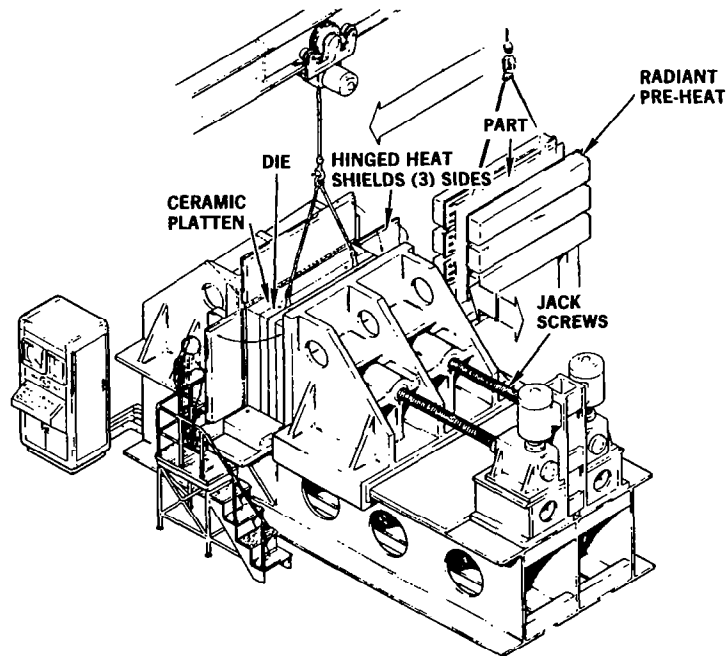


OPTIMUM PANEL SIZE

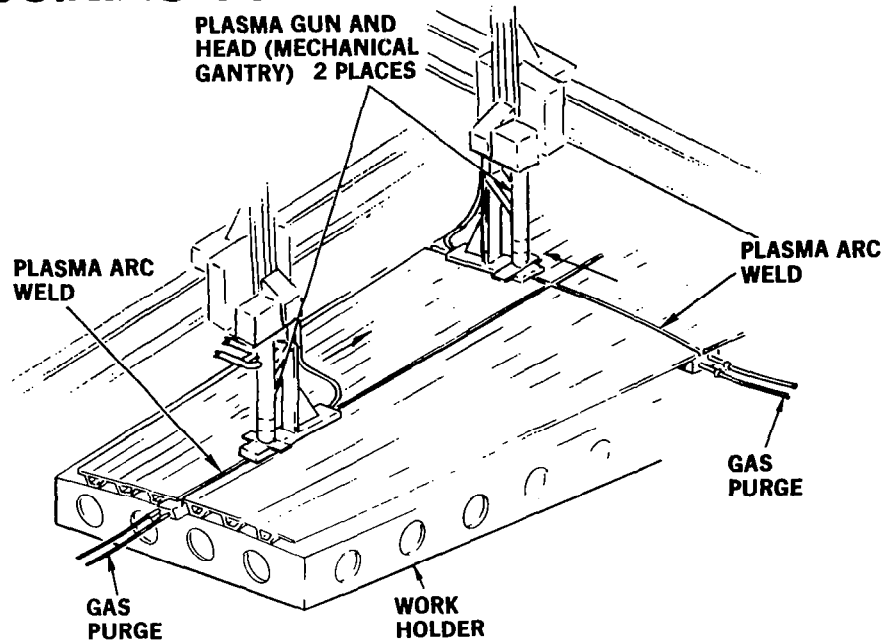
WING DIAGRAM



SPF/DB PANEL FABRICATION PRODUCTION CONCEPT

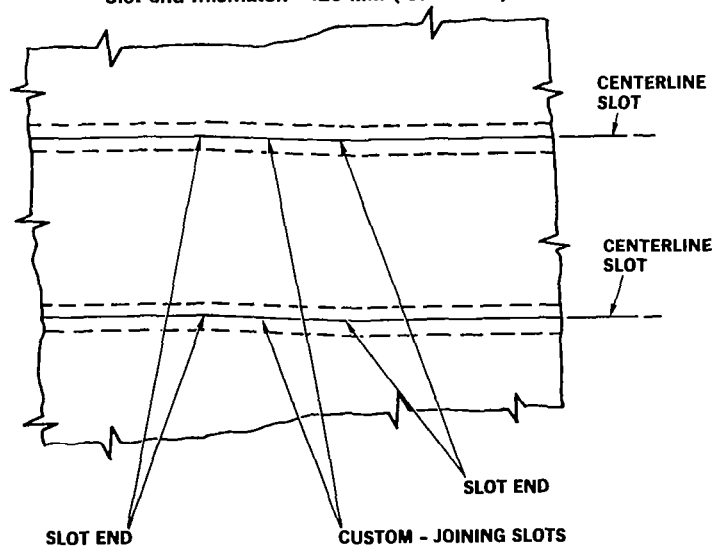


WING COVER FABRICATION JOINING CONCEPT



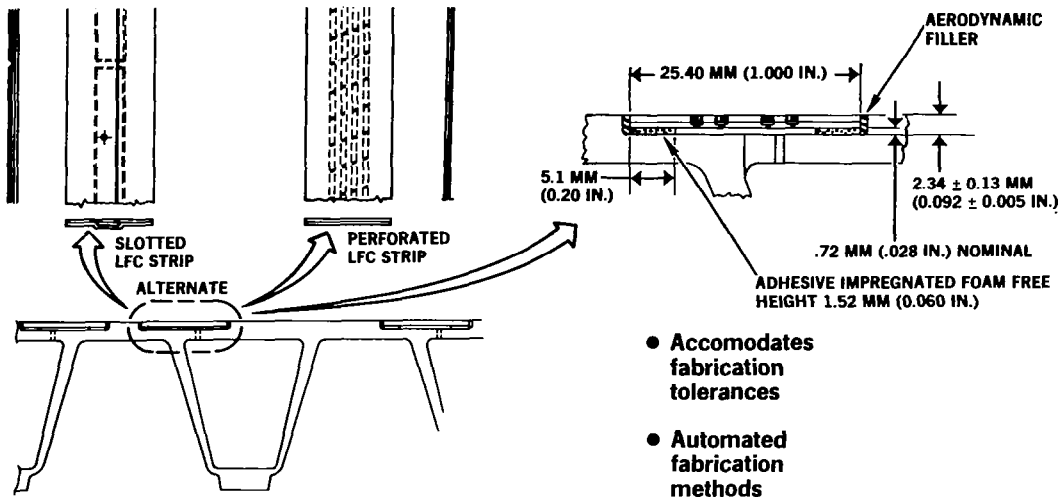
INTEGRAL LFC SLOT DIFFICULT TO MACHINE

- Slots - electric discharge machined (edm)
 - Max slot length - 760 MM (30 inches)
 - Slot end mismatch - .25 MM (.01 inches)



SELECTED DESIGN CONCEPT

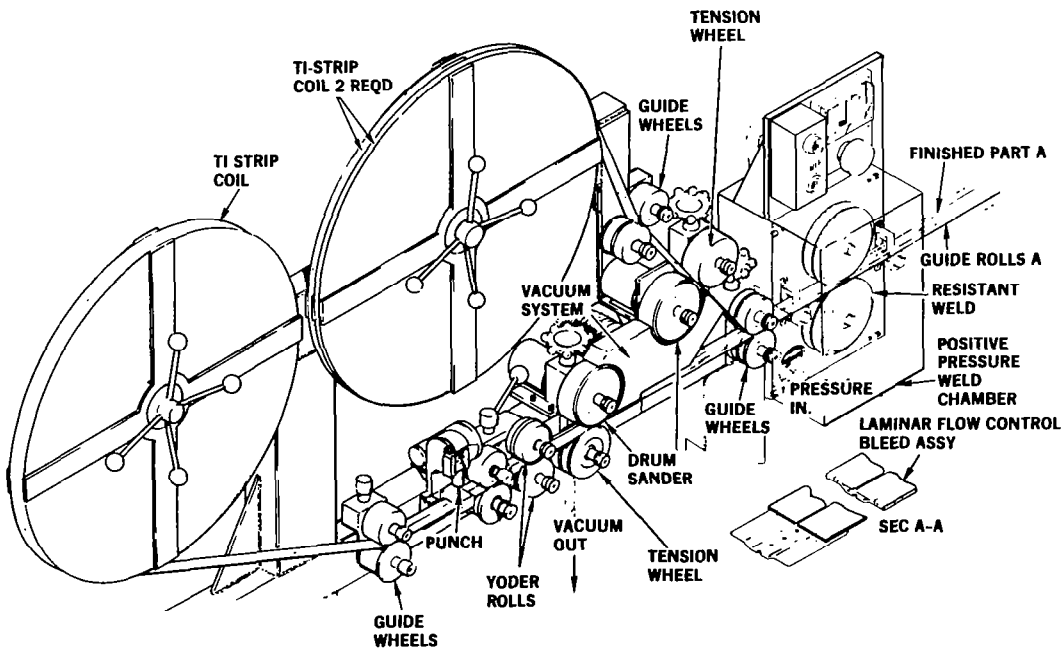
LFC REPLACEABLE STRIPS



- Accommodates fabrication tolerances
- Automated fabrication methods

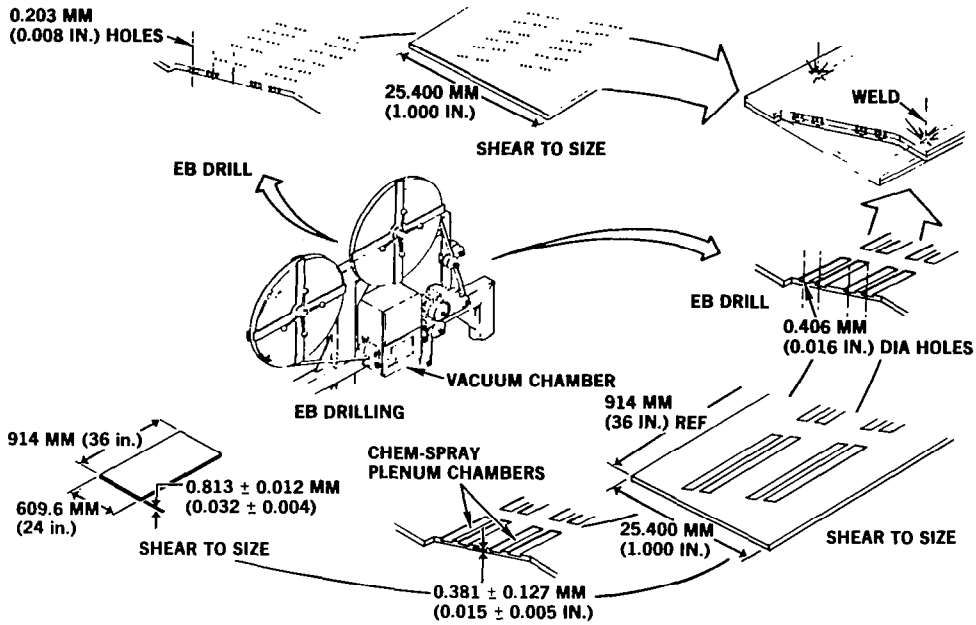
AUTOMATED FABRICATION CONCEPT

LFC SLOTTED STRIP

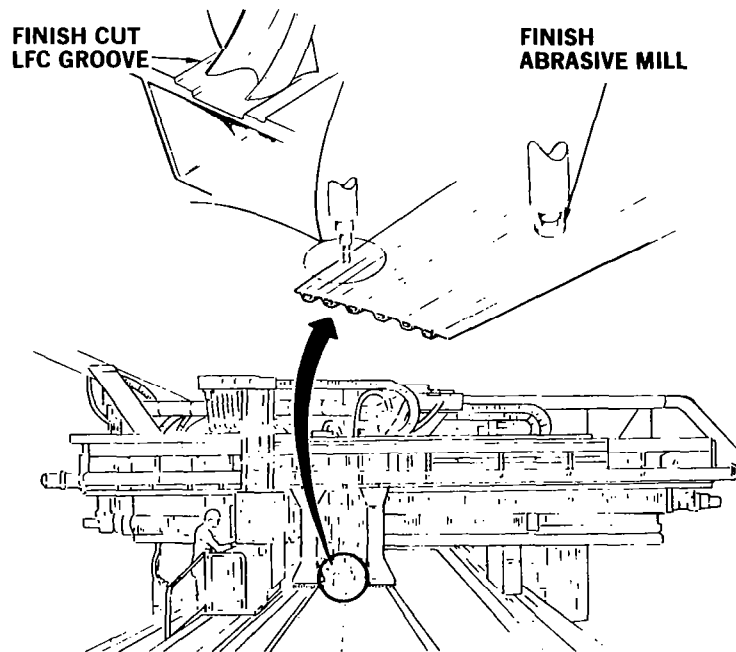


AUTOMATED FABRICATION CONCEPT

LFC PERFORATED STRIP



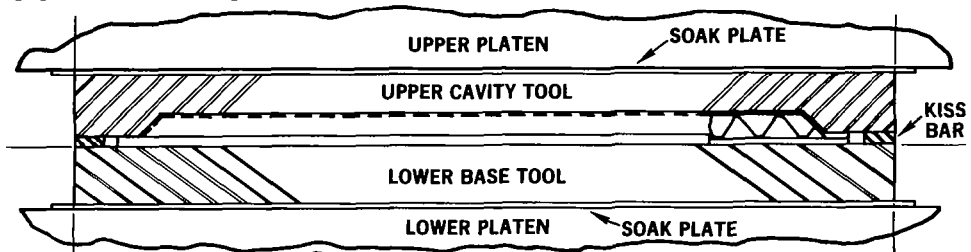
WING COVER MOLD LINE WILL MEET SURFACE FINISH REQUIREMENTS



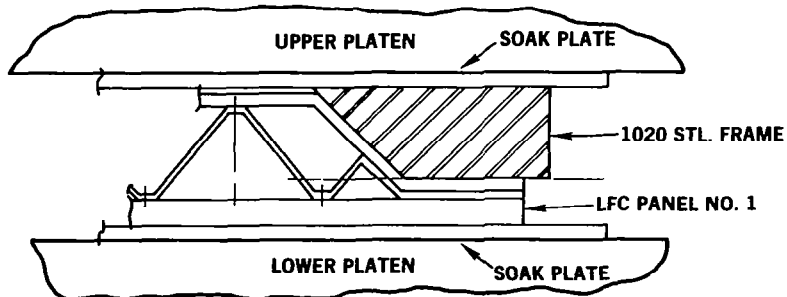
FEASIBILITY OF USING SPF/DB FOR LFC WINGS

PHASE	TASK	DESCRIPTION	MONTHS AFTER GO-AHEAD																				
			1	2	3	4	5	6	7	8	9	10	11	12	13	14	15	16	17	18	19	20	
			S	O	N	D	J	F	M	A	M	J	J	A	S	O	N	D	J	F	M	A	
I	1	<u>Panel fabrication</u>																					
		Design development	△	△																			
		Fabrication																					
2	3	Smooth panel																					
		Grooved panel																					
		Inspection																					
II	1	<u>Adhesive development</u>																					
		Survey																					
		Fabrication																					
2	3	Demonstrator																					
III		<u>Reports</u>																					
		Oral																					
		Final																					

FABRICATION PROCEDURE FOR LFC PANEL NO. 1

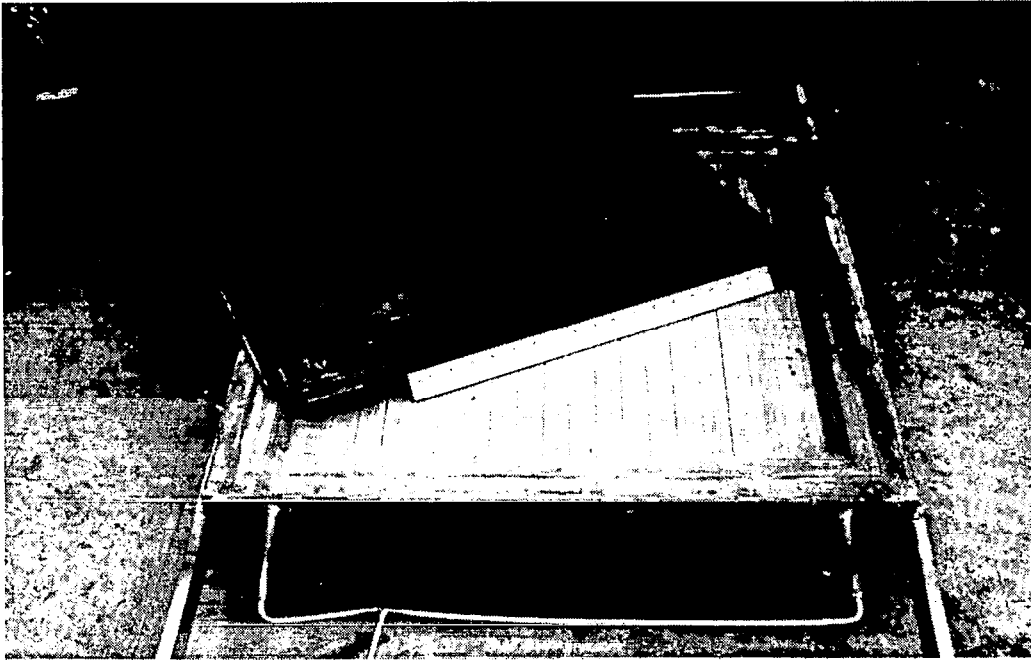


① BONDING & EXPANSION

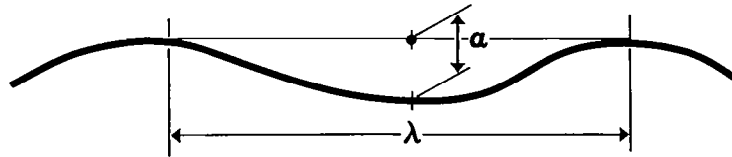


② HOT FLATTENING

PANEL NO. 1 WITH TOOLING



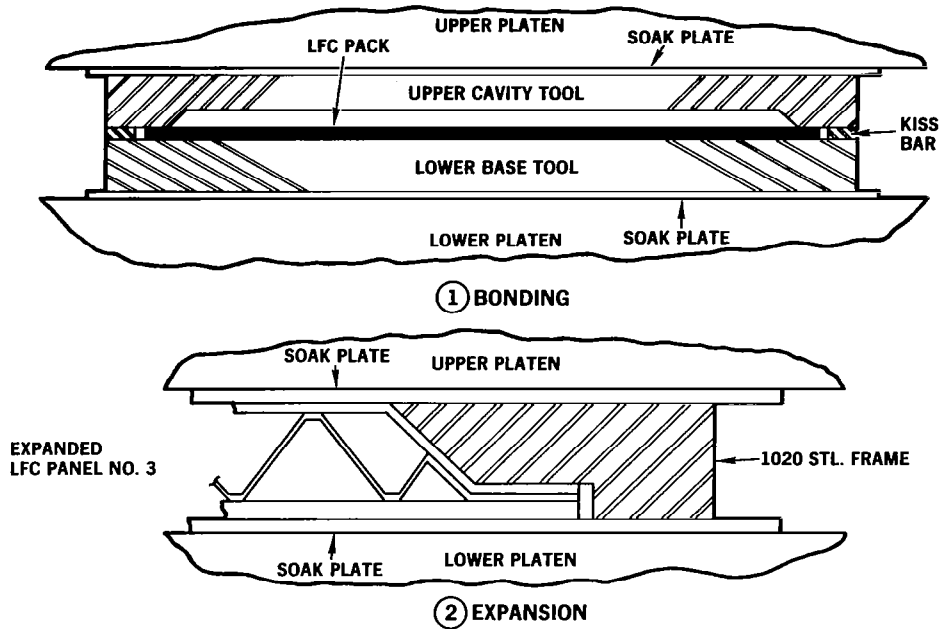
LFC PROGRAM PANEL SMOOTHNESS



DEPTH OF WAVE - α MM (IN.)

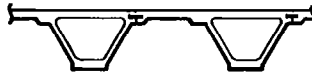
λ MM (IN.)	38.1 (1.5)	558.8 (22)
Required (max)	.079 (.003)	.300 (.012)
Panel no. 1		
As formed	0	1.27 (.050)
After creep forming	.203 (.008)	.279 (.011)
Panel no. 2		
As formed	0	.711 (.028)
After machining	0	.292 (.012)

FABRICATION PROCEDURE FOR LFC PANEL NO. 3



SUMMARY

- Three concepts demonstrated:



- Separate LFC strip concepts developed:



ADHESIVE
BONDED-BEST

- Fabrication methods concepts developed
- Required smoothness feasibility demonstrated
- Bonded LFC strip demo in works

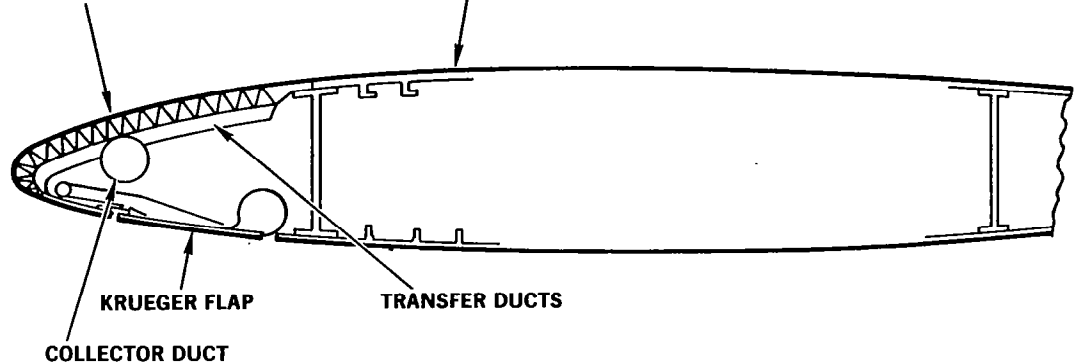
NEXT STEP

APPLICATION TO ADVANCED VARIABLE-SWEEP BOMBER AIRCRAFT

- Long range cruise configuration

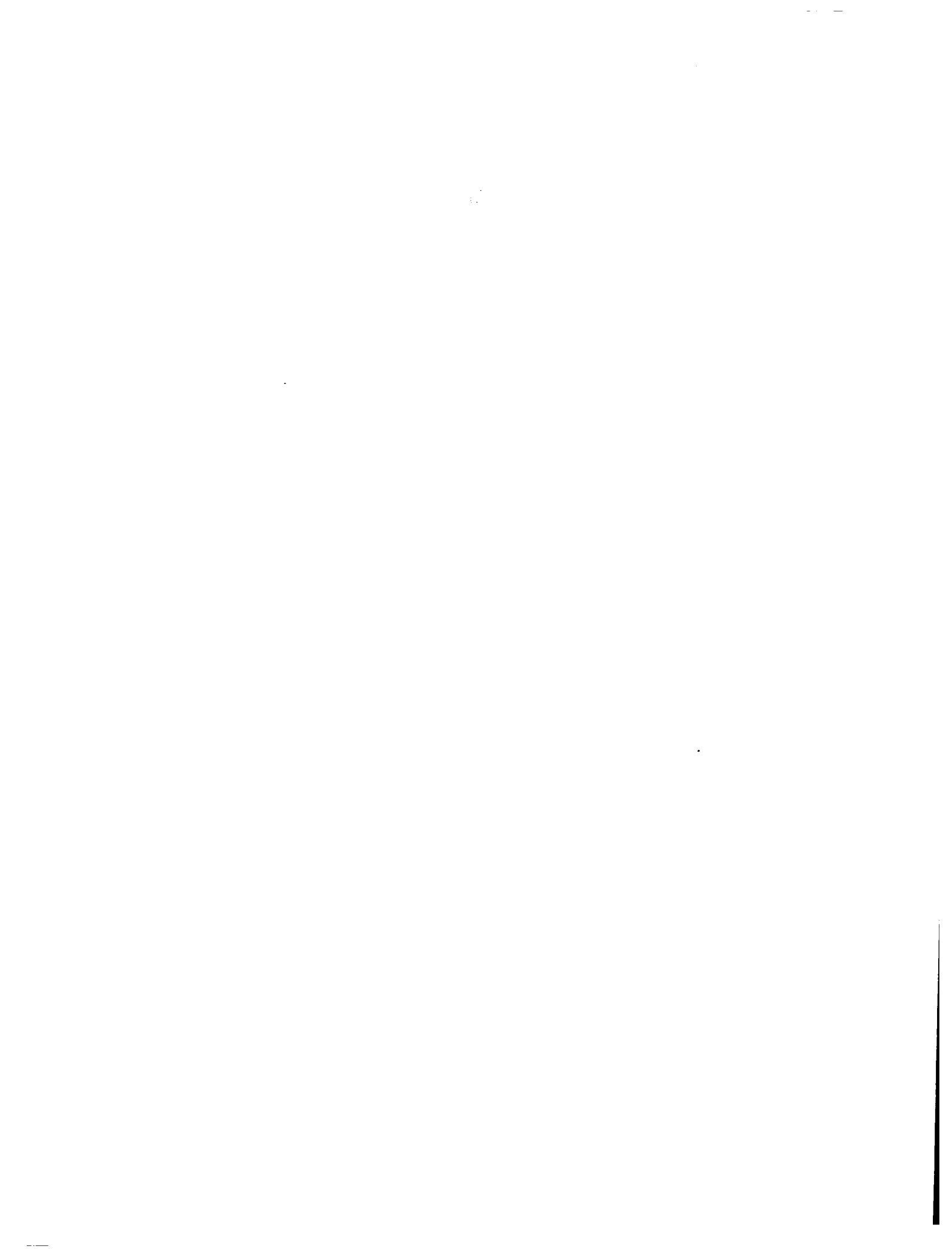
SPF/DB TI TRUSS-CORE SANDWICH WITH PERFORATED LFC SURFACE

PASSIVE LFC SURFACE



LFC PROVIDES MULTIPLE BENEFITS TO ADVANCED BOMBERS

- 1241 L (328 gal) fuel saved/training mission
- 118.4×10^6 L (31.3×10^6 gal) fuel saved/fleet in 20 years
- \$36.9M life cycle cost savings
- Reduced tanker fleet required



SPF/DB TITANIUM
LFC POROUS PANEL CONCEPT

Neil R. Williams

Douglas Aircraft Company
McDonnell Douglas Corporation
Long Beach, California

ABSTRACT

This program has resulted in the following:

- Production of SPF/DB panels using thin (0.016-in.) core and face sheets.
- Production of panels with smooth face sheets.
- Elimination of tool pickup on face sheets in contact with tooling material during the forming process.
- Production of panels with the configuration required for LFC applications.

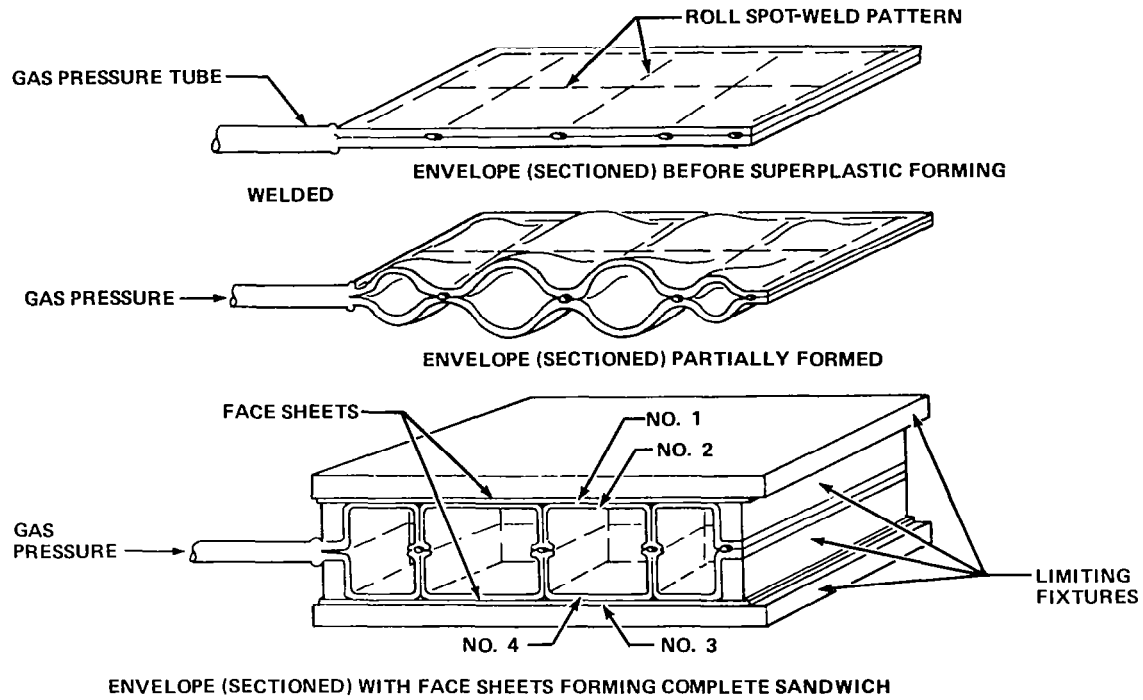
INTRODUCTION

A unique process has been developed at Douglas Aircraft Company combining welding and superplastic forming/diffusion bonding (SPF/DB) of titanium to fabricate expanded core sandwich panels.

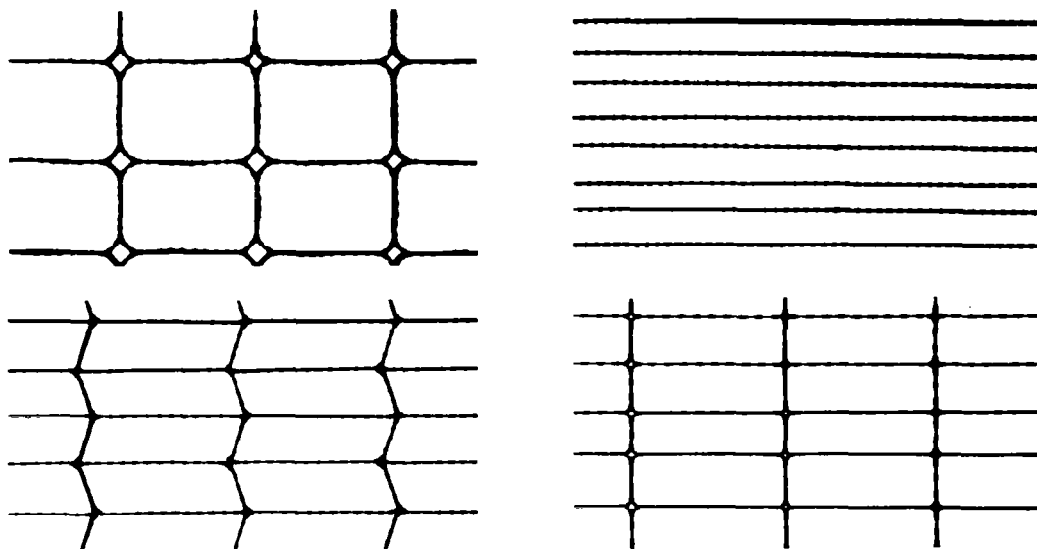
A variety of configurations has been developed, tested, and evaluated in the performance of CRAD and IRAD programs over the past several years. Because of this experience and the unique properties of SPF/DB titanium sandwich construction, this program demonstrated the capability of the SPF/DB process to produce structure having the smoothness and configuration to meet the design requirements for LFC applications.

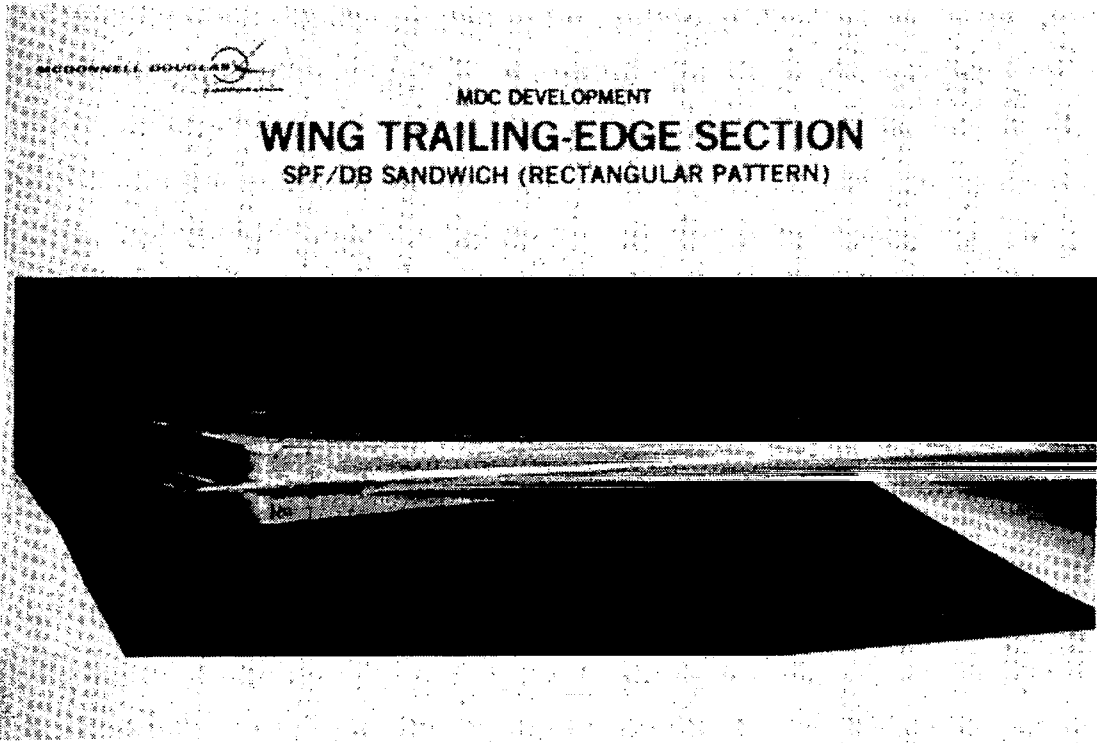
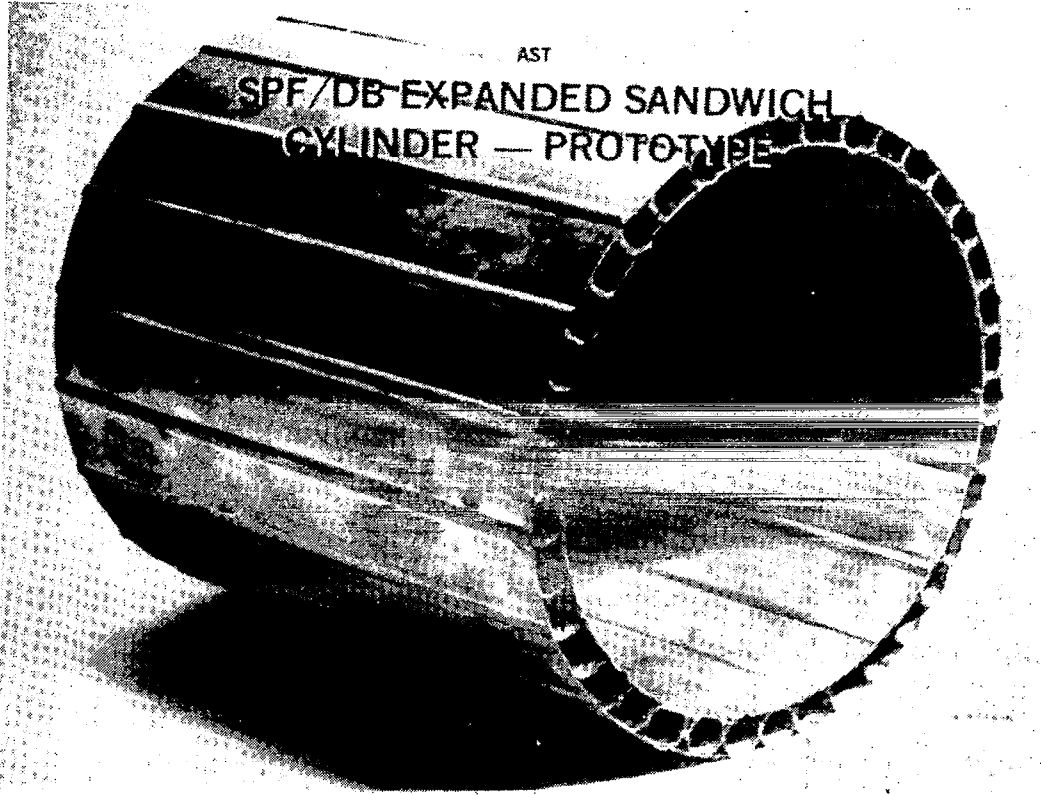
A brief explanation of the process is included along with comparative data on structural concepts to show how the process works and where SPF/DB titanium may be expected to be structurally competitive.

DOUGLAS DEVELOPMENT
SPF/DB PHASES OF FABRICATION
FOUR-SHEET SANDWICH



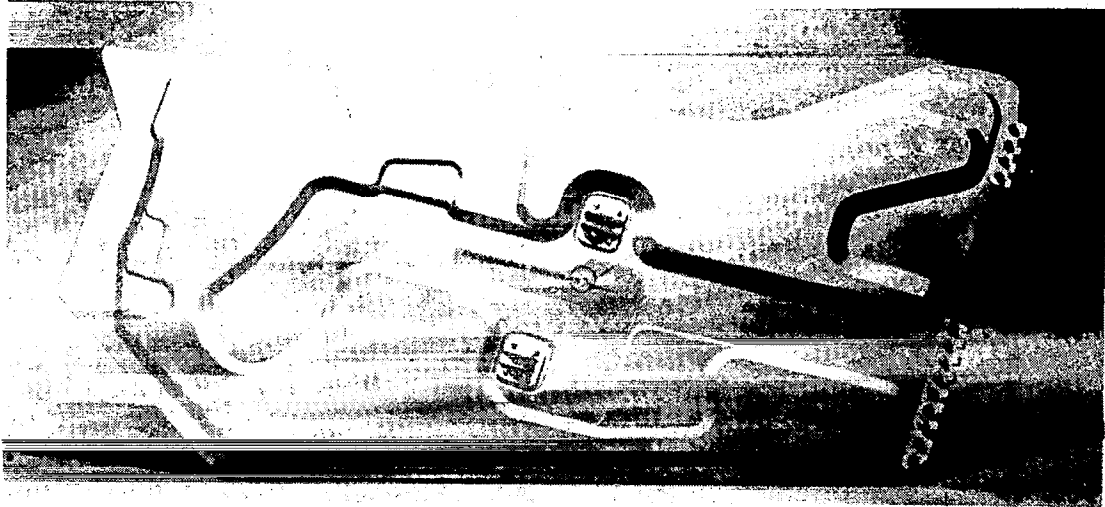
X-RAYS OF RECTANGULAR CORE CONCEPTS



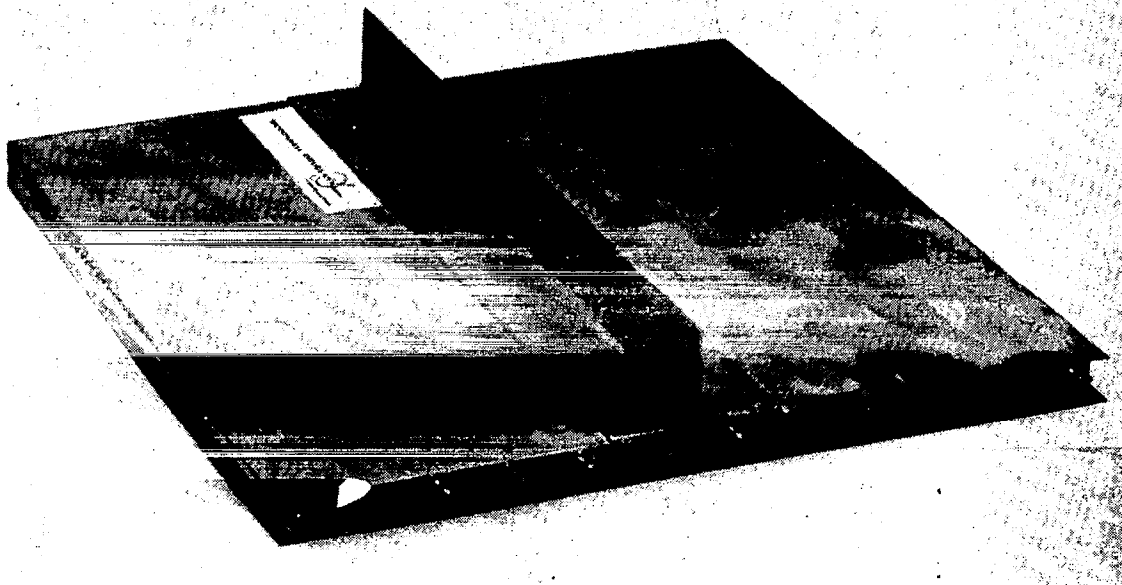


DOUGLAS DEVELOPMENT

T-38 MAIN LANDING GEAR DOOR
SPF/DB SANDWICH (RECTANGULAR PATTERN)



SPF/DB SANDWICH PANEL WITH INTEGRAL DOUBLERS AND ATTACHED TEE

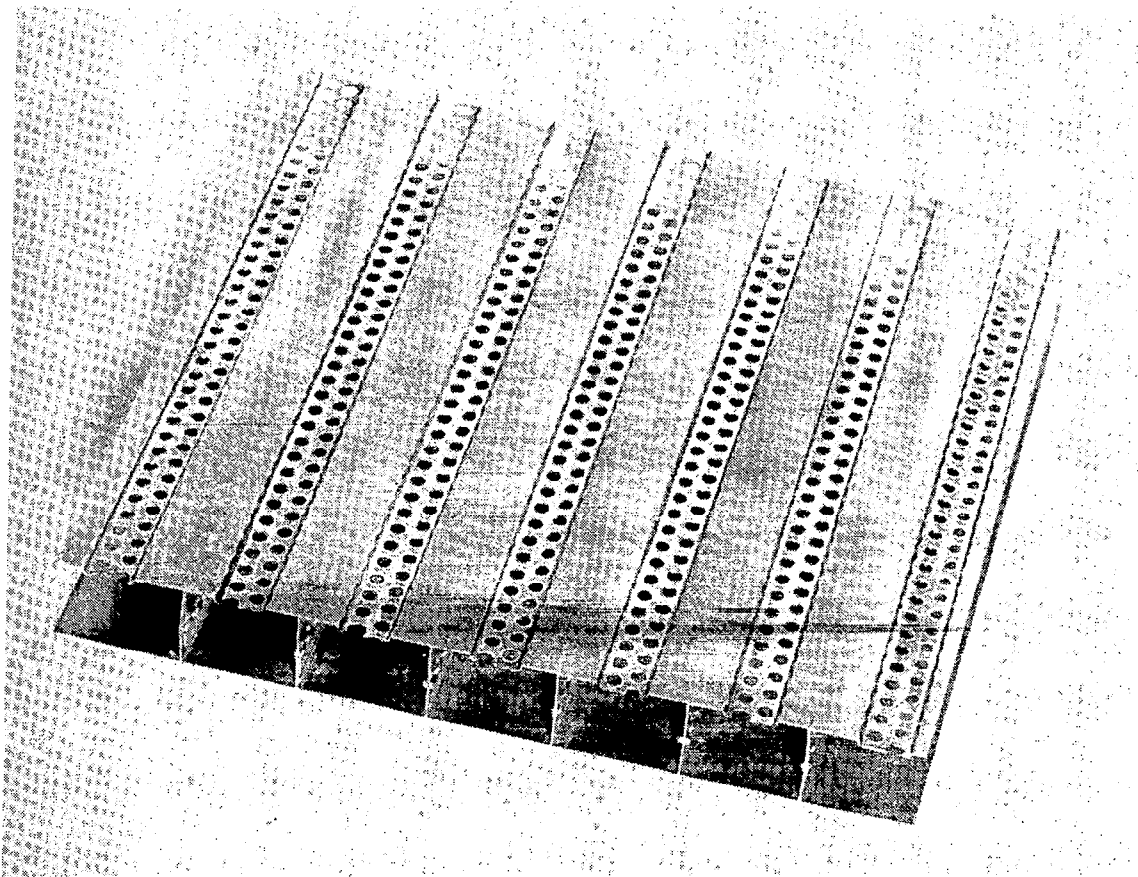


SMALL DEMONSTRATION PANEL SHOWING CONCEPT

Machined holes in face sheet channels

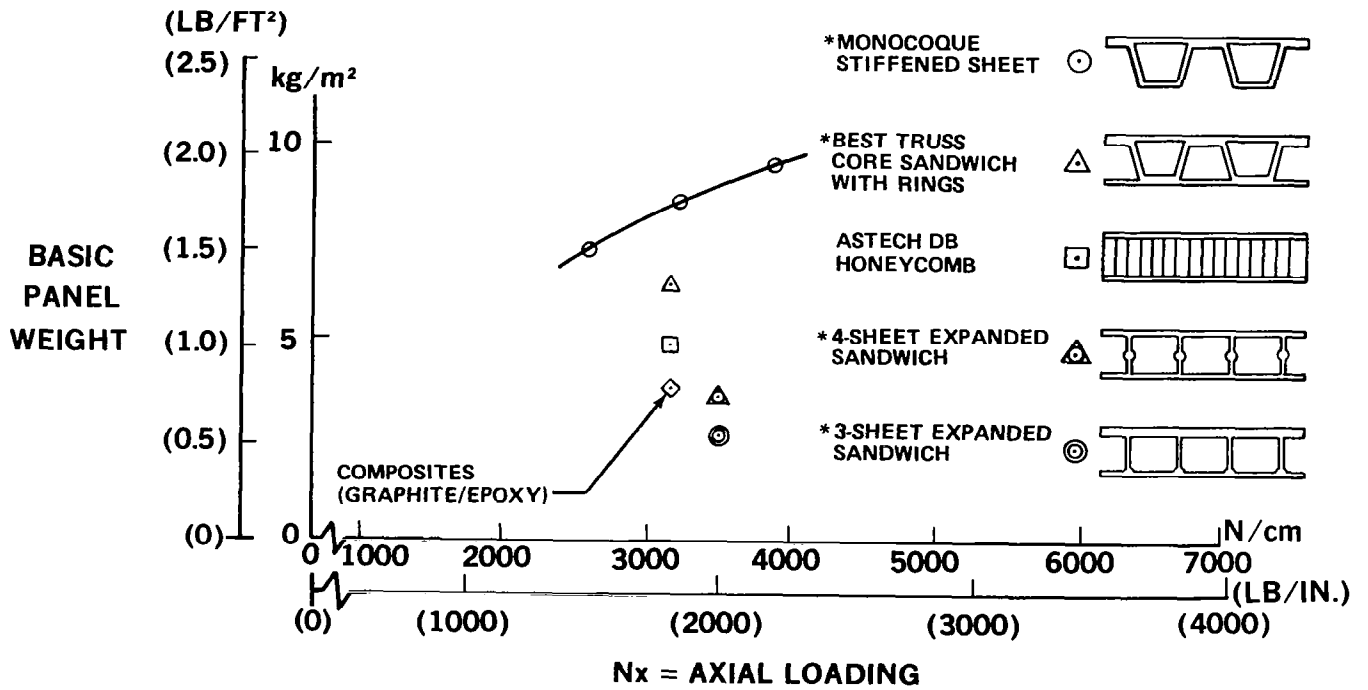
Uniform web location

No face sheet gas entrapment



STRUCTURAL CONCEPTS COMPARED

* TI SPF/DB

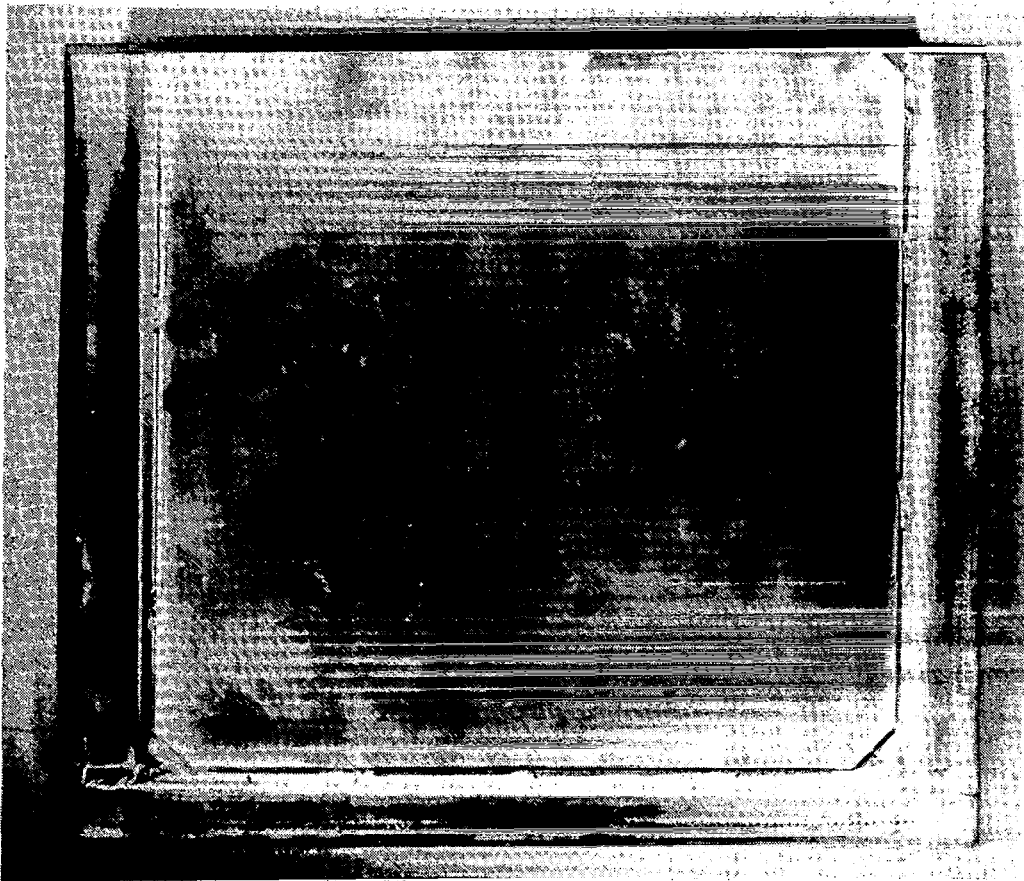


SURFACE CONTAMINATION STUDIES

Tool pickup

Slip sheets —Type 321 Cres sheet

Parting agent — Boron nitride with binder-acetone carrier

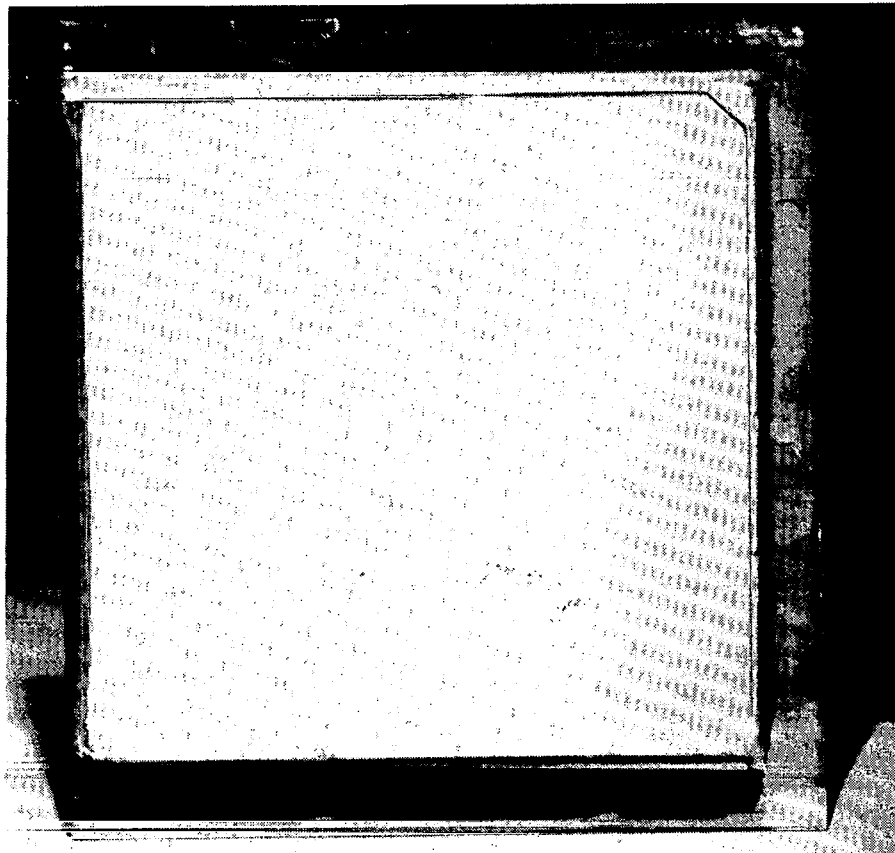


TOOL PICKUP AFTER CHEMICAL MILLING OF SURFACE

Tooling material constituents combined with titanium form barrier resisting chemical milling.

Pickup must be sanded clean to result in uniform material removal in chemical milling.

Depth of mechanical cleanup is limited by thickness of face sheets.

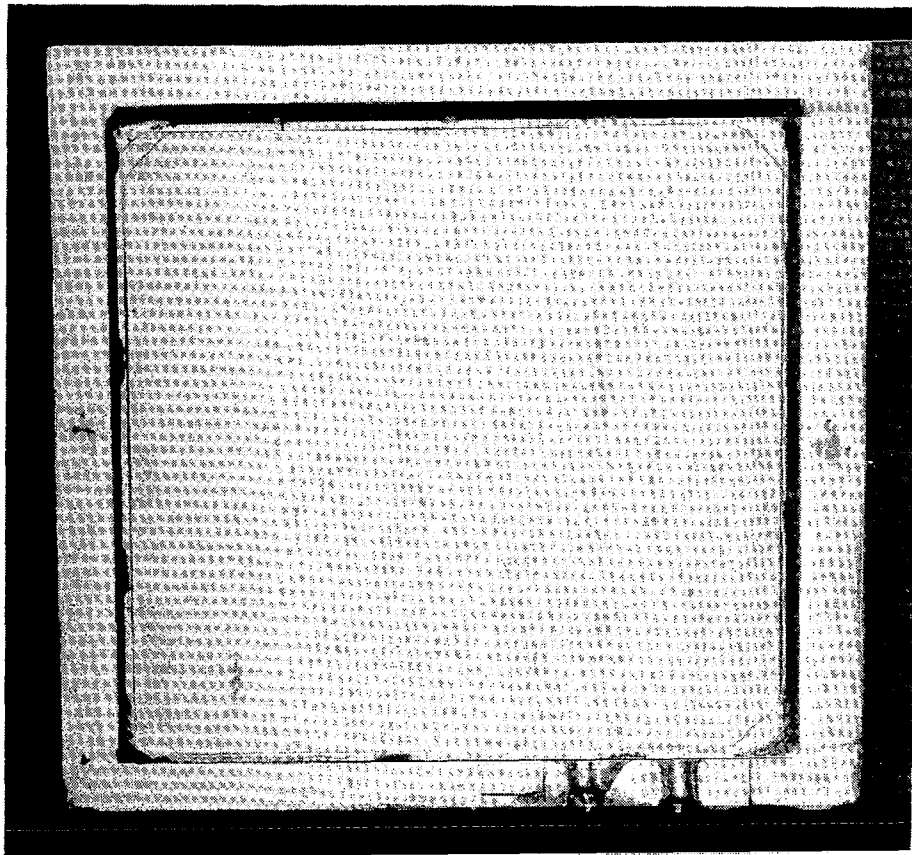


PANEL FORMED WITH NO FACE SHEET PICKUP

Slip sheets — Type 430 stainless steel

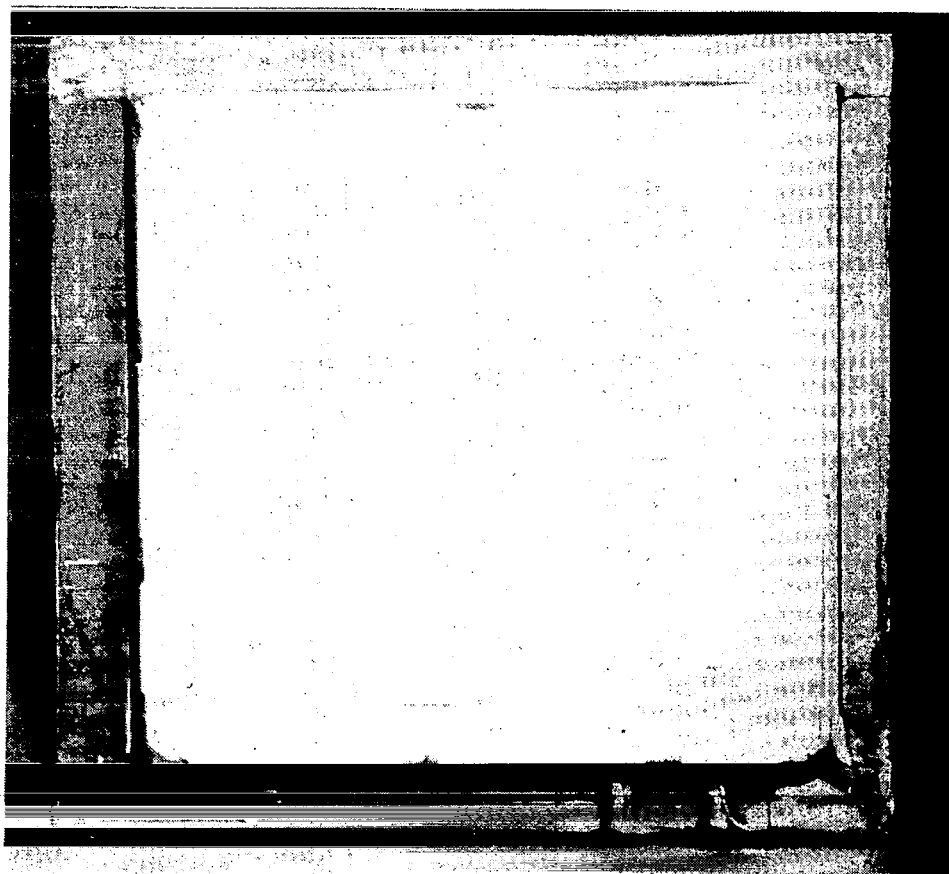
Parting agent — Boron nitride with binder-acetone carrier

Surface roughness — RMS 20



**PANEL WITH NO TOOL PICKUP
AFTER ALUMINUM OXIDE BLASTING AND CHEMICAL MILLING**

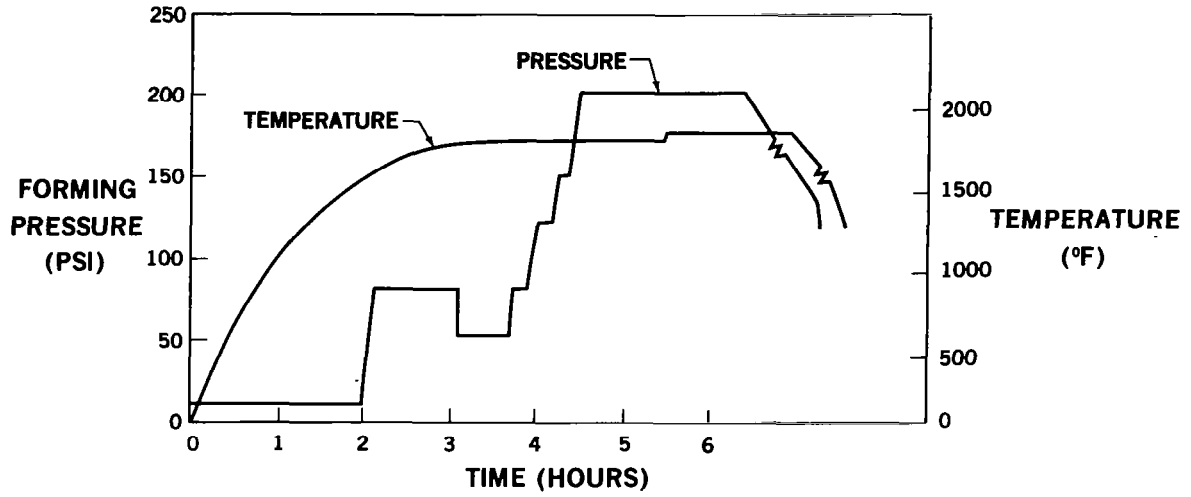
Surface roughness — RMS 40-50



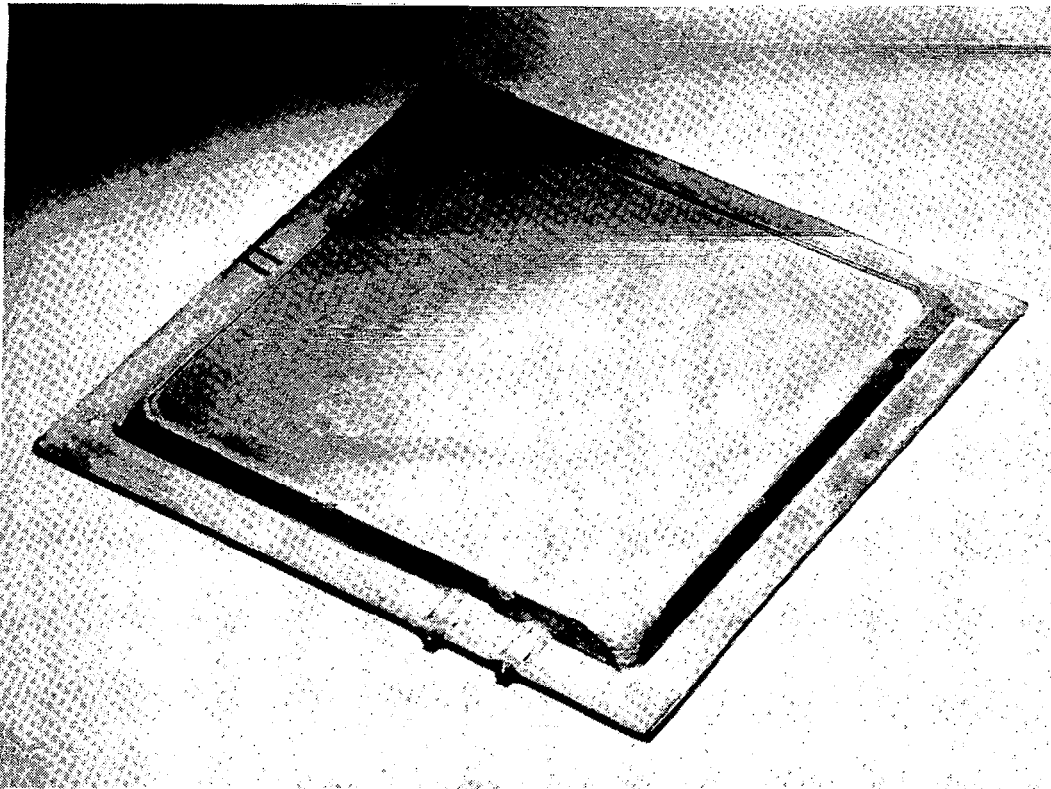
PARAMETERS PANEL — AS FORMED

CORE STARTING THICKNESS — 0.016 INCH

FACE SHEET THICKNESS — 0.016 INCH

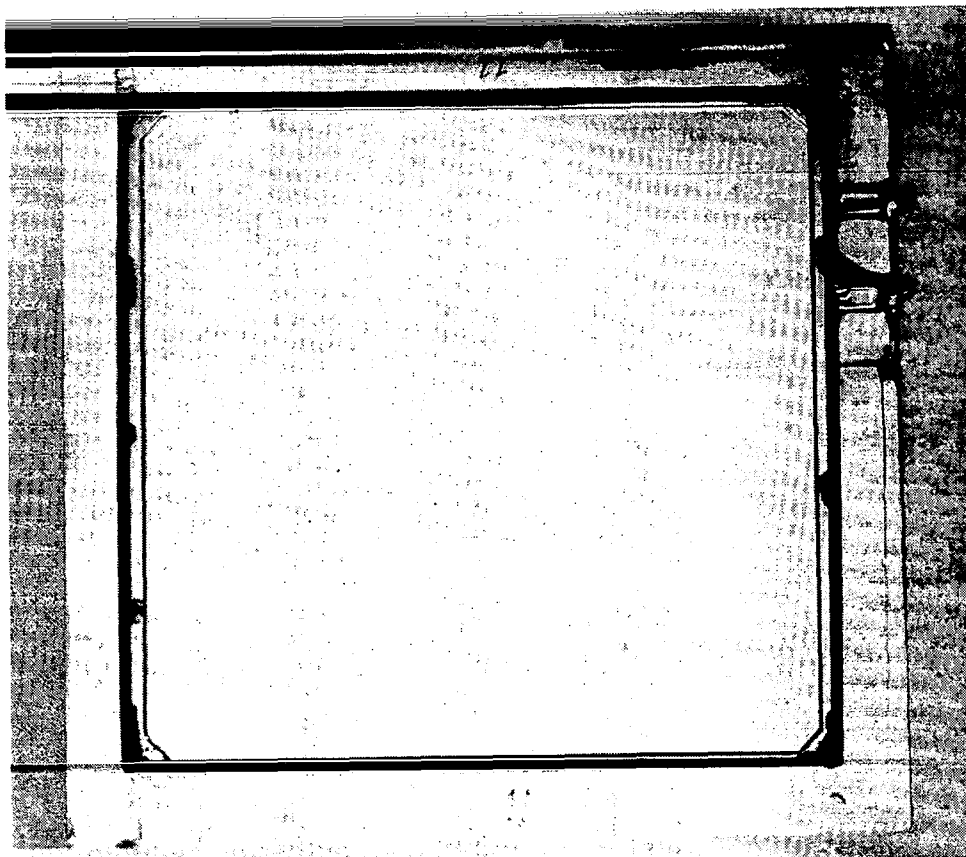


LFC PARAMETERS PANEL — PRESSURE CYCLE



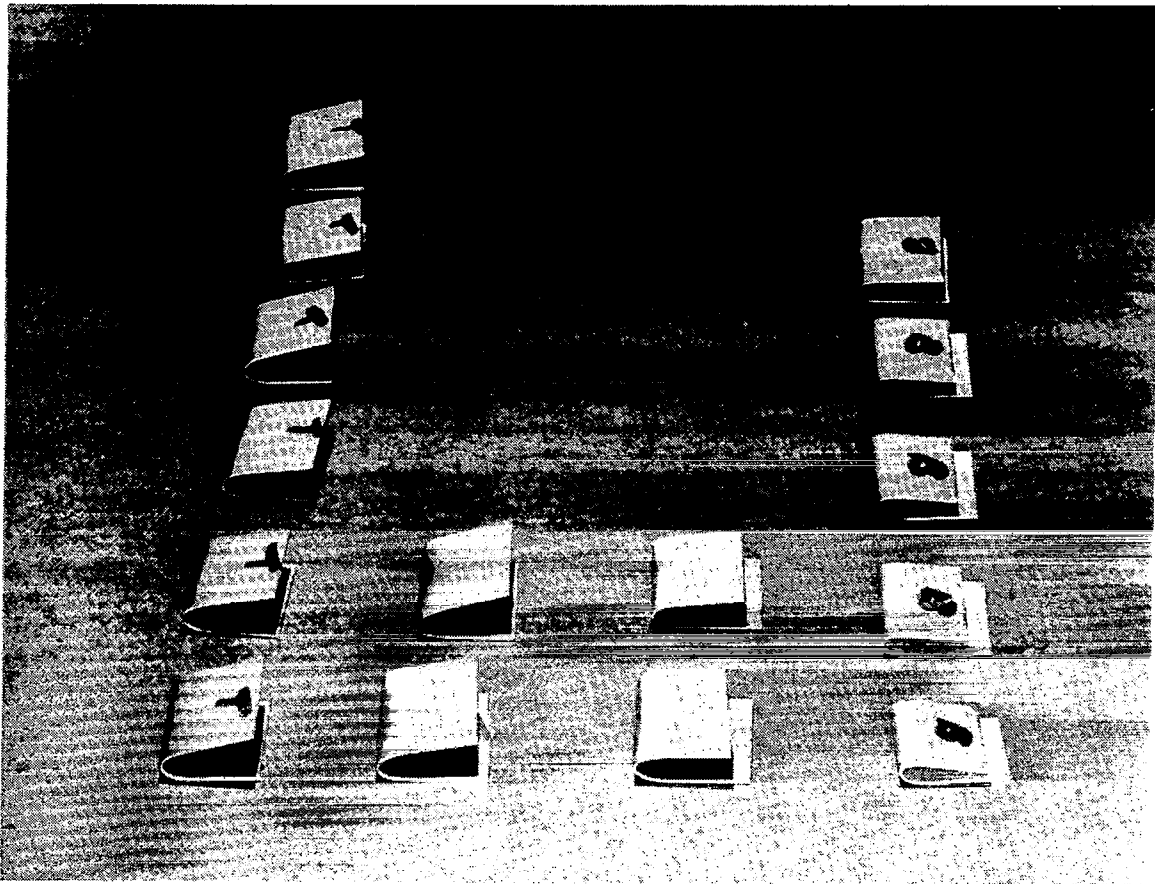
**PARAMETERS PANEL
AFTER ALUMINUM OXIDE BLASTING AND CHEMICAL MILLING**

Web grooves — 0.00025-inch maximum depth



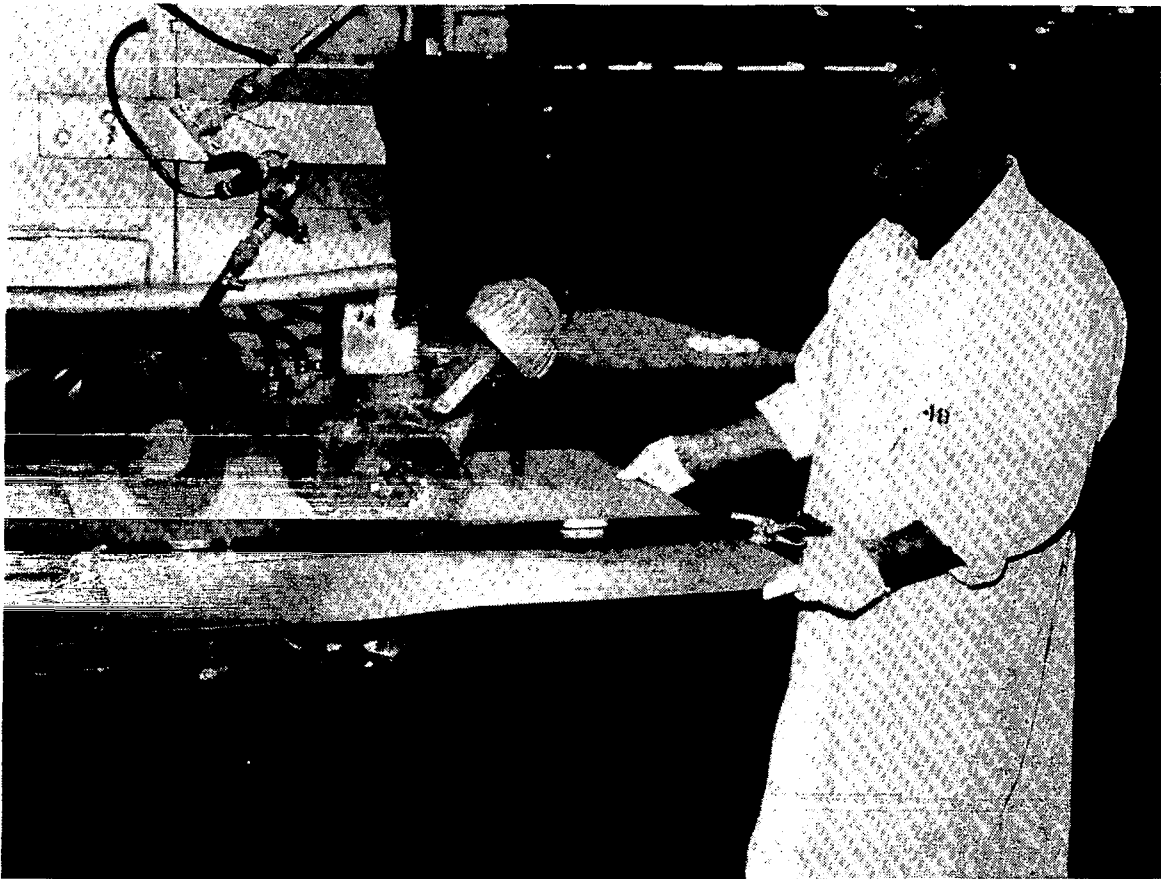
BEND TESTS FROM PARAMETERS PANEL

- Top — Top face sheet exterior surface bend
- Bottom — Bottom face sheet exterior surface bend
- Center — Top and bottom face sheets with interior surface (exposed to argon forming gas) on outside of bend



WELDING OF CORE SHEETS FOR LARGE FLAT PANEL

Seam weld — approximately 6 feet per minute

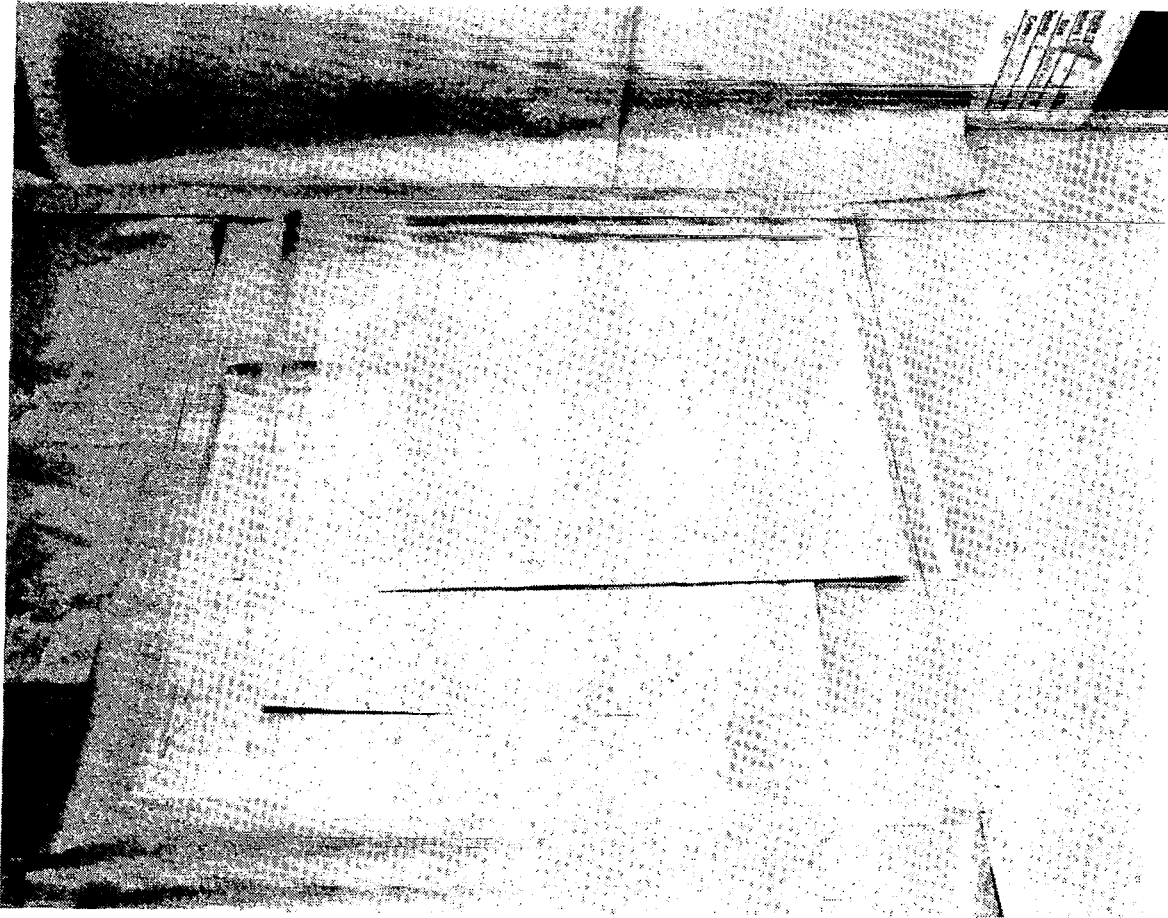


LAYUP FOR LARGE FLAT PANEL

Face sheets

Seam-welded core

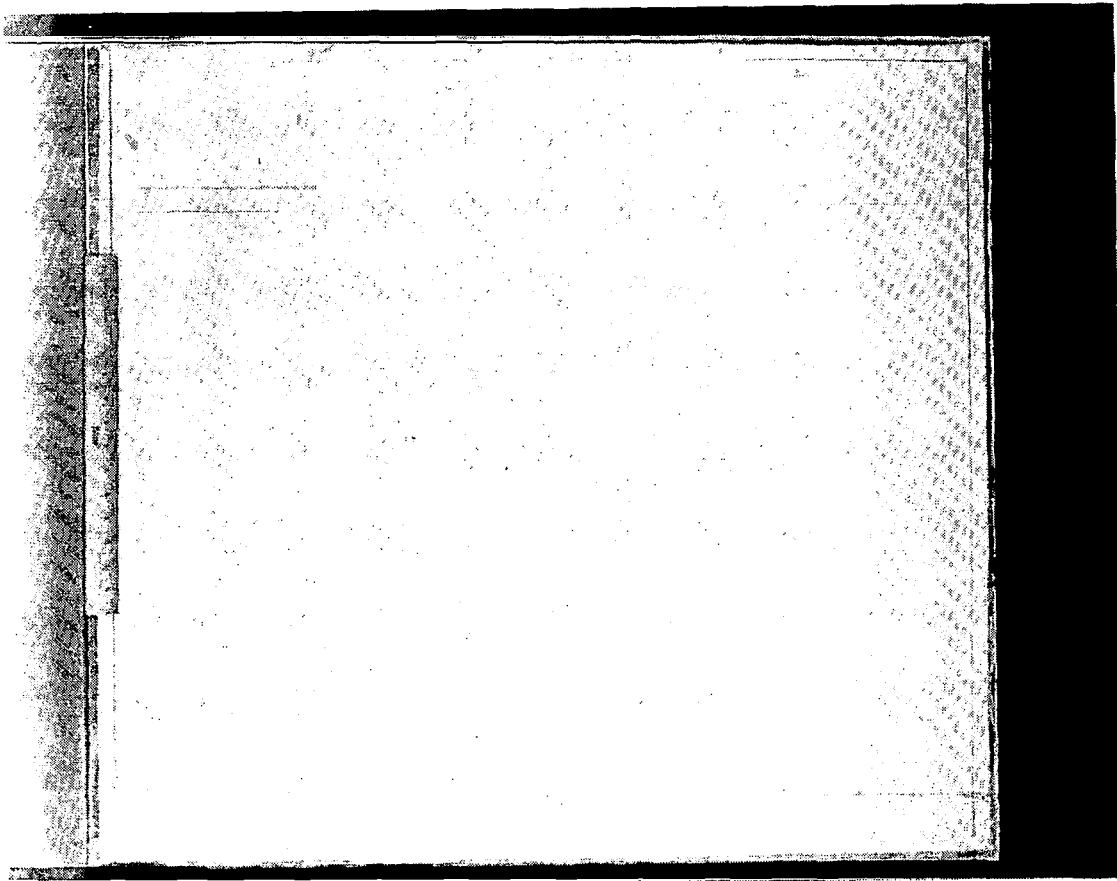
Edge doublers



TOP SURFACE OF LARGE FLAT PANEL

No web grooves.

Face sheet gas entrapment in core on top side caused wider core-to-face-sheet cleavage than on bottom side.

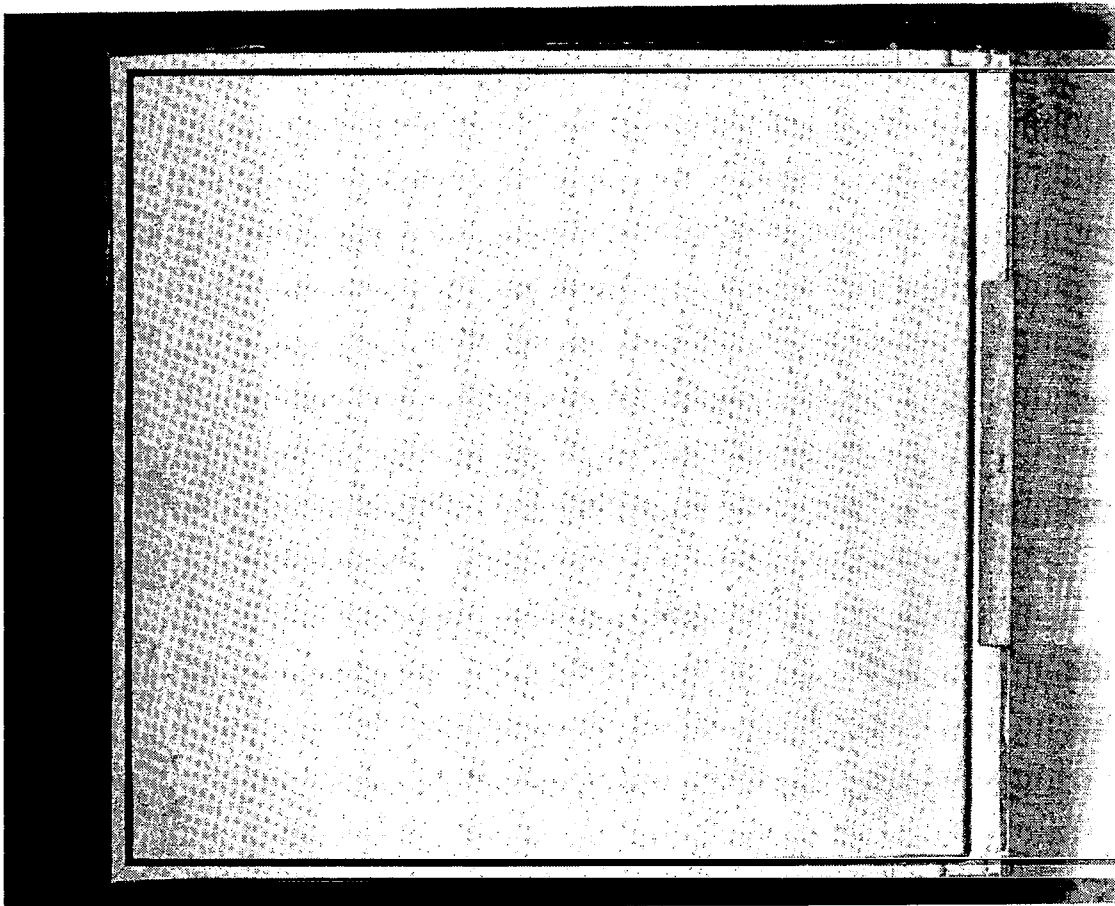


BOTTOM SURFACE OF SECOND LARGE FLAT PANEL

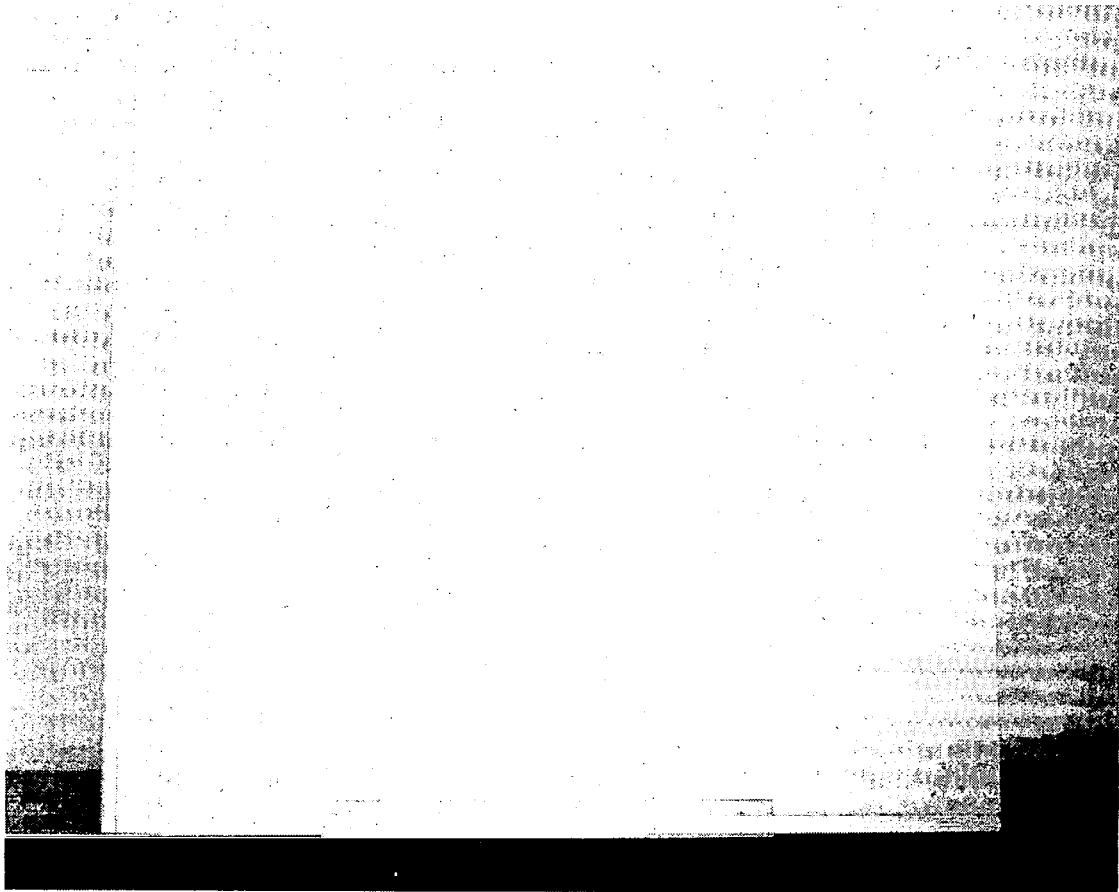
Web grooves 0.002 to 0.003 inch deep caused by reduction of face sheet pressure during final core forming.

This problem not characteristic in panels having face sheets thicker than core sheets.

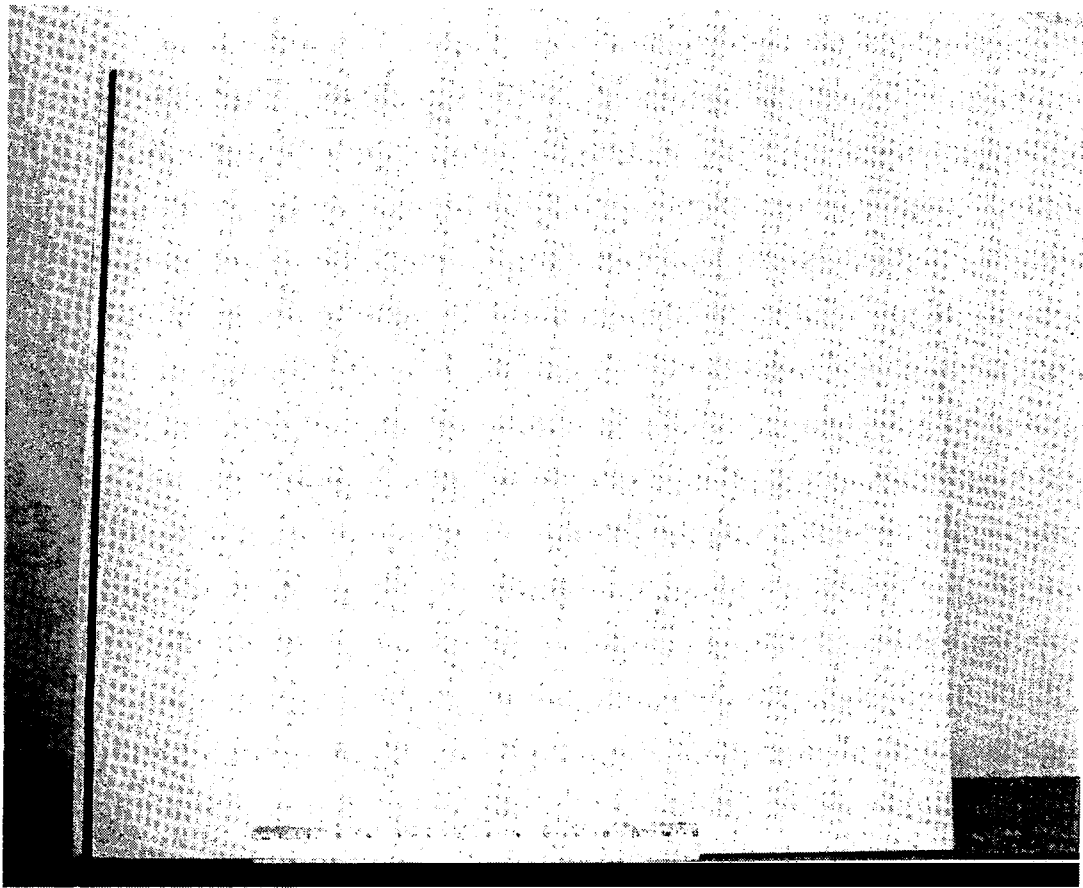
Cure: Maintain a higher face sheet pressure during final stages of core forming.



**TOP SURFACE OF LARGE FLAT PANEL
AFTER TRIMMING**

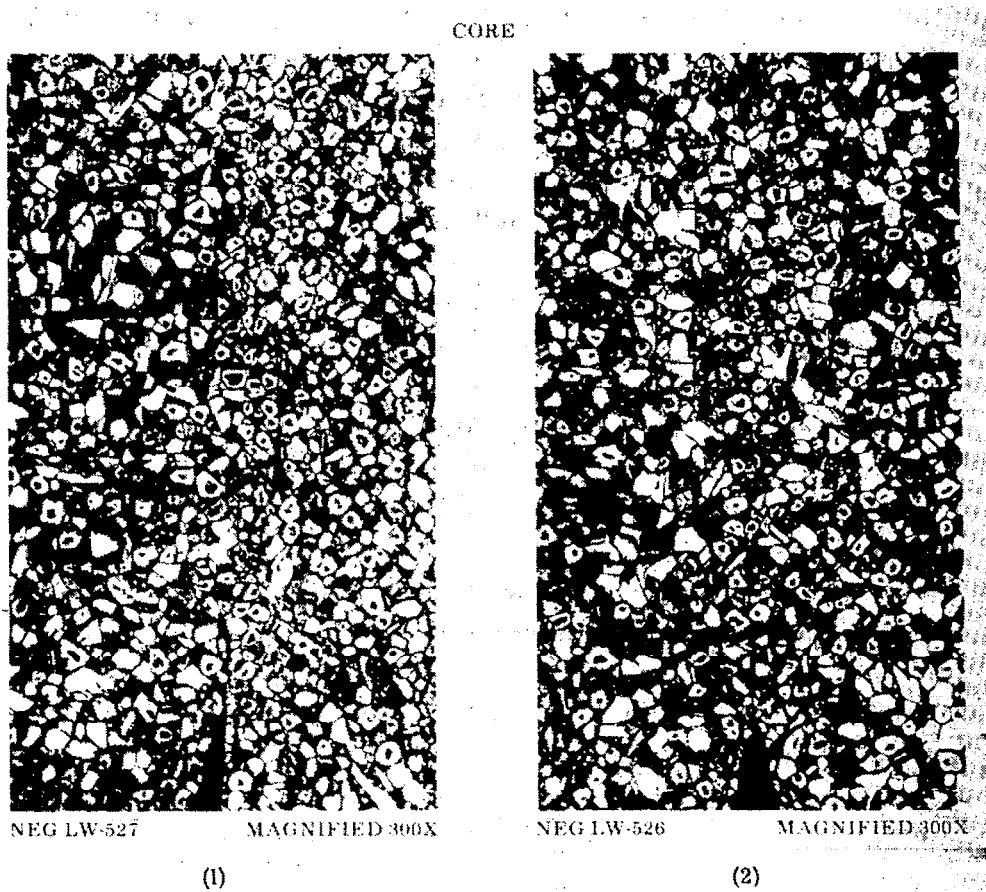


**BOTTOM SURFACE OF LARGE FLAT PANEL
AFTER TRIMMING**



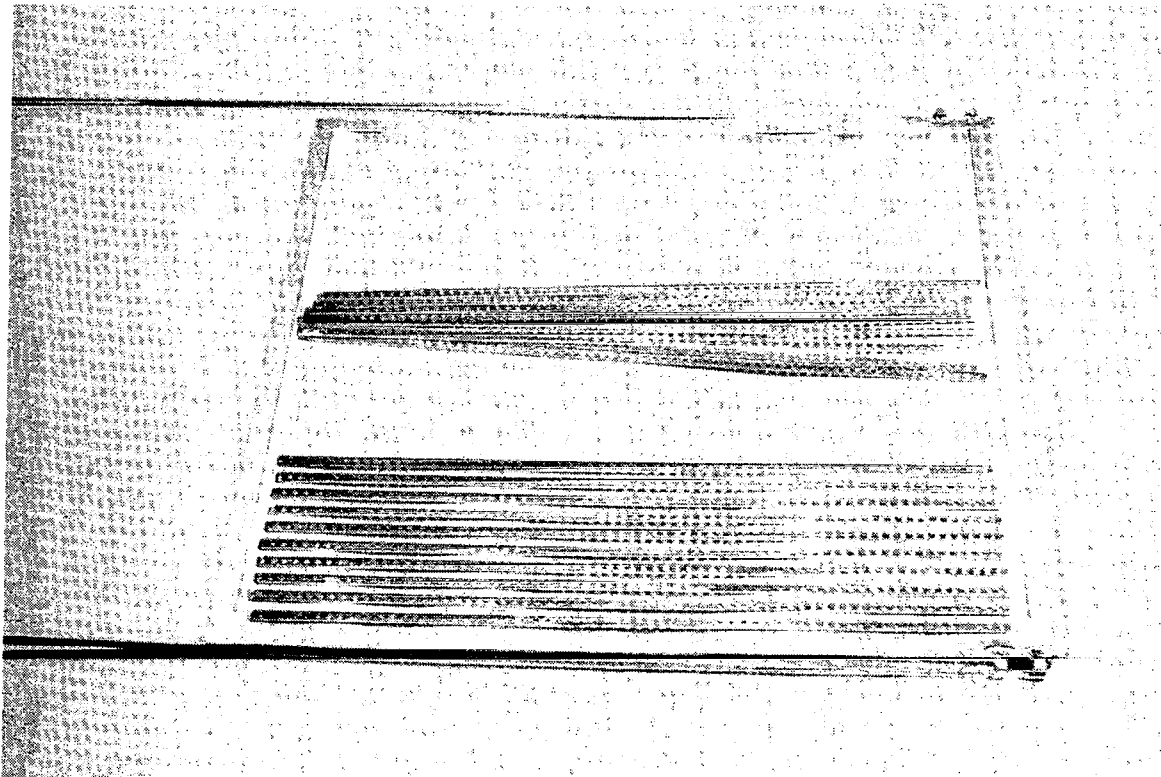
LARGE FLAT PANEL

Microstructure showing diffusion bond quality at face-sheet-to-core⁽¹⁾
and core-to-core⁽²⁾ interfaces.



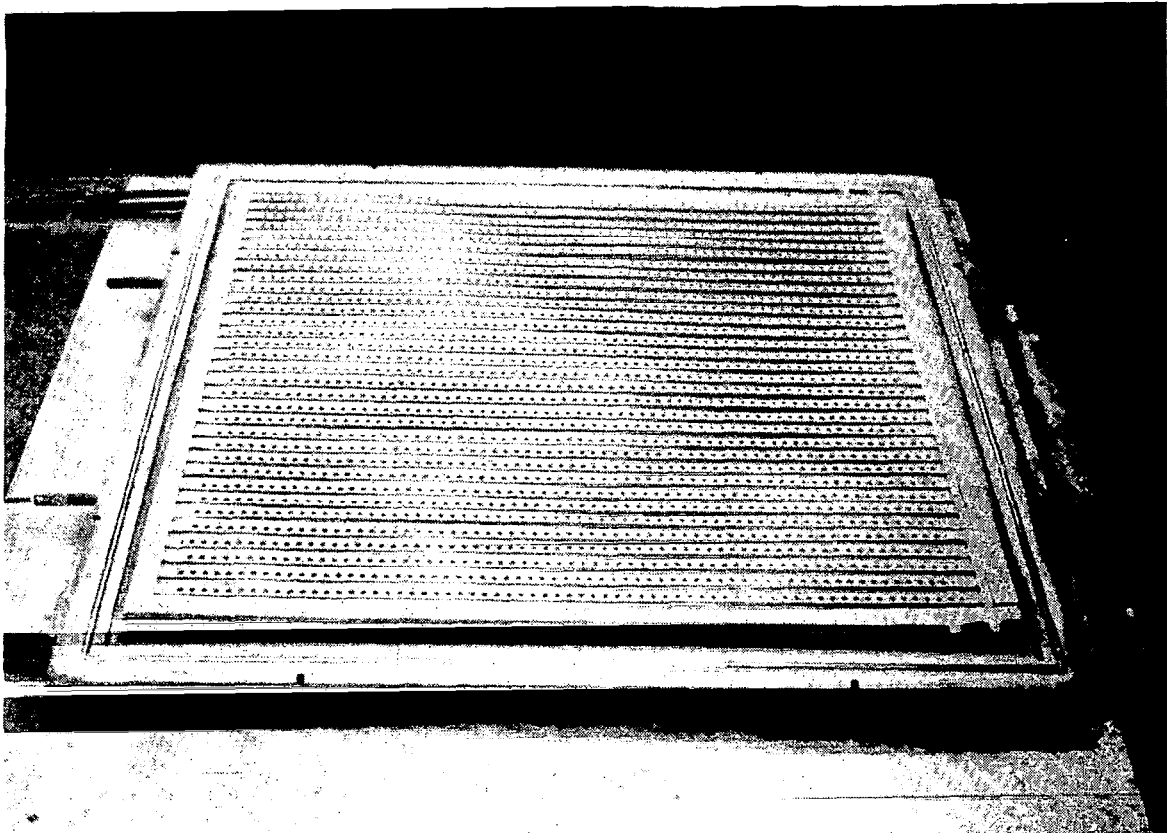
LAYUP OF LARGE DEMONSTRATION PANEL

Perforated strips and forming gas tube attachment are shown.

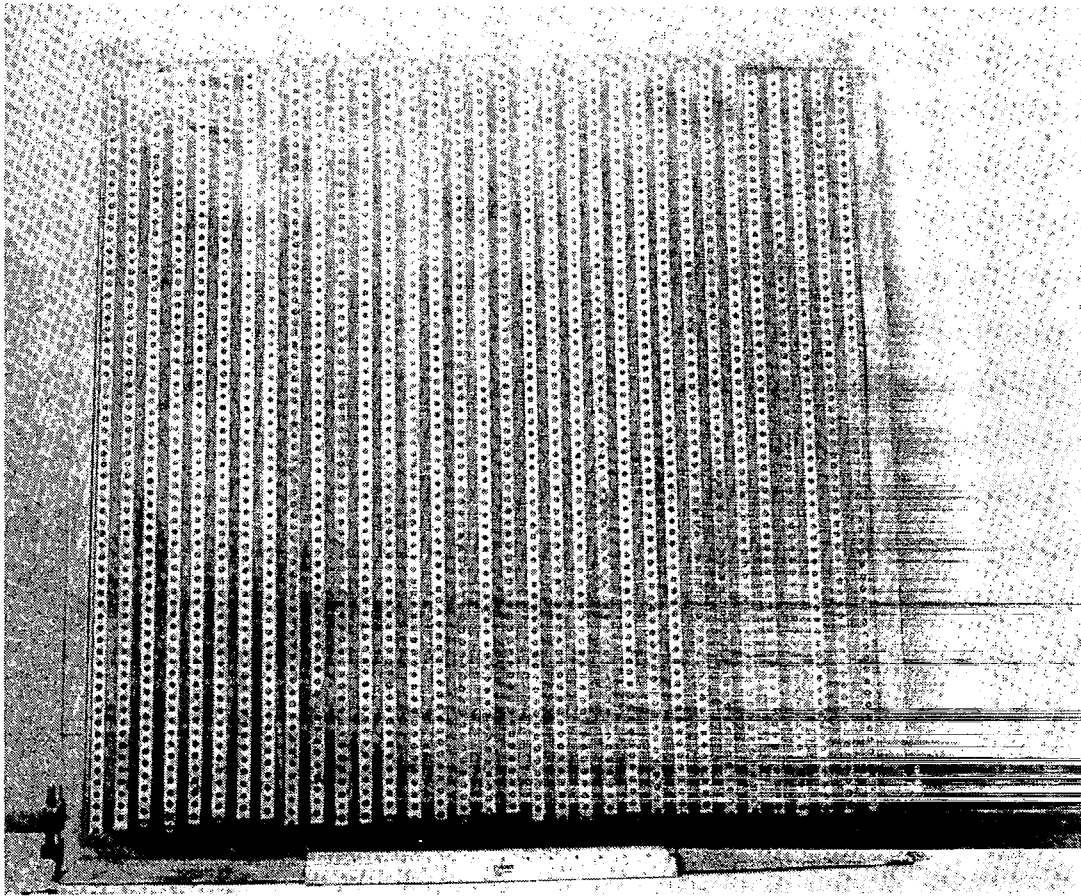


LARGE DEMONSTRATION PANEL IN FORMING RETORT

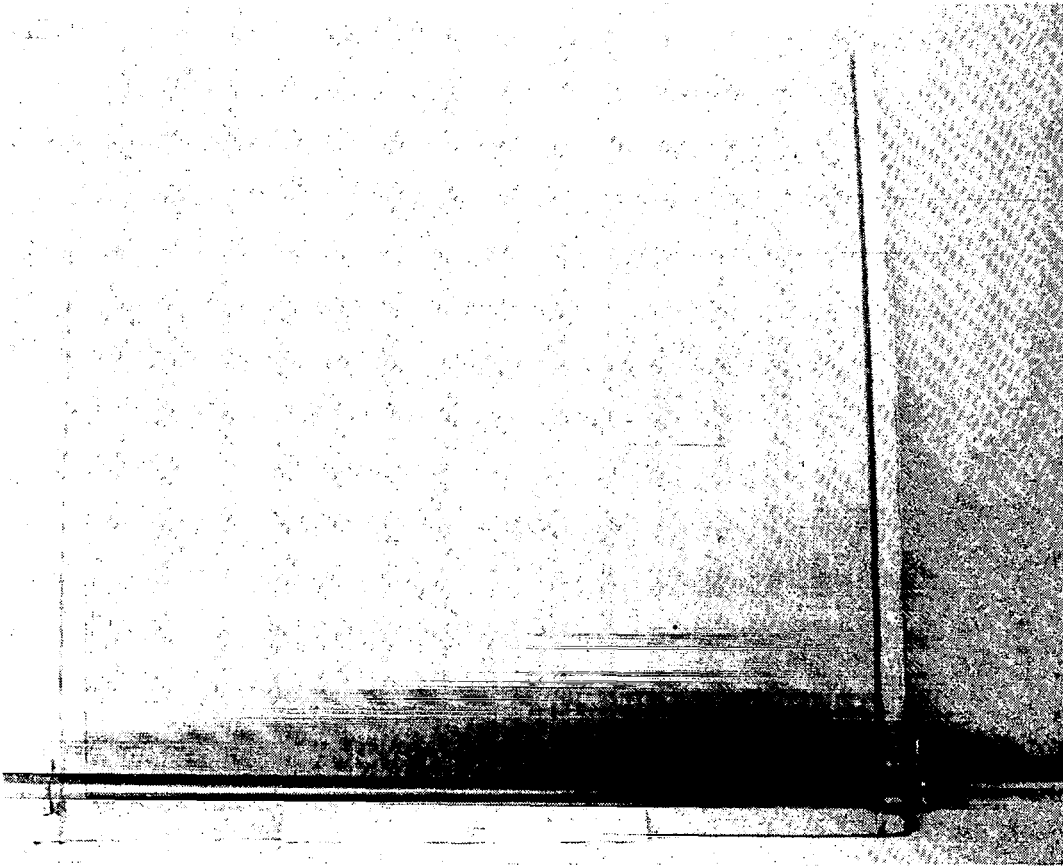
Location of perforated strips is shown.



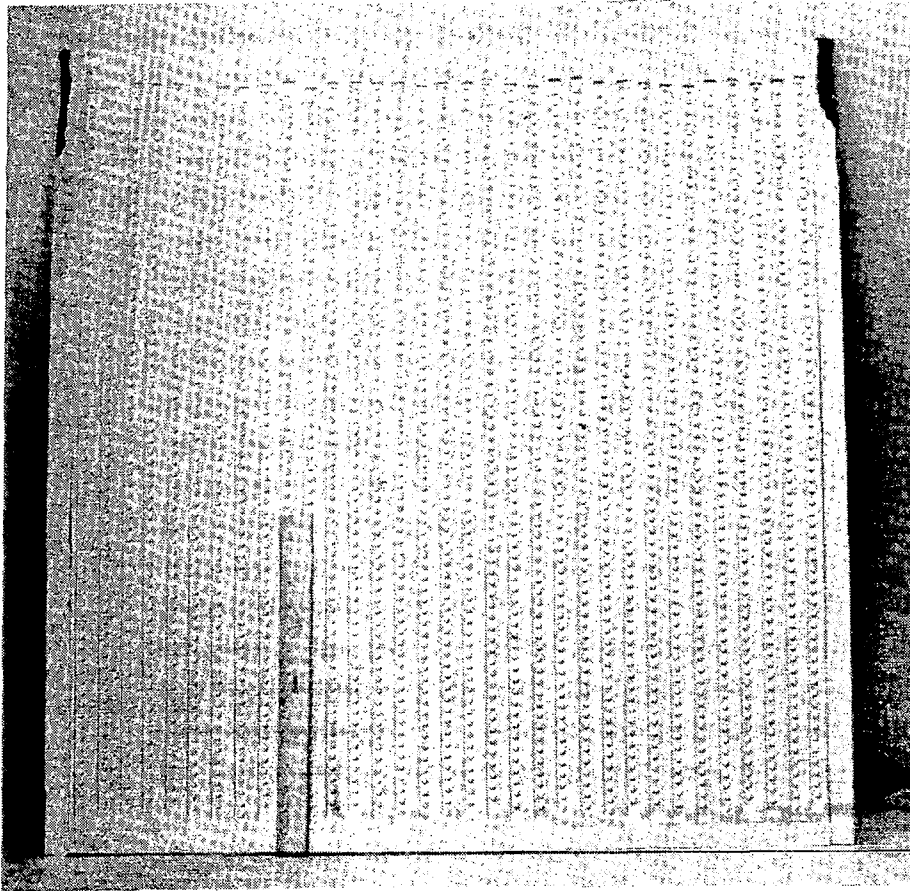
TOP SIDE OF LARGE DEMONSTRATION PANEL AFTER FORMING AND BEFORE REMOVAL OF PERFORATED STRIPS



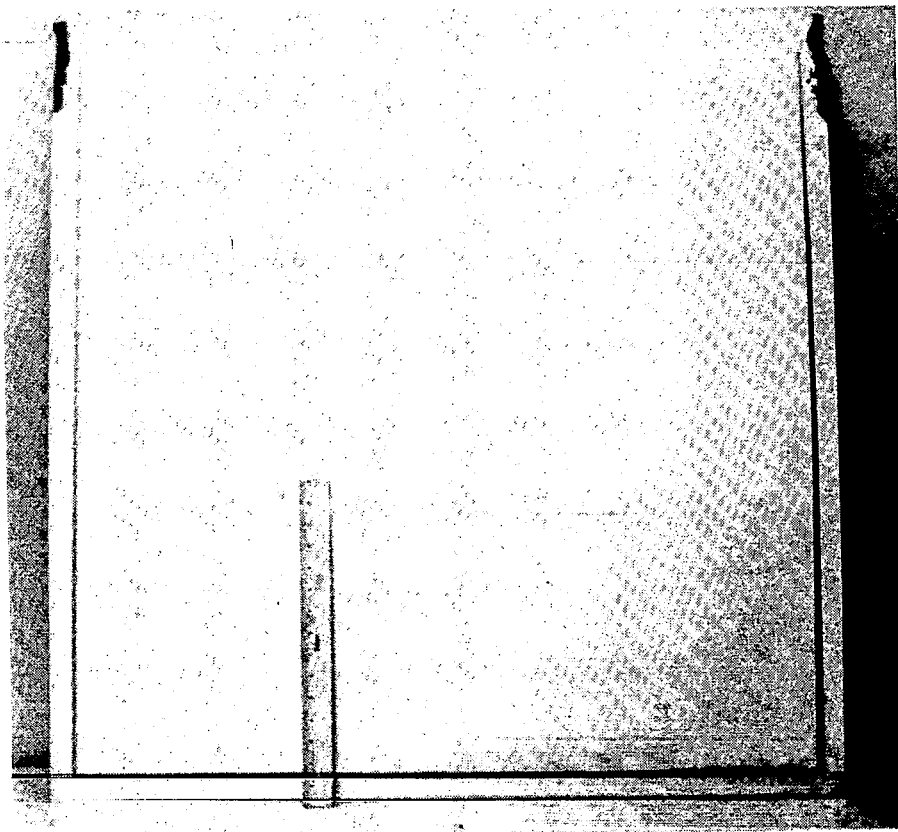
**BOTTOM SIDE OF LARGE DEMONSTRATION PANEL
AFTER FORMING**



**TOP SIDE OF LARGE DEMONSTRATION PANEL
AFTER REMOVAL OF PERFORATED STRIPS
AND CHEMICAL MILLING**



BOTTOM SIDE OF DEMONSTRATION PANEL AFTER CHEMICAL MILLING



CONCLUSIONS

Special procedures are required to produce smooth panels incorporating thin face sheets.

Tooling material in contact with the face sheets during forming is critical to avoid tooling pickup.

Type 430 stainless steel coated with boron nitride with a binder-acetone carrier was the only system which eliminated pickup.

SPF/DB titanium procedures developed in this program produced panels meeting the design requirements for LFC applications.

1. Report No. NASA CP-2218		2. Government Accession No.		3. Recipient's Catalog No.	
4. Title and Subtitle LAMINAR FLOW CONTROL - 1981 RESEARCH AND TECHNOLOGY STUDIES				5. Report Date March 1982	
				6. Performing Organization Code 534-01-13-06	
7. Author(s) Dal V. Maddalon, Editor				8. Performing Organization Report No. L-15084	
				10. Work Unit No.	
9. Performing Organization Name and Address NASA Langley Research Center Hampton, VA 23665				11. Contract or Grant No.	
				13. Type of Report and Period Covered Conference Publication	
12. Sponsoring Agency Name and Address National Aeronautics and Space Administration Washington, DC 20546				14. Sponsoring Agency Code	
15. Supplementary Notes					
16. Abstract This Conference Publication contains papers presented at the Oral Status Review of the NASA Aircraft Energy Efficiency (ACEE) Laminar Flow Control (LFC) Program held at the Dryden Flight Research Center in Edwards, California on September 17-18, 1981. Laminar flow control technology has undergone tremendous progress in recent years as focused research efforts in structures, materials, aerodynamics, and systems have begun to pay off. This work, conducted under the NASA Aircraft Energy Efficiency Laminar Flow Control Program, was begun in 1976. The objective is to demonstrate practical, reliable, LFC technology for application to commercial transport aircraft. Earlier work has shown that an LFC system greatly reduces both aircraft fuel use and operating cost. Ongoing research studies described in these papers compliment the major strides being made by industry airframe manufacturers (under NASA sponsorship) in LFC structures and materials and in the demonstration of flight systems. Research and technology developments discussed herein include, for example, fundamental studies of improved analytical techniques in boundary-layer stability prediction and a greatly expanded experimental data base characterized by detailed transonic wind-tunnel measurements on supercritical airfoils.					
17. Key Words (Suggested by Author(s)) Laminar flow control Boundary-layer Cloud effects stability Supercritical airfoil Superplastic formed/diffusion bonded structures			18. Distribution Statement Unclassified - Unlimited Subject Category 02		
19. Security Classif. (of this report) Unclassified		20. Security Classif. (of this page) Unclassified		21. No. of Pages 143	22. Price A07

National Aeronautics and
Space Administration

SPECIAL FOURTH CLASS MAIL
BOOK

Postage and Fees Paid
National Aeronautics and
Space Administration
NASA-451



Washington, D.C.
20546

Official Business

Penalty for Private Use, \$300

7 1 10, A, 030982 500903DS
DEPT OF THE AIR FORCE
AF WEAPONS LABORATORY
ATTN: TECHNICAL LIBRARY (SJT)
KIRTLAND AFB TX 77117

NASA

POSTMASTER: If Undeliverable (Section 158
Postal Manual) Do Not Return